2013

Experimental and Computational Studies of Environmentally Persistent Free Radicals (EPFRs) Formation

Lucy W. Kiruri
Louisiana State University and Agricultural and Mechanical College

EXPERIMENTAL AND COMPUTATIONAL STUDIES OF ENVIRONMENTALLY PERSISTENT FREE RADICALS (EPFRs) FORMATION

A Dissertation

Submitted to the Graduate Faculty of the
Louisiana State University and
Agricultural and Mechanical College
in partial fulfillment of the
requirements for the degree of
Doctorate of Philosophy

in

The Department of Chemistry

by

Lucy Wairimu Kiruri
B.Sc., Kenyatta University, Nairobi, Kenya, 2004
M.Sc., Kenyatta University, Nairobi, Kenya, 2009
December 2013

I dedicate this thesis to

my family, my husband, and my daughter

for all the support and patience

ACKNOWLEDGMENTS

Truly, it is a daunting task to pen down and appreciate y'all who contributed to my life and work at LSU. I had been greatly blessed by having three great advisors; Dr. Barry Dellinger, Dr. Randy Hall, and Dr. Ramu Ramachandran, who complemented one another in ways both academia and personal. Without their support and patience, I undoubtedly could not have presented this thesis.

Dr. Barry Dellinger is a renowned scientist whose depth of knowledge in Environmental chemistry of dioxins formation is quite amazing. His valuable instructions and constructive suggestions always inspired me to carry on with my study up to the completion of my PhD thesis. What I miss most about his session, is the inclusion of humor that sent everyone to laughter. I will always value his perspective in problem solving, both in science and academia.

I owe a great deal of appreciation to Dr. Hall and Dr. Ramu who constantly challenged me to try new *stuff* in the field of computational chemistry. Even after moving to San Francisco, Dr. Hall continued guiding me in my research through "hangouts" every Tuesday at 3pm. I also like to thank my committee member, Dr. Graça Vicente for her constructive suggestions, moral support, and chairing my defense. My endless thanks go to Dr. Erwin Poliakoff for his valuable instructions and support that saw me finish my PhD. Deep sincere gratitude equally goes to Dr. Slawomir Lomnicki, Dr. Cheri McFerrin, and Dr. Lavrent Khachatrayan, who immensely contributed to my success in my research work from the very beginning.

I salute past and present students of the Dellinger group: Dr. Eric Vejerano, Dr. Albert De La Cruz, Dr. William Gehling, Cholena Ren, Elizabeth Feld, and Phil Potter, who we always helped each other without any hesitation. My sincere thanks go to Ms. Tina for her kindness and care on matters both administrative and personal. Her sincere concerns about my daughter

always makes me feel good. Special thanks to my friend, Dr. John Peter Ngunjiri, for his continued help and advice throughout my PhD studies. I warmly thank Dr. Erastus and his wife Dr. Jess Hill…. I cherish the fun moments we shared.

I believe I have had the most fulfilling and amazing life after being raised by my loving parents, in the presence of great bro's: Jimmy, Dave, and Robert and sis: Joyce and Susan. My parents always provided me with support and unwavering love throughout my academic life. To my daughter Lilian, thanks for being strong. And to my niece Hanifa, am grateful for bringing joy to our family. Special thanks to my husband's wonderful family (*in-laws*) for being supportive and caring.

I cordially thank my best friend, soul-mate, and husband. John is the only person who can appreciate my quirkiness and sense of humor. He has been my true and great supporter and has unconditionally loved me during my high and low moments. Sometimes, life was not easy, but John was there for me during such times, and I truly thank him for loving me even when I was irritable and depressed. We have learnt a lot about life and ultimately strengthened our commitment and understanding so as to live life to the fullest.

Most importantly, I thank the Almighty God for His immeasurable blessings that have seen me realize my dream. My academic journey from a humble Kiguoya Primary School to the Louisiana State University was not easy, but God saw me through all challenges and turned every challenge into opportunity thus making me stronger at every turn.

To y'all, I salute you!

Shukrani!

TABLE OF CONTENTS

LIST OF TABLES

LIST OF FIGURES

LIST OF SCHEMES

LIST OF ABBREVIATIONS

EPFRs	-	environmentally persistent free radicals
LANL2DZ	-	Las Alamos National Laboratory 2 double zeta
aug-cc-pVDZ	-	augmented correlation-consistent polarized valence double zeta
ECP	-	effective core potential
B3LYP	-	Becke, three-parameter, Lee-Yang-Parr
PBE1PBE	-	Perdew, Burke and Ernzerhof (hybrid by Adamo)
M06	-	Minnesota functionals
BS1	-	basis set 1
BS2	-	basis set 2
GRRM	-	global reaction route mapping
PM	-	particulate matter
PM0.1	-	particulate matter (diameter of ≤ 0.1 μm)
PM2.5	-	particulate matter (diameter of ≤ 2.5 μm)
PM10	-	particulate matter (diameter of ≥ 10 μm)
UFP	-	ultrafine particles
FP	-	fine particles
PCDD/F	-	polychlorinated dibenzo-*p*-dioxin and dibenzofuran
1,2-DCBz	-	1,2-dichlorobenzene
2-CP	-	2-chlorophenol
PH	-	phenol
MCBz	-	monochlorobenzene
EPR	-	electron paramagnetic resonance

GC-MS	-	gas chromatography – mass spectrometry
ICP-AES	-	inductively coupled plasma – atomic emission spectroscopy
ROS	-	reactive oxygen species
DNA	-	deoxyribonucleic acid
DMPO	-	5,5-dimethyl-1-pyrroline-N-oxide
DPPH	-	2,2-di(4-tert-octylphenyl)-1-1picrylhydrazyl
PBS	-	phosphate buffer saline
NADPH	-	nicotinamide adenine dinucleotide phosphate
TB	-	tar balls
XANES	-	X-ray absorption near edge structures

ABSTRACT

The first part of the thesis investigates the use of theoretical quantum calculations for the study of EPFRs as the initial and fundamental step in the formation of polychlorinated dibenzo-*p*-dioxin and dibenzofuran. The computational model comprised of density functionals (B3LYP, PBE1PBE, and M06) and two types of basis set namely: LANL2DZ for all atoms and GEN (LANL2DZ for metals and aug-cc-pVDZ for non-metals). Full mechanisms of EPFRs formation over $(CuO)_{1-8}$, and aluminum oxide clusters were studied. The most stable intermediates and products have been determined and compared to available experimental data. In case of $(CuO)_{1-8}$ clusters, the small clusters are more exoergic and thus more reactive than larger clusters. However, Al_4O_6 cluster is more exoergic than Al_2O_3 cluster. Bader charge analysis was used to examine the degree of electron transfer from phenolic species to metal cluster. A low degree of electron transfer was observed for small clusters (CuO - Cu_5O_5). There was essentially no electron transfer for the large clusters studied (Cu_6O_6 - Cu_8O_8), and this suggests that the catalytic sites are likely to be small “islands" of metal oxide clusters. These studies serve to refine proposed mechanisms for EPFRs formation in Prof. Dellinger laboratory.

In the second part of the thesis, the dependency of EPFRs yield and their persistency on different CuO content on silica is reported. The EPFRs were generated through exposure of particles to adsorbate vapors of phenol, 2-chlorophenol, and 1,2-dichlorobenzene at 230 ^{0}C using a custom-made vacuum chamber. Adsorption resulted in the formation of surface-bound phenoxyl- and semiquinoine–type radicals with characteristic EPR spectra displaying a g-value ranging from ~2.0037 - 2.006. The highest EPFRs yield was observed for CuO concentrations between 1-3% in relation for 2-chlorophenol and phenol adsorption. The two longest lifetimes,

25 h and 23 h, were observed for phenoxyl-type radicals on 0.5% CuO and chlorophenoxyl-type radicals on 0.75% CuO, respectively. The EPFR-containing particle generated twice as much DMPO-OH compared to non-EPFR containing radical. On average, the ratio of OH radical concentration to the number of EPFRs was estimated to be 10:1 signaling a cyclic process.

CHAPTER 1 - INTRODUCTION

1.1 Background

The current status of knowledge concerning the origin, characterization, and health impacts of combustion-generated fine and ultrafine particles, emissions of dioxins, and the development of novel analytical/diagnostic tools was discussed at the 10th International Congress on Combustion Byproducts and their Health Effects held in Ischia, Italy, from June 17–20, 2007 [1]. The purpose of the discussion was to evaluate the current knowledge on the particle-associated organics, metals, and persistent free radicals (PFRs) generated from combustion sources that are the likely cause of the observed health impacts of airborne particulate matter (PM). This would help to identify research gaps and to come up with innovative solution-oriented recommendations.

The fact that our studies were highlighted at the meeting is a clear testimony to the importance of our research. Combustion-generated ultrafine and fine particles contain metals that catalyze the formation of toxic air pollutants such as polychlorinated dibenzodioxins and polychlorinated dibenzofurans (PCCD/Fs). A cycle of generating oxidative stress is presumed to occur in organisms once they are exposed to the metal-containing nanoparticles, organic carbon compounds, and persistent free radicals. Recommendations from the Congress included; studies of the interaction of gas-phase molecular pollutants with fine and ultrafine particles [2-4], epidemiologic studies that correlate incidence of disease with specific chemical components of fine and ultrafine particles [5, 6], and studies of the generation of reactive oxygen species (ROS) as a function of PFR concentration as well as particle size.

1.2 Overview of Environmentally Persistent Free Radicals

The research described herein is the detailed study on the formation of environmentally persistent free radicals (EPFRs) in combustion systems and in real environment using experimental and computational tools. First, we investigated the initial step in the formation of PCDD/Fs over hydroxylated copper oxide clusters and aluminum oxide clusters with phenol, *o*-chlorophenol, and *p*-chlorophenol using density functional theory (DFT) methods. Secondly, we focused on the formation and stabilization of EPFRs on different concentrations of Cu(II)O on silica surface. Copper is known to be a dominant transition metal in combustion-generated particles. A previous study was conducted using 5% Cu(II)O on silica which is higher than the typical concentrations of copper reported in combustion-generated and airborne PM [7]. We investigated the interaction of phenol, 2-chlorophenol, and 1,2-dichlorobenzene with x% Cu(II)O/silica, (x = 0.25, 0.5, 0.75, 1, 2, and 3), using electron paramagnetic resonance (EPR) spectroscopy. The persistency of EPFRs was examined by exposing them in air at ambient condition and then determining their concentration as a function of time. Thirdly, we investigated the propensity of EPFRs-particle systems in generating reactive oxygen species, specifically hydroxyl radicals using spin trapping methods in order to understand the mechanism of EPFR-induced ROS formation. Lastly, we investigated the formation of EPFRs on tar ball samples collected after the Deepwater Horizon (DH) incident of April 20, 2010 that resulted in 4.4 - 4.9 x 10^6 barrels of crude oil being released into the waters of the Gulf of Mexico [8-10].

1.2.1 The Nature and Origin of EPFRs

The typical sources of air pollution are derived from combustion and thermal processes [11, 12]. Size analysis of PM can be divided into three categories: coarse, fine, and ultrafine particles. Coarse particles have a mean aerodynamic diameter > 2.5 μm, fine particles, $PM_{2.5}$, are

particles with an aerodynamic diameter of < 2.5 μm, and ultrafine particles, $PM_{0.1}$, have an aerodynamic diameter of <0.1 μm [13-17]. Approximately, 90% of ultrafine and 70% airborne fine particles originate from combustion-generated processes such as internal combustion engines, industrial heating, power generation, flaring of hydrocarbon from refineries, and biomass burning. Combustion-generated particles can further be characterized as either primary or secondary particles [18]. The primary particles are those emitted directly from the sources such as vehicular emission, industrial processes, and biomass burning, whereas secondary particles are those formed when supersaturated vapors nucleate to form particles from gas phase

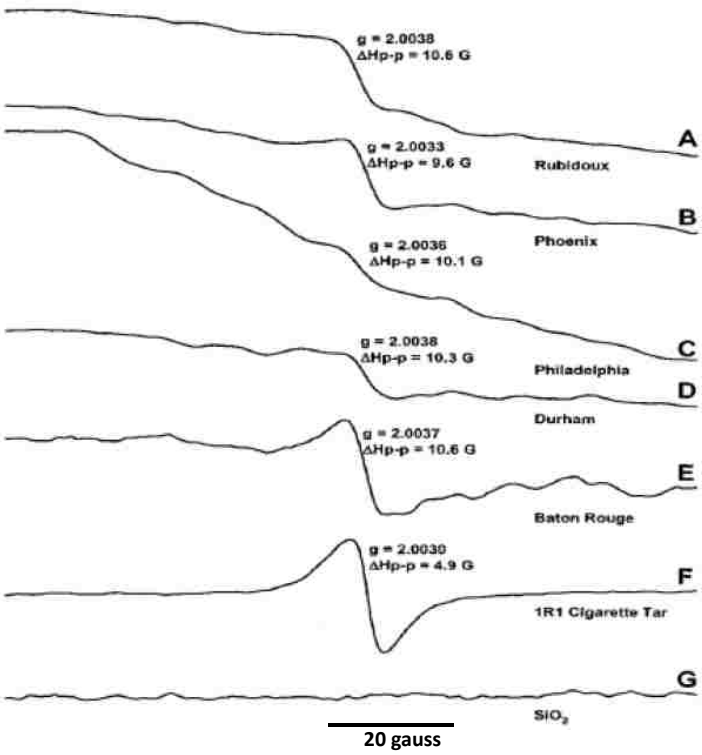

Figure 1.1 EPR Spectra of EPFRs in airborne fine particles collected from multiple cities in the United States. "Reprinted with permission from Reference [19]. Copyright 2001 American Chemical Society."

compounds. The nature of combustion by-products is determined by the composition of the chemicals and the conditions at which they react.

The presence of EPFRs in PM2.5 was first reported in samples collected from five different locations across the United States (cf. Figure 1.1) [19]. The EPR signals revealed presence of EPFRs from semiquinones family with slightly different g-values that can be attributed to both the inhomogeneity of the sample and the different degrees of interactions with metal ions [20]. The spectra displayed in Figure 1.1 are similar to those of cigarette tar radicals [21, 22]. High concentrations of EPFRs (10^{17} – 10^{18} radicals/g) were detected in PM2.5 samples which were from a highly industrialized area in Baton Rouge [23] in a recent study.

The lifetimes range from several days to several months and are comparable to those observed in the laboratory studies (cf. Figure 1.2) on fly ash surrogates of Cu(II)O/silica,

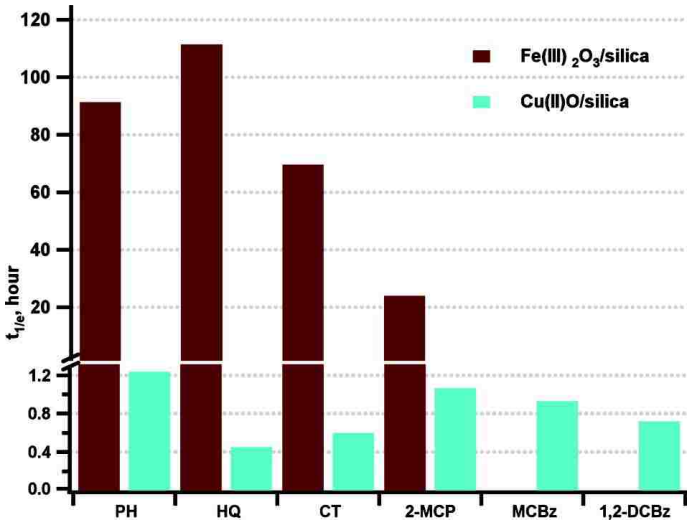

Figure 1.2 The lifetimes of EPFRs over 5% Fe(III)2O3/silica and 5% Cu(II)O/silica surfaces dosed at 230 °C and exposed to air at room temperature. “Reprinted with permission from Reference [3]. Copyright 2001 American Chemical Society.”

$Fe(III)_3O_2$/silica, and Ni(II)O/silica [2-4]. This suggests that EPFRs can easily be transported to the atmosphere and can eventually participate in atmospheric reactions directly or indirectly causing health and environmental effects [7].

1.2.2 Sources of PM2.5 and EPFRs

In combustion processes, high-temperatures initiate a cascade of chemical reactions which forms semiquinone- and phenoxyl-type of radicals depending on the precursor present [24, 25]. The combustion process is divided into four parts that can be explained by the zone theory [26]. These zones include: zone 1, the pre-flame zone (fuel zone), zone 2, the high temperature flame zone, zone 3, the postflame thermal zone, and zone 4, the gas quench cool zone and the surface catalysis zone (cf. Figure 1.3).

Surface-mediated processes are observed in zone 4 characterized by temperatures ranging from about 150 – 600 ^{0}C and result in the formation and emission of combustion-generated particulate matter that contain free radicals as well as PCDD/F [28, 29]. The free radicals are surface-stabilized on metals via interaction of an organic compound with the metal ion center [30-35]. Such an association has been demonstrated to result into highly resonance-stabilized semiquinone and phenoxyl radicals at the combustion exit [36-38]. The radicals are then desorbed and emitted to the environment with little or no destruction due to low temperature that

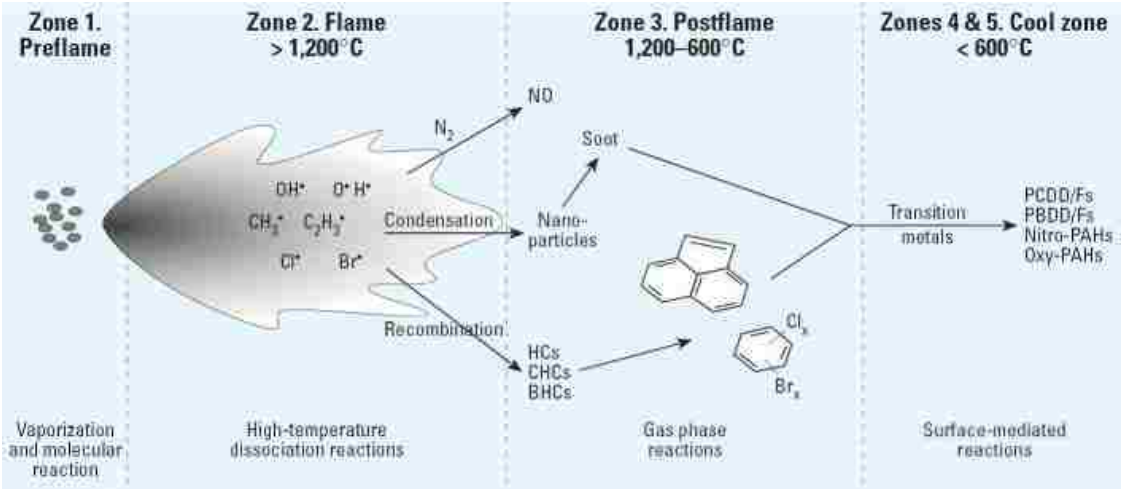

Figure 1.3 Zone theory of combustion in the formation of surface-associated free radical.

does not destroy these pollutants. Research from our laboratory has demonstrated the formation and stabilization of EPFRs on temperature ranging from about 150 – 400 ^{0}C [2-4, 19, 36] and these reactions are known to be catalyzed by transition metals [30-33, 39].

The EPFRs formation and stabilization is initiated by physisorption of EPFRs precursors on hydroxylated surface of the metal oxide (cf. Scheme 1.1). This is followed by chemisorption step via either removal of water, hydrogen chloride, or both molecules. Once the chemisorption process is reached, an electron is transferred from the organic precursor to the metal surface leading to reduction of the metal cation center. The formation of EPFRs has been demonstrated

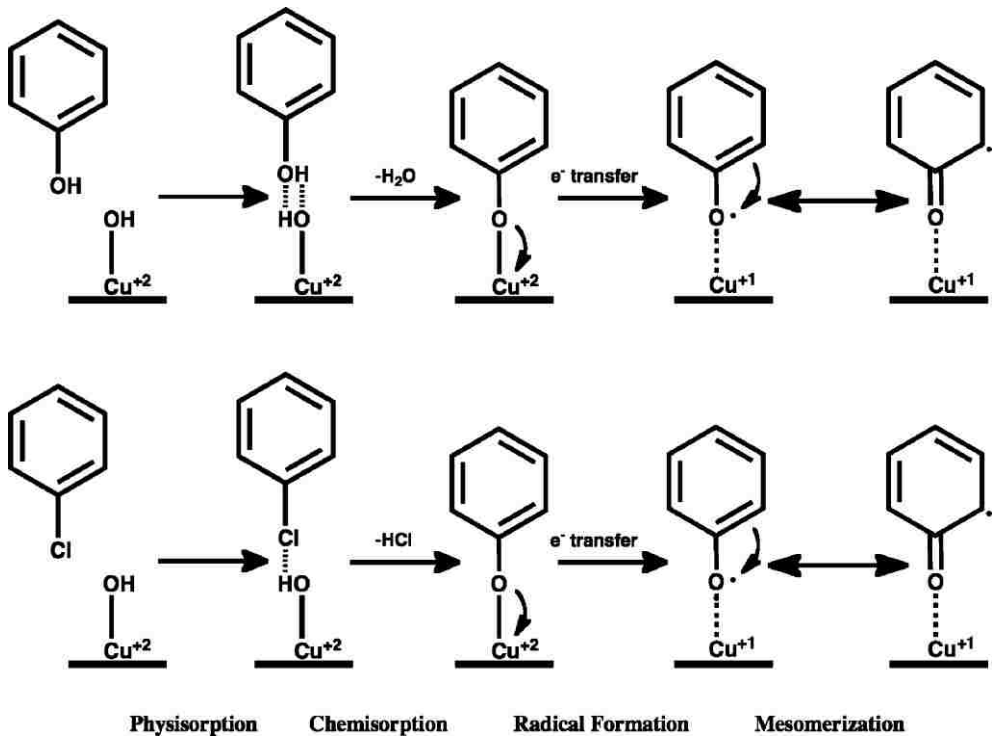

Scheme 1.1 Physisorption, chemisorption and radical formation from phenol and monochlorobenzene on a Cu(II)O Surface. "Reprinted with permission from reference [172]. Copyright 2008 American Chemical Society."

through past and on-going research [2, 4, 36] using electron paramagnetic resonance (EPR) spectroscopy. In additional study, the reduction of metal cation center has been confirmed by X-ray absorption near edge structure (XANES) spectroscopy indicating reduction caused by

chemisorbed organic compound [39-41].

Because of the association of the radical with the particle, EPFRs have shown to possess a highly-stable properties toward decomposition and significant resistant to reaction with molecular oxygen hence, the reference, environmentally persistent free radicals. This allows the concentration and decay of EPFRs to be detected by EPR as function of time.

1.3 Transition Metals in Combustion-Generated Particles

A plethora of laboratory research has demonstrated that transition metals enhance formation and stabilization of EPFRs [2, 36, 42, 43]. The typical size of a metal cluster derived from combustion-generated processes has been reported to be within ultrafine size [44, 45]. The ultrafine metallic aerosols are formed in the high-temperature (zone 2) which result from wood burning, industrial activities, combustion power generation, and other anthropogenic activities as well as non-anthropogenic sources such as natural fires and volcanic eruptions [46]. Transition metals such as copper and iron are some of the dominant transition metals. Nickel and zinc are present in combustion system and thermal processes [47-51]. The analysis and characterization of transition metals from combustion systems and municipal incinerators reveals 2.35% iron(III) oxide and 0.05% copper oxide by mass [52, 53]. In addition, characterization of particulate matter from both anthropogenic and non-anthropogenic revealed the presence of iron and other transition metals in combustion-derived particles [54]. Ambient particulate air pollution contains most transition metals with iron being the most abundant forming about 4.6% by mass [55-58]. Similarly, copper contributes significantly to ultrafine particles in indoor environment and is also found in cigarette smoke as well as gas stove emissions [59]. Copper, iron, nickel, and zinc are in high concentration in PM10 and PM2.5 [47-49]. High amounts of iron, copper, nickel, and zinc are also emitted from vehicular sources and correlate with the high presence of copper and zinc

in high traffic areas. In fly ash, copper species was studied by the least-squares fitted X-ray absorption near edge structural (XANES) spectroscopy and reported $CuCO_3$, $Cu(OH)_2$, and CuO in fractions of 0.09, 0.33, and 0.51, respectively [60]. These redox-active metals are particularly important in various electron transfer reactions and are believed to mediate formation of radicals from organic precursors [54].

Alumina is widely used as both a catalyst and as a catalyst support [61, 62]. In the manufacturing process, alumina is present in 10-20 Å films on metal surfaces whereby it exerts strong catalytic influence [63]. In the environment [64], its major role is as an adsorbent [65] as well as coagulants that render bacteria and viruses inactive [66]. In the upper atmosphere, aluminum oxides particles are generated from solid rocket boosters and are likely to play a role in atmospheric reactions [67-69]. When released to the atmosphere, the surfaces of all oxides become covered with a surface layer of water. The adsorbed water on the surface can be present in the form of hydrogen bonded or coordinated molecular H_2O, and in a dissociated form as surface hydroxyl. Infrared spectroscopy has been used to observe the O-H stretching of hydroxyl adsorbed on Al_2O_3 at a frequency region ~ 2500 cm^{-1} [70]. The adsorbed hydroxyl group has been demonstrated to exist even at 870 K. Table 1.1 displays the concentration of transition metals present in particulate matter as a function of origin and type of fuel generating the particles.

1.4 Electronic Properties of Copper Oxide Clusters

Studies of small copper oxide clusters have been accomplished both experimentally [71-77] and theoretically [78-83]. Understanding the properties of transition metals (TM) is one of the most challenging and important subjects within physical chemistry. Catalytic metal oxide nanoclusters have been reported to be present in airborne fine particles and play a key role in

Table 1.1 Metals in Environmental Nanoparticles and Fuels [85]

	PM 2.5 (μg/g)	Coal		Fuel Oil	
		Fuel (%)	Emission (%)	Fuel (ppmv)	Emission (%)
Metal					
Ni	~0.2		0.015	3-21	12.8
V	13,000-60,000		0.03	3-48	17.6
Fe	$1\text{-}5*10^3$	6-20 (ox)	4-20	27,800	34
Mg	~1	1-4 (ox)	1-5	7,120	6.2
Ca		2-23 (ox)	1-22	41,200	14.8
Co			0.005	2,040	1.2-1.5
Cr	~1		0.02	4,400	5.8-9.0
Cu	~2		0.02	2,780	3.3-3.8
Mn			0.07	1,040	1.2-3.5
Pb	5-10		0.015	2,040	0.7-1.0
Sr			0.1	713	1.7-3
Zn	500-22,000		0.023	5,630	3.3-3.8
Zr			0.015		
Mo			0.001	4,270	5.5-10
Si		35-45 (ox)	22-61	46,000	15-20
K			0.3-4		
Al		15-40 (ox)	13-36	32,000	19.5-28

PCCD/Fs formation. TM, particularly copper and iron have been shown to be effective catalysts in the formation and stabilization of EPFRs that basically play a key role in the initial step of PCDD/Fs formation. The structure and electronic spectra of copper monoxide (CuO) were first reviewed using intermodulated fluorescence [84].

The laser photoelectron spectroscopy has also been used to study the neutral and anionic CuO molecule. The bond length of CuO was found to be 1.704 Å and its vibrational frequency to be 682 cm^{-1}. Two geometric structures of CuO_2 are reported in literature: CuOO (bent) and CuO_2 (side-on, C_{2v}). Evidence of the bent complex of CuOO has been reported both in experiment and in theory.

Figure 1.4 displays the electronic structures of Cu_2O_n (n =1-4) investigated using anion photoelectron spectroscopy and density functional calculations. The geometries of Cu_2O and

Cu_2O_2 are triangle and rhombus, respectively. For Cu_2O_3, two isomers were found to have close energies (bipyramid and bent structure with an O-Cu-O-Cu-O atomic arrangement); the bipyramid structure is in good agreement with the experimental electron affinity (EA). The stable structure of Cu_2O_4 has hexagonal ring with two O-O bond (cf. Figure 1.4).

Figure 1.5 illustrates the structures of some $(CuO)_n$ clusters with n = 1−8 clusters [86] that will be used in chapter IV as the starting point for reactions with EPFRs precursors (phenol, *o*-chlorophenol, and *p*-chlorophenol). The calculated bond length of neutral and anionic CuO are 1.81 Å and 1.74 Å and they compare well with the measured values of 1.72 Å and 1.67 Å [87]. It is well known that the geometrical structures and chemical reactivity of metal oxide depend on cluster's size. Therefore, one can elucidate catalytic behavior as a function of cluster size. Unlike surface or condensed phase, clusters can be isolated in the gas phase and are thus amenable to

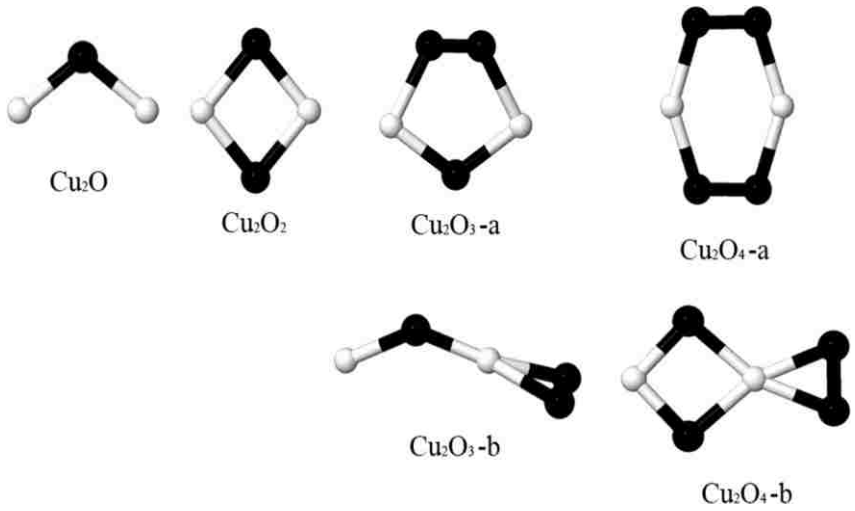

Figure 1.4 Lowest energy clusters for Cu_2On, n = 1−4. Copper/oxygen atoms are colored white/black. "Reprinted with permission from reference [86]. Copyright 2008 American Chemical Society."

individual access both experimentally and theoretically. The size of the metal nanoclusters in combustion-generated particles has been suggested to range from a micrometer down to just a

few atoms. For this reason, knowledge of the detailed geometrical and electronic structures of these atomic clusters can be essential in understanding dioxin formation [86].

1.5 EPFRs in "Real" Environmental Samples

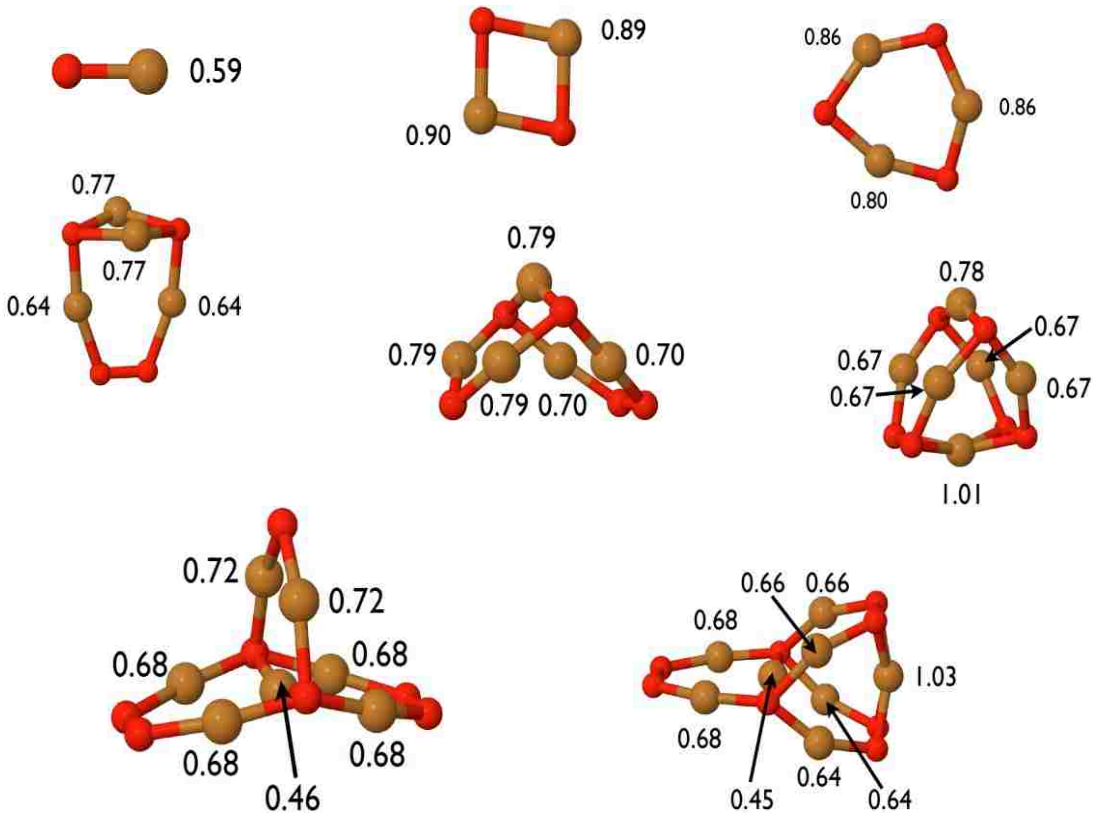

Figure 1.5 Re-Optimized structures of neutral (CuO)n clusters with n = 1−8 using the B3LYP/GEN model chemistry. Bader charges for the copper atoms are shown in parentheses. Copper/oxygen atoms are colored gold/red. "Reprinted with permission from reference [86]. Copyright 2008 American Chemical Society."

It is now clear that EPFRs are formed on the surface of combustion-generated particulate matter containing different transition metals. However, recent findings indicate that EPFRs can be formed not only in combustion systems but also in the environment at ambient temperatures [88-91]. Soot contains catalytically active metals and a strong EPR signal that indicate the presence of unpaired electrons as reported in coal dusts, diesel exhaust particulate, and coal fly ash. The process of soot formation in a combustion system is through gas-phase nucleation,

molecular growth, and aggregation/agglomeration of organic species. These radicals are entrapped in the matrix and fail to migrate to the surface, therefore; cannot undergo oxidation in air. Figure 1.6 shows EPR spectra of soot generated from a wood-burning fireplace with chlorinated organics from a pilot-scale hazardous waste incinerator. Soot from tetrachloroethylene and bromoform demonstrated the presence of both oxidized carbon and a semiquinone-type radical [20].

Recent investigation of EPFRs on soil samples collected from superfund site

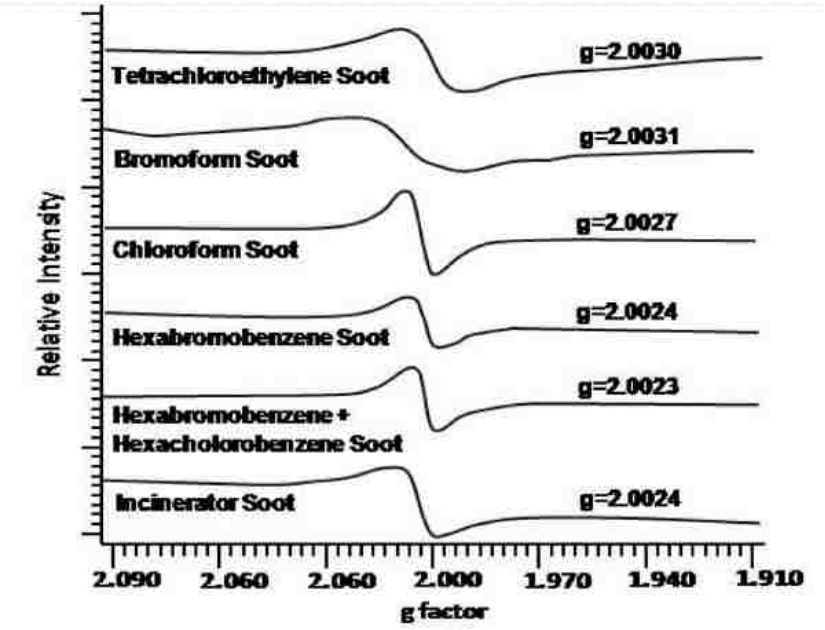

Figure 1.6 EPR spectra for various combustion-generated particulate samples from combustion process.

(contaminated with pentachlorophenol) and outside the superfund site (non-contaminated) revealed the presence of radicals as displayed in Figure 1.7. The contaminated soil contained higher concentration of EPFRs than non-contaminated soil. Pentachlorophenol (PCP) presence was verified through extraction (followed by GC-MS analysis) and by introducing vapors of PCP onto a clean soil [88]. Semiquinone-type radicals are generated during formation of humic acid

from organic matter through radical polymerization [92-95]. EPFRs similar to those formed from combustion-generated process were expected to be present due to the presence of redox-active metals in soil. The main difference between EPFRs formed in soil and those in combustion systems, is the reaction times and temperatures. Whereas the reaction time in a combustion system is in seconds under high temperatures, in soils, the reaction time is years at ambient conditions.

It has been found out that PM10 and PM2.5 from vehicle emissions are the most dangerous [96] to human health. As stated earlier, fine and ultrafine particles are composed of inorganic, organic, and elemental carbon, sulfates, and nitrates [97]. The composition of PM depends on site and location [98, 99]. For instance, particulate matter in Europe are higher in sulfate and organic compounds due to prevalent use of coal which contributes to submicron size particles [100, 101].

1.6 Health and Environment Impacts of PM

Epidemiological studies have shown high correlation between exposure to particulate matter (PM) and increased adverse health effects. Particulate matter (PM) exposure is associated with death from cardiopulmonary disorders and lung cancer according to the studies done in six cities [102, 103] and 151 metropolitan areas [104] in the United States, with 1% increase in daily mortality for each 10 $\mu g/m^3$ increase in PM10. Although a plethora of studies exist on the mortality and morbidity of PM, the components that are responsible for its toxicity and the observed adverse effects remains a quagmire [105, 106]. Many researchers on PM agree that the level of toxicity depends on the chemical composition [107], particle size [108], and shape [109, 110]. The serious health risk is associated with ultrafine particles due to their high surface area and large amount (high concentration) of toxic pollutants condensing on the surface [111].

Ultrafine particles ($PM_{0.1}$) can penetrate deeper into interstitial spaces of the lungs where they can be deposited to the alveoli, bronchi, and other parts of the lower respiratory system [112-115]. This has led to increased asthmatic symptoms [116, 117] and increased hospitalization rates for respiratory disorder and lung malfunction [118-121]. Ultrafine particles can also penetrate into the bloodstream and be deposited into the mitochondria causing oxidative stress and major structural damage [107]. The ability of PM to induce damage through its biological potency depends on the redox cycling ability of organic compounds adsorbed on its surface.

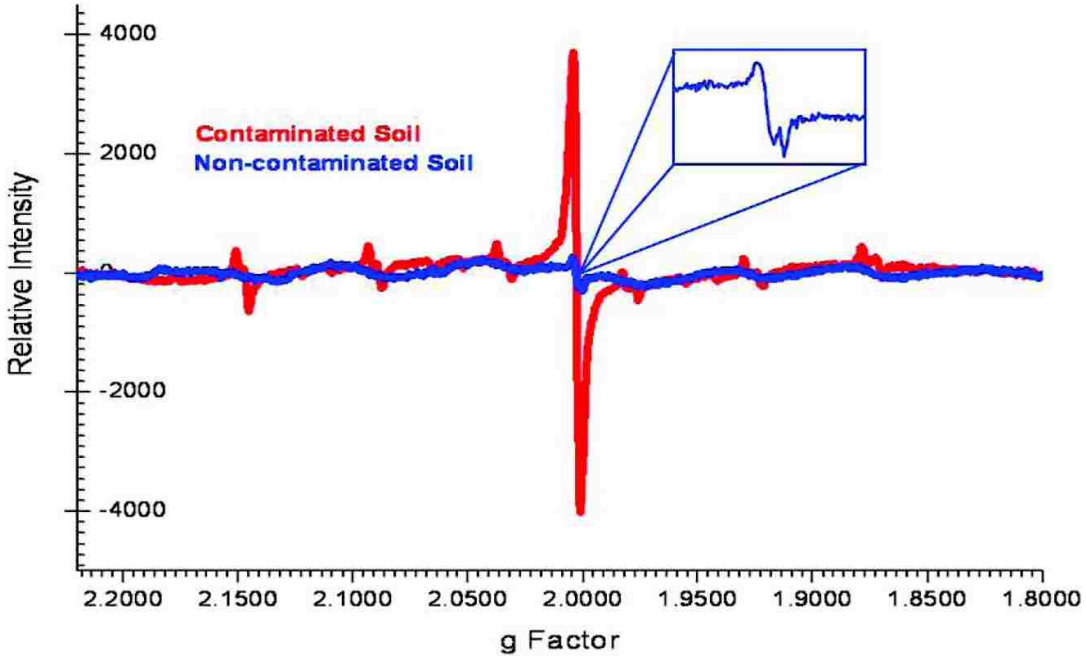

Figure 1.7 EPR spectra of the whole soils of contaminated (red) and non-contaminated soils (blue). "Reprinted with permission from reference [88]. Copyright 2008 American Chemical Society.

Indoor pollution from cigarette smoke and/or biomass combustion from cooking stoves contains similar organic species as outdoor air pollutant. The indoor pollutant pose a greater risk to people exposed to it for the longest period of time e.g. women, infants, young children, and the elderly and especially those with immune/pulmonary/cardiovascular disorders. Nearly two million premature deaths are caused by acute lower respiratory tract infections in children under

five. Chronic obstructive pulmonary disease in adults and respiratory tract cancers in adults are underlying impacts linked to indoor pollution [122, 123].

As aforementioned, the size, shape, and composition are important factors in determining the toxicity of particles [109, 110]. Organic pollutants are often associated with particulate matter [110]. Studies have demonstrated that organic pollutant are surface-bound to PM and are resistant to removal implying a rather stronger chemical bond [124]. The persistency of the radical in air is attributed to stabilization on the surface of the particle, whereas the persistency in biological systems is attributed to cyclic mechanism involving the biological regeneration of reactive oxygen species (ROS) which include hydrogen peroxide, superoxide, and hydroxyl radical. Although ROS are essential in the maintenance of cellular processes, such as energy source, chemical signal transduction, and immune function, the overproduction of ROS can cause the defense system to fail leading to structural damage of the cellular components [107]. The particulate matter triggers the production of ROS, [125, 126] which cause oxidative stress that can result to acute and chronic diseases [127, 128]. Some redox-active transition metals in particulate matter can also catalyze generation of ROS, particularly iron in producing oxidant-mediated injury to the gastric mucosa [129] and proinflammatory effects [105, 108, 130-133].

One acceptable experimental model (cf. Figure 1.8) in the toxicity of particulate matter proposes that surface bound persistent quinoid and semiquinone-type radicals generate ROS by reducing molecular oxygen to superoxide [109, 134-143]. The superoxide radical then undergoes dismutation with biological reducing agents[144] such as NADPH to produce hydrogen peroxide, which upon reaction with a transition metal (Fe(II) or Cu(I)) forms hydroxyl radicals via Fenton reaction which elicits DNA damage [145]. Each cycle in the proposed form produces a net output of one hydroxyl radical per EPFR, with the regeneration of the starting radical-

particle system [146, 147]. The number of OH radicals generated by one EPFR-particle system is dependent on the cycle termination reaction, such as EPFRs recombination or scavenging by antioxidant agent. It is postulated that hydroxyl radical are produced within affected cells due to their relative short half-life of 10^{-9} s [148].

A key question from a variety of studies is how the exogenous iron found in PM was capable of generating hydroxyl radicals yet it is inactive toward Fenton reaction [145]. Recently, it has been discovered that superoxide not only dismutate to hydrogen peroxide but it is also

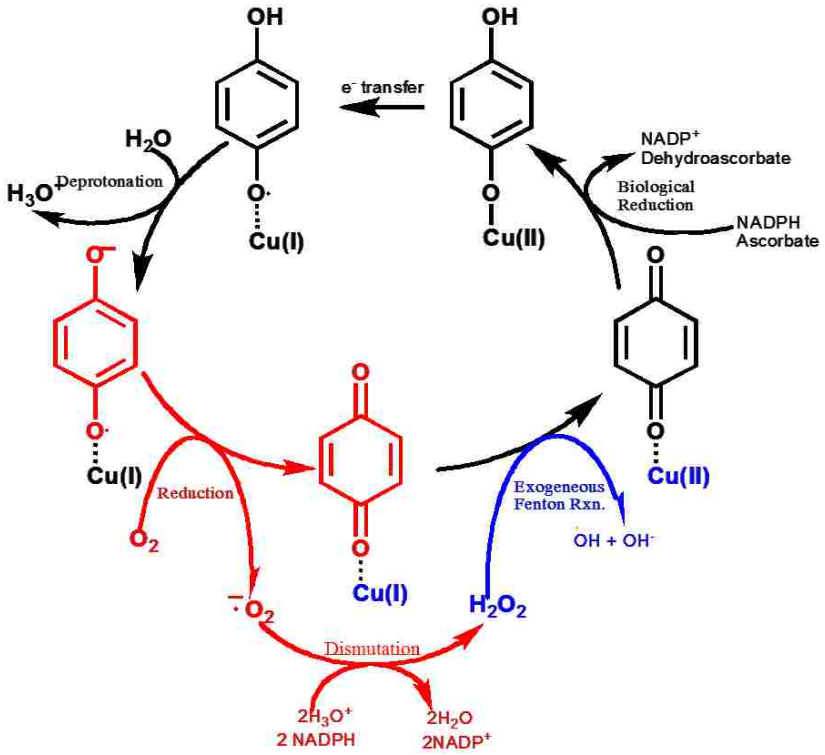

Figure 1.8 Selected steps of the proposed cycle chain involved in the ROS generation in the presence of EPFR-particle system in biological media

capable of attacking Fe-S cluster protein in biological systems liberating the bound iron and making it available for the Fenton reaction [149].

Although the health impact of EPFRs is in its infancy owing to its recent discoveries, few researches demonstrate their potential for causing dire health consequences stressing the need to

understand their mechanism. The EPFRs, by definition, persist for long periods of time (hours – months) [2-4] in air and at least 12 hr in biological fluid [150]. The particles containing EPFRs promote DNA damage and induce pulmonary dysfunction consistent with free radical reactivity through ROS generation [19, 27, 146, 147, 151, 152]. A significant increase of the GSSG (oxidized glutathione)/total glutathione ratio was observed (cf. Figure 1.9) and depletion of gluthathione peroxidase enzyme [153] when HEp-2 cells was exposured to EPFRs particles [153] due to oxidative stress in human epithelial cells. Thus, increase in GSSG/total glutathione ratio is an indication of the higher ROS activity level. Copper oxide/silica particles without EPFRs have also shown oxidative stress activity thus, stimulating inflammatory changes which are expressed as increased levels of various cytokines. However, the presence of radicals on the surface of particles dramatically enhanced this effect [154, 155].

1.6.1 EPFRs in Tar Balls

The research on the ecological and toxic effects of oil spills is concentrated around the toxicity of the water-soluble polycyclic aromatic hydrocarbon (PAH) and other aromatic compounds [156]. The heavier and insoluble fractions of the crude oil, as in tar balls, has not been considered a significant environmental threat except as coating agent of animals and plants surfaces (birds, turtles, shore flora) [157]. In the case of sea turtles, tar ball ingestion and blockage of oral cavities have been reported [158]. The formation of tar balls and oil mineral aggregates (OMA) during the emulsification and weathering of spilled oil results in adsorption of aromatic molecules and their chemical interaction with minerals. Since the suspended minerals and sediments contain crystallites and domains of transition metals [159-161], the metal-crude interaction is inevitable. Experimental studies of the surrogates of combustion borne particulate matter containing metal oxides have shown aromatic molecules chemisorb on the metal ion

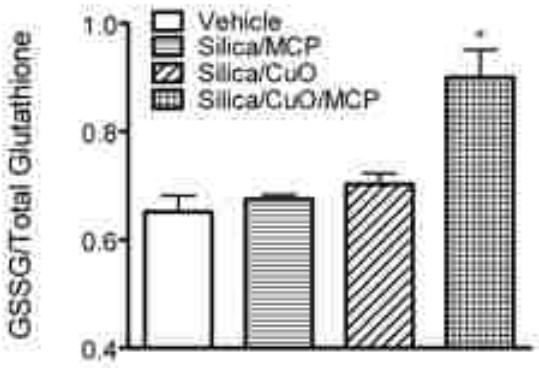

Figure 1.9 Ratio of cellular oxidized to total glutathione in epithelial cells.

centers to produce surface stabilized EPFRs [162, 163]. The mechanism of the EPFRs formation from interaction with metal ions has been shown to occur at elevated temperatures in combustion systems, and also recently in ambient conditions such as in soils at contaminated Superfund sites [88]. From these evidences, we postulated EPFRs can exist in other real world environmental samples such as the tar balls washed on the shores of Gulf of Mexico as a result of Deepwater Horizon oil spill.

Tar balls are a physical mixture of the heavier components of crude oil, mineral inorganic particles, and biological debris from aquatic ecosystem. The major components of the tar balls are asphaltenes, nanosized particles of polymeric aromatic polar compounds. The presence of the paramagnetic signal in crude oil is associated with the asphaltenes. The paramagnetism of asphaltenes was detected long time ago [164, 165], and application of EPR measurements of crude oil was suggested as a mean of quantitative estimation of asphaltenes in crudes [165]. Two major factors contribute to the spectral features: paramagnetic vanadyl VO^{2+} species in a porphyrin like structures and free radicals signals. There have been attempts to correlate the free radical signals in asphaltenes with vanadyl content. However, the correlations are not obvious and also not well understood. Other metals such as Fe^{3+} or Mn^{2+} present in the asphaltenes can

contribute to their paramagnetic spectrum. Since the tar balls are particularly enriched in heavy components of the crudes and asphaltenes, paramagnetic signal is anticipated to be observed. Of special interest, is a free radical signal associated with the asphaltenes. The g-value of the radical signal associated with asphaltenes observed vary from 2.0028 - 2.004 [166, 167]. The position of the signal and its asymmetry indicates the presence of different paramagnetic species. Depending on the level of aromaticity and the presence of heteroatoms of the asphaltene fragment associated with the radical, a shift in g-value occurs; with aromatic radicals centered at ~2.0028, phenoxyl at 2.004 and sulphur containing radicals at 2.008 [168]. Thus, the study of the formation of stabilized radicals in crude remnants appears warranted. The stabilized radicals can have a critical impact on the affected ecosystems, since EPFRs have been shown to be potent ROS generators in aqueous media [146].

1.7 Formation of Dioxins and Furans in Combustion System

As previously mentioned, the initial step in PCDD/F formation from chlorinated phenols through surface-mediated reactions is the adsorption of chlorophenoxyl radical on the catalytic site. The adsorbed chlorophenoxyl then reacts with another surface-bound chlorophenoxyl via the Langmuir-Hinshelwood mechanism (L-H) or with a gaseous chlorophenol via the Eley-Rideal mechanism (E-R). These two mechanisms has been investigated using Cu(II)O/silica in which a positive reaction order was assigned for PCDD formation indicating an L-H mechanism while a negative order indicating an E-R mechanism was observed for PCDF formation [169, 170]. A pyrolysis study carried out using the same system reported that PCDD formation is a side reaction for oxidation of 2-chlorophenol via a Mars-van Krevelen mechanism that involves transfer of oxygen atom from a Cu oxidized surface to the adsorbed 2-chlorophenoxy radical, which is formed by H-abstraction from its hydroxyl

group by surface oxygen [171].

1.8 Research Aims and Objectives

We started by investigating the reactions of metal oxide clusters with phenol and chlorinated phenol using *ab initio* based methods. Secondly, we investigated the formation of EPFRs on the surface of surrogate combustion-generated particulate matter on different copper oxide concentrations. Thirdly, we investigated the generation of ROS from EPFRs-containing particles using spin trapping method. Finally, we investigated the presence of EPFRs in tar ball collected at the Gulf of Mexico after the BP oil spill.

In general, metal oxide particles catalyze the formation of toxic pollutants such as PCDD/Fs in combustion systems. We employed density functional theory to study the reactions of phenol, *o*-, and *p*-chlorophenol with hydroxylated neutral copper oxide and also hydroxylated aluminum oxide clusters. Our starting copper oxide clusters had been previously reported elsewhere (cf. Figure 1.7) [86]. When exposed to external environment, metal oxides show a strong tendency to become saturated by chemically reacting with water in a process known as hydroxylation. The first step in the surface-mediated process thus involved addition of water to copper atom followed by a proton transfer to the adjacent oxygen presumably causing hydroxyl groups on the surface. The hydroxylated surface reacted with a phenolic/or chlorophenolic compound through physisorption and chemisorption processes. Various thermodynamic and electronic properties such as reaction energies (ΔE_{rxn}), enthalpies (ΔH_{rxn}), and free energies (ΔG_{rxn}) were established so as to determine the most probable reaction sites on the clusters. There is evidence of an electron transfer from the chemisorbed species to the metal cation center as have been demonstrated by numerous EPR signals from metal oxide particles containing EPFRs. We assessed the degree of charge transfer using Bader analysis method.

In the second part, we investigated formation and stabilization of EPFRs on different concentrations of copper oxide on silica matrix. Copper oxide is a dominant transition metal found in combustion-generated particulate matter [54] and it interacts with aromatic organic compound to form surface-stabilized EPFRs. A previous study on formation of EPFRs on 5% Cu(II)O on silica [7, 172] is higher than the typical concentrations reported in combustion-generated and airborne PM in dioxin literature [173]. This prompted to investigation of different concentrations of Cu(II)O on silica so as to get insight into the properties of copper that could affect the catalytic activity, such as copper loading, copper dispersion, and copper redox properties, and establish how this can influence formation of EPFRs. Although the presence of metal merits formation of EPFRs, a study to show how metal concentration affects the EPFRs yield is still lacking. The size dependency of nanoparticles has been examined as a pivotal property in determining the catalytic activity [174]. Generally, the catalytic activity per unit cluster increases with decreasing particle size. In the current study, a set of CuO/silica catalysts with different metal loading, were prepared, characterized and tested for EPFRs formation.

In the adsorption studies, different CuO/silica concentrations (0.25, 0.5, 0.75, 1, 2, and 3%) were dosed with 1,2-dichlorobenzene, 2-chlorophenol, and phenol. The two chlorinated EPFRs precursor are present in combustion sources containing chlorine such as hazardous waste and municipal waste incinerators [175-177]. Phenol was chosen because it is a dominant component in biomass combustion [178-181]. EPFRs were formed using our custom-made vacuum system and analyzed using EPR spectroscopy. We performed hydroxyl radical generation studies with EPFRs-particles dosed with 2-CP and non-EPFR particles to analyze the amount of hydroxyl generated. Spin-trapping techniques of 5,5-dimethyl-pyrroline-N-oxide (DMPO) was used in phosphate buffer saline solution.

Lastly, we identified and analyzed EPFRs originating from tar balls in the sediment and sand deposits of the Louisiana Gulf Coast. We postulated that tar balls and oil material upon interaction with sand sediments and after weathering will form EPFRs similar to those observed upon interaction of transition metal oxides with aromatic molecules. In the proposed study, we evaluated the formation of the EPFRs in the tar balls and oil contaminated shore sand. Chemical analysis combined with the extraction process was performed to identify a specific molecular species responsible for EPFRs formation. We also evaluated the lifetime of the EPFRs present in tar balls. In addition, we established the ROS generation potency of the EPFRs contaminated sands in physiological conditions. Identification of the molecular precursor is an important indication of a potential health hazard of EPFR containing deposits.

1.9 References

1. Dellinger, B., et al., *Report: Combustion byproducts and their health effects: Summary of the 10th International Congress.* Environmental engineering science, 2008. **25**(8): p. 1107-1114.

2. Lomnicki, S., et al., *Copper oxide-based model of persistent free radical formation on combustion-derived particulate matter.* Environ Sci Technol, 2008. **42**: p. 4982 - 4988.

3. Vejerano, E., S. Lomnicki, and B. Dellinger, *Formation and Stabilization of Combustion-Generated Environmentally Persistent Free Radicals on an Fe(III)2O3/Silica Surface.* Environmental Science & Technology, 2010. **45**(2): p. 589-594.

4. Vejerano, E., S.M. Lomnicki, and B. Dellinger, *Formation and Stabilization of Combustion-Generated, Environmentally Persistent Radicals on Ni(II)O Supported on a Silica Surface.* Environmental Science & Technology, 2012. **46**(17): p. 9406-9411.

5. Buzea, C., I.I. Pacheco, and K. Robbie, *Nanomaterials and nanoparticles: sources and toxicity.* Biointerphases, 2007. **2**(4): p. MR17-MR71.

6. Brook, R.D., et al., *Air pollution and cardiovascular disease A statement for healthcare professionals from the expert panel on population and prevention science of the American Heart Association.* Circulation, 2004. **109**(21): p. 2655-2671.

7. Lomnicki, S., et al., *Copper Oxide-Based Model of Persistent Free Radical Formation on Combustion-Derived Particulate Matter.* Environmental Science & Technology, 2008. **42**(13): p. 4982-4988.

8. Crone, T.J. and M. Tolstoy, *Magnitude of the 2010 Gulf of Mexico Oil Leak.* Science, 2010. **330**(6004): p. 634.

9. Ramseur, J.L., *Deepwater Horizon Oil Spill: The fate of Oil*, 2010, Congressional Research Service.

10. Owens, E.H., et al., *Tar ball frequency data and analytical results from a long-term beach monitoring program.* Marine Pollution Bulletin, 2002. **44**(8): p. 770-780.

11. Zambon, P., et al., *Sarcoma risk and dioxin emissions from incinerators and industrial plants: a population-based case-control study (Italy).* Environ Health, 2007. **6**(19).

12. Floret, N., et al., *A municipal solid waste incinerator as the single dominant point source of PCDD/Fs in an area of increased non-Hodgkin's lymphoma incidence.* Chemosphere, 2007. **68**(8): p. 1419-1426.

13. Sioutas, C., R.J. Delfino, and M. Singh, *Exposure assessment for atmospheric ultrafine particles (UFPs) and implications in epidemiologic research.* Environmental Health Perspectives, 2005. **113**(8): p. 947.

14. Ntziachristos, L., et al., *Relationship between redox activity and chemical speciation of size-fractionated particulate matter.* Part Fibre Toxicol, 2007. **4**(5).

15. Zhu, Y., et al., *Concentration and size distribution of ultrafine particles near a major highway.* Journal of the air & waste management association, 2002. **52**(9): p. 1032-1042.

16. Barmpadimos, I., et al., *One decade of parallel fine (PM 2.5) and coarse (PM 10–PM 2.5) particulate matter measurements in Europe: trends and variability.* Atmospheric Chemistry and Physics, 2012. **12**(7): p. 3189-3203.

17. Cusack, M., et al., *Trends of particulate matter (PM 2.5) and chemical composition at a regional background site in the Western Mediterranean over the last nine years (2002–2010).* Atmospheric Chemistry and Physics, 2012. **12**(18): p. 8341-8357.

18. Bølling, A.K., et al., *Health effects of residential wood smoke particles: the importance of combustion conditions and physicochemical particle properties.* Particle and fibre toxicology, 2009. **6**(29): p. 20.

19. Dellinger, B., et al., *Role of free radicals in the toxicity of airborne fine particulate matter.* Chemical Research in Toxicology, 2001. **14**(10): p. 1371-1377.

20. Dellinger, B., et al., *The role of combustion-generated radicals in the toxicity of PM2.5.* Proceedings of the Combustion Institute, 2000. **28**(2): p. 2675-2681.

21. Maskos, Z. and B. Dellinger, *Formation of the secondary radicals from the aging of tobacco smoke.* Energy & Fuels, 2007. **22**(1): p. 382-388.

22. Maskos, Z., L. Khachatryan, and B. Dellinger, *Formation of the persistent primary radicals from the pyrolysis of tobacco.* Energy & Fuels, 2008. **22**(2): p. 1027-1033.

23. Walsh, M., et al., *By-products of the Thermal Treatment of Hazardous Waste: Formation and Health Effects.* EM (Pittsburgh, Pa.), 2010: p. 26.

24. Lomnicki, S., H. Truong, and B. Dellinger, *Mechanisms of product formation from the pyrolytic thermal degradation of catechol.* Chemosphere, 2008. **73**(4): p. 629-633.

25. Truong, H., S. Lomnicki, and B. Dellinger, *Mechanisms of molecular product and persistent radical formation from the pyrolysis of hydroquinone.* Chemosphere, 2008. **71**(1): p. 107-113.

26. Taylor D, D. and C. Flagan R, *Aerosols from a Laboratory Pulverized Coal Combustor*, in *Atmospheric Aerosol*. 1981, AMERICAN CHEMICAL SOCIETY. p. 157-172.

27. Cormier, S.A., et al., *Origin and health impacts of emissions of toxic by-products and fine particles from combustion and thermal treatment of hazardous wastes and materials.* Environmental health perspectives, 2006. **114**(6): p. 810.

28. Altwicker, E.R., *Some laboratory experimental designs for obtaining dynamic property data on dioxins.* Science of The Total Environment, 1991. **104**(1–2): p. 47-72.

29. Gullett, B.K., P.M. Lemieux, and J.E. Dunn, *Role of combustion and sorbent parameters in prevention of polychlorinated dibenzo-p-dioxin and polychlorinated dibenzofuran formation during waste combustion.* Environmental Science & Technology, 1994. **28**(1): p. 107-118.

30. Olie, K., R. Addink, and M. Schoonenboom, *Metals as catalysts during the formation and decomposition of chlorinated dioxins and furans in incineration processes.* Journal of the Air & Waste Management Association, 1998. **48**(2): p. 101-105.

31. Cains, P.W., et al., *Polychlorinated dibenzo-p-dioxins and dibenzofurans formation in incineration: Effects of fly ash and carbon source.* Environmental science & technology, 1997. **31**(3): p. 776-785.

32. Addink, R. and K. Olie, *Mechanisms of formation and destruction of polychlorinated dibenzo-p-dioxins and dibenzofurans in heterogeneous systems.* Environmental science & technology, 1995. **29**(6): p. 1425-1435.

33. Gullett, B.K., A. Touati, and C.W. Lee, *Formation of Chlorinated Dioxins and Furans in a Hazardous-Waste-Firing Industrial Boiler.* Environmental Science & Technology, 2000. **34**(11): p. 2069-2074.

34. Sun, Q., et al., *Catalytic Effect of CuO and Other Transition Metal Oxides in Formation of Dioxins: Theoretical Investigation of Reaction Between 2,4,5-Trichlorophenol and CuO.* Environmental Science & Technology, 2007. **41**(16): p. 5708-5715.

35. Altarawneh, M., et al., *A first-principles density functional study of chlorophenol adsorption on CuO (110): CuO.* The Journal of chemical physics, 2009. **130**: p. 184505.

36. Dellinger, B., et al., *Formation and stabilization of persistent free radicals.* Proceedings of the Combustion Institute, 2007. **31**(1): p. 521-528.

37. Kodomari, M., H. Satoh, and S. Yoshitomi, *Selective halogenation of aromatic hydrocarbons with alumina-supported copper (II) halides.* The Journal of Organic Chemistry, 1988. **53**(9): p. 2093-2094.

38. McFerrin, C.A., R.W. Hall, and B. Dellinger, *Ab initio study of the formation and degradation reactions of semiquinone and phenoxyl radicals.* Journal of Molecular Structure: THEOCHEM, 2008. **848**(1–3): p. 16-23.

39. Patterson, M.C., et al., *EPFR formation from phenol adsorption on Al2O3 and TiO2: EPR and EELS studies.* Chemical Physics, (0).

40. Farquar, G.R., et al., *X-ray Spectroscopic Studies of the High Temperature Reduction of Cu(II)O by 2-Chlorophenol on a Simulated Fly Ash Surface.* Environmental Science & Technology, 2003. **37**(5): p. 931-935.

41. Alderman, S.L., et al., *Reaction of 2-chlorophenol with CuO: XANES and SEM analysis.* Proceedings of the Combustion Institute, 2005. **30**(1): p. 1255-1261.

42. Kobylecki, R.P., et al., *Dioxin and fly ash free incineration by ash pelletization and reburning.* Environmental science & technology, 2001. **35**(21): p. 4313-4319.

43. Stieglitz, L., et al., *On the de-novo synthesis of PCDD/PCDF on fly ash of municipal waste incinerators.* Chemosphere, 1989. **18**(1): p. 1219-1226.

44. Flagan, R.C. and J.H. Seinfeld, *Fundamentals of air pollution engineering*. 2012: DoverPublications. com.

45. Wei, Q., et al., *Effect of nanocrystalline and ultrafine grain sizes on the strain rate sensitivity and activation volume: fcc versus bcc metals.* Materials Science and Engineering: A, 2004. **381**(1): p. 71-79.

46. André, E., et al., *Inhalation of ultrafine carbon particles triggers biphasic pro-inflammatory response in the mouse lung.* European Respiratory Journal, 2006. **28**(2): p. 275-285.

47. Okeson, C.D., et al., *Impact of the composition of combustion generated fine particles on epithelial cell toxicity: influences of metals on metabolism.* Chemosphere, 2003. **51**(10): p. 1121-1128.

48. Allouis, C., F. Beretta, and A. D'Alessio, *Structure of inorganic and carbonaceous particles emitted from heavy oil combustion.* Chemosphere, 2003. **51**(10): p. 1091-1096.

49. Nielsen, M.T., et al., *Formation and emission of fine particles from two coal-fired power plants.* Combustion science and technology, 2002. **174**(2): p. 79-113.

50. Catallo, W.J., T.F. Shupe, and R.P. Gambrell, *Hydrothermal treatment of CCA-and penta-treated wood.* Wood and fiber science, 2004. **36**(2): p. 152-160.

51. Wasson, S.J., et al., *Emissions of chromium, copper, arsenic, and PCDDs/Fs from open burning of CCA-treated wood.* Environmental science & technology, 2005. **39**(22): p. 8865-8876.

52. Dreher, K.L., et al., *Soluble transition metals mediate residual oil fly ash induced acute lung injury.* Journal of Toxicology and Environmental Health Part A, 1997. **50**(3): p. 285-305.

53. Karamanov, A., et al., *Sintered glass-ceramics from incinerator fly ashes. Part II. The influence of the particle size and heat-treatment on the properties.* Journal of the European ceramic society, 2003. **23**(10): p. 1609-1615.

54. Ghio, A.J., *Metals associated with both the water-soluble and insoluble fractions of an ambient air pollution particle catalyze an oxidative stress.* Inhalation Toxicology, 1999. **11**(1): p. 37-49.

55. Makkonen, U., et al., *Size distribution and chemical composition of airborne particles in south-eastern Finland during different seasons and wildfire episodes in 2006.* Science of the Total Environment, 2010. **408**(3): p. 644-651.

56. Demuynck, M., et al., *Chemical analysis of airborne particulate matter during a period of unusually high pollution.* Atmospheric Environment (1967), 1976. **10**(1): p. 21-26.

57. Smith, K.R. and A.E. Aust, *Mobilization of iron from urban particulates leads to generation of reactive oxygen species in vitro and induction of ferritin synthesis in human lung epithelial cells.* Chemical research in toxicology, 1997. **10**(7): p. 828-834.

58. Mamane, Y., *Estimate of municipal refuse incinerator contribution to Philadelphia aerosol-I. Source analysis.* Atmospheric Environment (1967), 1988. **22**(11): p. 2411-2418.

59. Cyrys, J., et al., *Elemental composition and sources of fine and ultrafine ambient particles in Erfurt, Germany.* Science of the Total Environment, 2003. **305**(1): p. 143-156.

60. Hsiao, M.-C., H.P. Wang, and Y.-W. Yang, *EXAFS and XANES studies of copper in a solidified fly ash.* Environmental science & technology, 2001. **35**(12): p. 2532-2535.

61. Knözinger, H. and P. Ratnasamy, *Catalytic Aluminas: Surface Models and Characterization of Surface Sites.* Catalysis Reviews, 1978. **17**(1): p. 31-70.

62. Ertl, G. and H.-J. Freund, *Catalysis and Surface Science.* Physics Today, 1999. **52**(1): p. 32-38.

63. Sercombe, T.B. and G.B. Schaffer, *Rapid Manufacturing of Aluminum Components.* Science, 2003. **301**(5637): p. 1225-1227.

64. Brown, G.E., et al., *Metal Oxide Surfaces and Their Interactions with Aqueous Solutions and Microbial Organisms.* Chemical Reviews, 1998. **99**(1): p. 77-174.

65. Evans, L.J., *Chemistry of metal retention by soils.* Environmental Science & Technology, 1989. **23**(9): p. 1046-1056.

66. Matsui, Y., et al., *Virus Inactivation in Aluminum and Polyaluminum Coagulation.* Environmental Science & Technology, 2003. **37**(22): p. 5175-5180.

67. Hanning-Lee, M., et al., *Ozone decomposition on alumina: Implications for solid rocket motor exhaust.* Geophysical research letters, 1996. **23**(15): p. 1961-1964.

68. Denison, M., et al., *Solid rocket exhaust in the stratosphere-Plume diffusion and chemical reactions.* Journal of Spacecraft and Rockets, 1994. **31**(3): p. 435-442.

69. Cofer III, W., et al., *Space shuttle exhausted aluminum oxide: A measured particle size distribution.* Journal of Geophysical Research, 1991. **96**(D9): p. 17371-17,376.

70. Morterra, C. and G. Magnacca, *A case study: surface chemistry and surface structure of catalytic aluminas, as studied by vibrational spectroscopy of adsorbed species.* Catalysis Today, 1996. **27**(3): p. 497-532.

71. Ozin, G.A., S.A. Mitchell, and J. Garcia-Prieto, *Dioxygen activation by photoexcited copper atoms.* Journal of the American Chemical Society, 1983. **105**(21): p. 6399-6406.

72. Tevault, D., *Laser-induced emission spectrum of CuO in argon matrices.* The Journal of Chemical Physics, 1982. **76**: p. 2859.

73. Bondybey, V. and J. English, *Structure of copper oxide (CuO2) and its photochemistry in rare gas matrixes.* The Journal of Physical Chemistry, 1984. **88**(11): p. 2247-2250.

74. Howard, J., R. Sutcliffe, and B. Mile, *Cryochemical studies. Part 8. Electron spin resonance spectra of dioxygen complexes of Group IB metal atoms.* The Journal of Physical Chemistry, 1984. **88**(19): p. 4351-4354.

75. Kasai, P.H. and P.M. Jones, *Copper, silver, and gold atom-molecular oxygen complexes: matrix isolation ESR study.* The Journal of Physical Chemistry, 1986. **90**(18): p. 4239-4245.

76. Madhavan, P. and M. Newton, *Electronic states of CuO.* The Journal of chemical physics, 1985. **83**: p. 2337.

77. Hippe, D. and S. Peyerimhoff, *Theoretical spectroscopy of copper monoxide.* Molecular Physics, 1992. **76**(2): p. 293-318.

78. Deng, K., et al., *A theoretical study of the linear OCuO species.* The Journal of Chemical Physics, 1999. **111**(4): p. 1477-1482.

79. Igel, G., et al., *Cu and Ag as one-valence-electron atoms: Pseudopotential CI results for CuO and AgO.* The Journal of chemical physics, 1984. **81**: p. 2737.

80. Massobrio, C. and Y. Pouillon, *Structural properties of CuO and CuO clusters: A density functional study.* The Journal of chemical physics, 2003. **119**: p. 8305.

81. Jadraque, M. and M. Martín, *DFT calculations of clusters: Evidence for Cu 2 O building blocks.* Chemical Physics Letters, 2008. **456**(1): p. 51-54.

82. Ekuma, C., et al., *Electronic Structure and Spectra of CuO.* arXiv preprint arXiv:1305.6283, 2013.

83. Himmetoglu, B., R.M. Wentzcovitch, and M. Cococcioni, *First-principles study of electronic and structural properties of CuO.* Physical Review B, 2011. **84**(11): p. 115108.

84. Steimle, T.C. and Y. Azuma, *An intermodulated fluorescence study of the $A^2\Sigma^- - X^2\Pi_i$ band system of copper monoxide.* Journal of Molecular Spectroscopy, 1986. **118**(1): p. 237-247.

85. Huffman, G.P., et al., *Characterization of fine particulate matter produced by combustion of residual fuel oil.* Journal of the Air & Waste Management Association, 2000. **50**(7): p. 1106-1114.

86. Bae, G.-T., B. Dellinger, and R.W. Hall, *Density Functional Calculation of the Structure and Electronic Properties of CunOn (n = 1−8) Clusters.* The Journal of Physical Chemistry A, 2011. **115**(11): p. 2087-2095.

87. Polak, M.L., et al., *Photoelectron spectroscopy of copper oxide (CuO-).* The Journal of Physical Chemistry, 1991. **95**(9): p. 3460-3463.

88. dela Cruz, A.L.N., et al., *Detection of Environmentally Persistent Free Radicals at a Superfund Wood Treating Site.* Environmental Science & Technology, 2011. **45**(15): p. 6356-6365.

89. Cruz, A.L.N.d., et al., *Effect of Low Temperature Thermal Treatment on Soils Contaminated with Pentachlorophenol and Environmentally Persistent Free Radicals.* Environmental Science & Technology, 2012. **46**(11): p. 5971-5978.

90. Ingram, D., et al., *Paramagnetic resonance in carbonaceous solids.* 1954.

91. Jankovic, J., et al., *Measurement of short-lived reactive species and long-lived free radicals in air samples from structural fires.* Applied Occupational and Environmental Hygiene, 1993. **8**(7): p. 650-654.

92. Polewski, K., et al., *The effect of UV and visible light radiation on natural humic acid: EPR spectral and kinetic studies.* Geoderma, 2005. **126**(3): p. 291-299.

93. Rosa, A.H., et al., *Multimethod study of the degree of humification of humic substances extracted from different tropical soil profiles in Brazil's Amazonian region.* Geoderma, 2005. **127**(1): p. 1-10.

94. Christoforidis, K.C., S. Un, and Y. Deligiannakis, *High-field 285 GHz electron paramagnetic resonance study of indigenous radicals of humic acids.* The Journal of Physical Chemistry A, 2007. **111**(46): p. 11860-11866.

95. Jezierski, A., et al., *Electron paramagnetic resonance (EPR) and stable isotope records of paleoenvironmental conditions during peat formation.* Spectrochimica Acta Part A: Molecular and Biomolecular Spectroscopy, 2008. **69**(5): p. 1311-1316.

96. Oberdörster, G. and M.J. Utell, *Ultrafine particles in the urban air: to the respiratory tract--and beyond?* Environmental Health Perspectives, 2002. **110**(8): p. A440.

97. Lighty, J.S., J.M. Veranth, and A.F. Sarofim, *Combustion aerosols: factors governing their size and composition and implications to human health.* Journal of the Air & Waste Management Association, 2000. **50**(9): p. 1565-1618.

98. Kleeman, M.J., J.J. Schauer, and G.R. Cass, *Size and composition distribution of fine particulate matter emitted from motor vehicles.* Environmental science & technology, 2000. **34**(7): p. 1132-1142.

99. Linak, W.P., C.A. Miller, and J.O. Wendt, *Comparison of particle size distributions and elemental partitioning from the combustion of pulverized coal and residual fuel oil.* Journal of the Air & Waste Management Association, 2000. **50**(8): p. 1532-1544.

100. Kleeman, M.J., et al., *Source contributions to the size and composition distribution of atmospheric particles: Southern California in September 1996.* Environmental science & technology, 1999. **33**(23): p. 4331-4341.

101. Kleeman, M.J., J.J. Schauer, and G.R. Cass, *Size and composition distribution of fine particulate matter emitted from wood burning, meat charbroiling, and cigarettes.* Environmental Science & Technology, 1999. **33**(20): p. 3516-3523.

102. Dockery, D.W., et al., *An association between air pollution and mortality in six US cities.* New England journal of medicine, 1993. **329**(24): p. 1753-1759.

103. Krewski, D., et al., *Reanalysis of the Harvard Six Cities Study and the American Cancer Society Study of particulate air pollution and mortality.* Cambridge, MA: Health Effects Institute, 2000. **295**.

104. Pope III, C.A., et al., *Particulate air pollution as a predictor of mortality in a prospective study of US adults.* American journal of respiratory and critical care medicine, 1995. **151**(3_pt_1): p. 669-674.

105. Nel, A.E., D. Diaz-Sanchez, and N. Li, *The role of particulate pollutants in pulmonary inflammation and asthma: evidence for the involvement of organic chemicals and oxidative stress.* Current opinion in pulmonary medicine, 2001. **7**(1): p. 20-26.

106. Peters, A., et al., *Increased particulate air pollution and the triggering of myocardial infarction.* Circulation, 2001. **103**(23): p. 2810-2815.

107. Li, N., et al., *Ultrafine particulate pollutants induce oxidative stress and mitochondrial damage.* Environmental health perspectives, 2003. **111**(4): p. 455.

108. Brown, D.M., et al., *Size-dependent proinflammatory effects of ultrafine polystyrene particles: a role for surface area and oxidative stress in the enhanced activity of ultrafines.* Toxicology and applied pharmacology, 2001. **175**(3): p. 191-199.

109. Valavanidis, A., K. Fiotakis, and T. Vlachogianni, *Airborne particulate matter and human health: toxicological assessment and importance of size and composition of particles for oxidative damage and carcinogenic mechanisms.* Journal of Environmental Science and Health, Part C, 2008. **26**(4): p. 339-362.

110. Franck, U., et al., *Respiratory effects of indoor particles in young children are size dependent.* Science of the Total Environment, 2011. **409**(9): p. 1621-1631.

111. Oberdörster, G., *Pulmonary effects of inhaled ultrafine particles.* International archives of occupational and environmental health, 2000. **74**(1): p. 1-8.

112. Calderon-Garciduenas, L., et al., *Canines as sentinel species for assessing chronic exposures to air pollutants: part 1. Respiratory pathology.* Toxicological sciences, 2001. **61**(2): p. 342-355.

113. Calderon-Garciduenas, L., et al., *Canines as sentinel species for assessing chronic exposures to air pollutants: part 2. Cardiac pathology.* Toxicological Sciences, 2001. **61**(2): p. 356-367.

114. Nemmar, A., et al., *Passage of inhaled particles into the blood circulation in humans.* Circulation, 2002. **105**(4): p. 411-414.

115. Nemmar, A., et al., *Passage of intratracheally instilled ultrafine particles from the lung into the systemic circulation in hamster.* American journal of respiratory and critical care medicine, 2001. **164**(9): p. 1665-1668.

116. Von Klot, S., et al., *Increased asthma medication use in association with ambient fine and ultrafine particles.* European Respiratory Journal, 2002. **20**(3): p. 691-702.

117. Penttinen, P., et al., *Ultrafine particles in urban air and respiratory health among adult asthmatics.* European respiratory journal, 2001. **17**(3): p. 428-435.

118. Pope III, C.A., et al., *Respiratory health and PM10 pollution: a daily time series analysis.* American Review of Respiratory Disease, 1991. **144**(3_pt_1): p. 668-674.

119. Pope III, C.A. and D.W. Dockery, *Acute health effects of PM10 pollution on symptomatic and asymptomatic children.* American Review of Respiratory Disease, 1992. **145**(5): p. 1123-1128.

120. Roemer, W., G. Hoek, and B. Brunekreef, *Effect of ambient winter air pollution on respiratory health of children with chronic respiratory symptoms.* American review of respiratory disease, 1993. **147**(1): p. 118-124.

121. Penttinen, P., et al., *Number concentration and size of particles in urban air: effects on spirometric lung function in adult asthmatic subjects.* Environmental health perspectives, 2001. **109**(4): p. 319.

122. Martin, W.J., et al., *A major environmental cause of death.* Science, 2011. **334**(6053): p. 180-181.

123. Lopez, A.D., et al., *Global and regional burden of disease and risk factors, 2001: systematic analysis of population health data.* The Lancet, 2006. **367**(9524): p. 1747-1757.

124. Martens, D., et al., *Determination of pentachlorophenol (PCP) in samples of the environmental specimen bank using isotope dilution.* International journal of environmental analytical chemistry, 1997. **68**(4): p. 415-427.

125. Hamade, A.K., R. Rabold, and C.G. Tankersley, *Adverse cardiovascular effects with acute particulate matter and ozone exposures: interstrain variation in mice.* Environmental health perspectives, 2008. **116**(8): p. 1033.

126. Li, N., T. Xia, and A.E. Nel, *The role of oxidative stress in ambient particulate matter-induced lung diseases and its implications in the toxicity of engineered nanoparticles.* Free Radical Biology and Medicine, 2008. **44**(9): p. 1689-1699.

127. Kodavanti, U.P., et al., *The spontaneously hypertensive rat as a model of human cardiovascular disease: evidence of exacerbated cardiopulmonary injury and oxidative stress from inhaled emission particulate matter.* Toxicology and applied pharmacology, 2000. **164**(3): p. 250-263.

128. Ling, S.H. and S.F. van Eeden, *Particulate matter air pollution exposure: role in the development and exacerbation of chronic obstructive pulmonary disease.* International journal of chronic obstructive pulmonary disease, 2009. **4**: p. 233.

129. Hiraishi, H., et al., *Role for iron in reactive oxygen species-mediated cytotoxicity to cultured rat gastric mucosal cells.* American Journal of Physiology-Gastrointestinal and Liver Physiology, 1991. **260**(4): p. G556-G563.

130. Kumagai, Y., et al., *Generation of reactive oxygen species during interaction of diesel exhaust particle components with NADPH-cytochrome P450 reductase and involvement of the bioactivation in the DNA damage.* Free Radical Biology and Medicine, 1997. **22**(3): p. 479-487.

131. Saldiva, P.H., et al., *Lung inflammation induced by concentrated ambient air particles is related to particle composition.* American Journal of Respiratory and Critical Care Medicine, 2002. **165**(12): p. 1610-1617.

132. Dick, C.A., et al., *The role of free radicals in the toxic and inflammatory effects of four different ultrafine particle types.* Inhalation toxicology, 2003. **15**(1): p. 39-52.

133. Li, X.Y., et al., *Short-term inflammatory responses following intratracheal instillation of fine and ultrafine carbon black in rats.* Inhalation toxicology, 1999. **11**(8): p. 709-731.

134. Pryor, W.A., et al., *The radicals in cigarette tar: their nature and suggested physiological implications.* Science, 1983. **220**(4595): p. 425-427.

135. Pryor, W.A., et al., *Fractionation of aqueous cigarette tar extracts: fractions that contain the tar radical cause DNA damage.* Chemical research in toxicology, 1998. **11**(5): p. 441-448.

136. Hirakawa, K., et al., *Catechol and hydroquinone have different redox properties responsible for their differential DNA-damaging ability.* Chemical research in toxicology, 2002. **15**(1): p. 76-82.

137. Seike, K., et al., *Oxidative DNA damage induced by benz [a] anthracene metabolites via redox cycles of quinone and unique non-quinone.* Chemical research in toxicology, 2003. **16**(11): p. 1470-1476.

138. Squadrito, G.L., et al., *Quinoid redox cycling as a mechanism for sustained free radical generation by inhaled airborne particulate matter.* Free Radical Biology and Medicine, 2001. **31**(9): p. 1132-1138.

139. Donaldson, K., et al., *Oxidative stress and calcium signaling in the adverse effects of environmental particles (PM< sub> 10</sub>).* Free Radical Biology and Medicine, 2003. **34**(11): p. 1369-1382.

140. Li, Y. and M.A. Trush, *Reactive oxygen-dependent DNA damage resulting from the oxidation of phenolic compounds by a copper-redox cycle mechanism.* Cancer research, 1994. **54**(7 Supplement): p. 1895s-1898s.

141. Schweigert, N., et al., *DNA degradation by the mixture of copper and catechol is caused by DNA-copper-hydroperoxo complexes, probably DNA-Cu (I) OOH.* Environmental and molecular mutagenesis, 2000. **36**(1): p. 5-12.

142. Stone, K., et al., *The ESR properties, DNA nicking, and DNA association of aged solutions of catechol versus aqueous extracts of tar from cigarette smoke.* Archives of biochemistry and biophysics, 1995. **319**(1): p. 196-203.

143. Borish, E.T., et al., *Cigarette tar causes single-strand breaks in DNA.* Biochemical and biophysical research communications, 1985. **133**(2): p. 780-786.

144. Dellinger, B., et al., *Role of free radicals in the toxicity of airborne fine particulate matter.* Chemical Research in Toxicology, 2001. **14**: p. 1371-1377.

145. Kukier, U., et al., *Composition and element solubility of magnetic and non-magnetic fly ash fractions.* Environmental Pollution, 2003. **123**(2): p. 255-266.

146. Khachatryan, L., et al., *Environmentally Persistent Free Radicals (EPFRs). 1. Generation of Reactive Oxygen Species in Aqueous Solutions.* Environmental Science & Technology, 2011. **45**(19): p. 8559-8566.

147. Khachatryan, L. and B. Dellinger, *Environmentally Persistent Free Radicals (EPFRs)-2. Are Free Hydroxyl Radicals Generated in Aqueous Solutions?* Environmental Science & Technology, 2011. **45**(21): p. 9232-9239.

148. Pryor, W.A., *Oxy-radicals and related species: their formation, lifetimes, and reactions.* Annual Review of Physiology, 1986. **48**(1): p. 657-667.

149. Kohanski, M.A., et al., *A common mechanism of cellular death induced by bactericidal antibiotics.* Cell, 2007. **130**(5): p. 797-810.

150. Saravia, J., et al., *Particulate Matter Containing Environmentally Persistent Free Radicals and Adverse Infant Respiratory Health Effects: A Review.* Journal of biochemical and molecular toxicology, 2013. **27**(1): p. 56-68.

151. Knaapen, A., et al., *Soluble metals as well as the insoluble particle fraction are involved in cellular DNA damage induced by particulate matter.* Molecular and Cellular Biochemistry, 2002. **234-235**(1): p. 317-326.

152. Maskos, Z., L. Khachatryan, and B. Dellinger, *Precursors of Radicals in Tobacco Smoke and the Role of Particulate Matter in Forming and Stabilizing Radicals.* Energy & Fuels, 2005. **19**(6): p. 2466-2473.

153. Fahmy, B., et al., *In vitro and in vivo assessment of pulmonary risk associated with exposure to combustion generated fine particles.* Environmental Toxicology and Pharmacology.

154. Balakrishna, S., et al., *Environmentally persistent free radicals amplify ultrafine particle mediated cellular oxidative stress and cytotoxicity.* Part. Fibre Toxicol., 2009. **6**: p. 11.

155. Balakrishna, S., et al., *Resveratrol Ameliorates the Redox Imbalances in Human Airway Epithelial Cells Exposed to Combustion Generated Nanoparticles.* Free Radical Biology and Medicine, 2008. **45**: p. S44-S44.

156. Council, N.R., *Spills of Emulsified Fuels:Risks and Responses*. 2001: The National Academies Press.

157. ATSDR, *Light Crude Oil Information for Health professionals*, Center for Desease Control, Editor 2010.

158. Witham, R., *A review of some petroleum impacts on sea turtles.*, in *Proceedings of the Workshop on Cetaceans and Sea Turtles in the Gulf of Mexico: Study Planning for Effects of Outer Continental Shelf Development.* , C.E.K.a.J.K. Adams, Editor 1983.

159. Preda, M. and M.E. Cox, *Chemical and mineralogical composition of marine sediments, and relation to their source and transport, Gulf of Carpentaria, Northern Australia.* Journal of Marine Systems, 2005. **53**(1,Äì4): p. 169-186.

160. Macias-Zamora, J.V., et al., *Trace metals in sediment cores from the Campeche shelf, Gulf of Mexico.* Environmental Pollution, 1999. **104**(1): p. 69-77.

161. Vazquez, F.G. and V.K. Sharma, *Major and trace elements in sediments of the Campeche Sound, southeast Gulf of Mexico.* Marine Pollution Bulletin, 2004. **48**(1,Äì2): p. 87-90.

162. Lomnicki, S., et al., *A Copper Oxide-Based Model of Persistent Free Radical Formation on Combustion Derived Particulate Matter* Environmental Science & Technology, 2008. **42**(13): p. 4982-4988.

163. Vejerano, E., S. Lomnicki, and B. Dellinger, *Formation and Stabilization of Combustion-Generated Environmentally Persistent Free Radicals on an Fe(III)(2)O-3/Silica Surface.* Environmental Science & Technology, 2011. **45**(2): p. 589-594.

164. Guedes, C.L.B., et al., *EPR and Fluorescence Spectroscopy in the Photodegradation Study of Arabian and Colombian Crude Oils.* International Journal of Photoenergy, 2006. **2006**.

165. Montanari, L., et al., *Asphaltene radicals and their interaction with molecular oxygen: an EPR probe of their molecular characteristics and tendency to aggregate.* Applied Magnetic Resonance, 1998. **14**(1): p. 81-100.

166. Di Mauro, E., C.L.B. Guedes, and M.T. Piccinato, *EPR of Marine Diesel.* Applied Magnetic Resonance, 2007. **32**(3): p. 303-309.

167. Tagirzyanov, M., M. Yakubov, and G. Romanov, *A study of the processes related to coagulation of asphaltenes by electronic spin resonance.* Journal of Canadian Petroleum Technology, 2007. **46**(9).

168. MR, Y., *Stable Radicals in Heavy Pyrolyis Tar.* Petroleum Chemistry, 2003. **43**(4): p. 255-257.

169. Alderman, S.L., et al., *An Infrared and X-ray Spectroscopic Study of the Reactions of 2-Chlorophenol, 1,2-Dichlorobenzene, and Chlorobenzene with Model CuO/Silica Fly Ash Surfaces.* Environmental Science & Technology, 2005. **39**(19): p. 7396-7401.

170. Lomnicki, S. and B. Dellinger, *A Detailed Mechanism of the Surface-Mediated Formation of PCDD/F from the Oxidation of 2-Chlorophenol on a CuO/Silica Surface.* The Journal of Physical Chemistry A, 2003. **107**(22): p. 4387-4395.

171. Lomnicki, S. and B. Dellinger, *Formation of PCDD/F from the pyrolysis of 2-chlorophenol on the surface of dispersed copper oxide particles.* Proceedings of the Combustion Institute, 2002. **29**(2): p. 2463-2468.

172. Truong, H., S. Lomnicki, and B. Dellinger, *Potential for Misidentification of Environmentally Persistent Free Radicals as Molecular Pollutants in Particulate Matter.* Environmental Science & Technology, 2010. **44**(6): p. 1933-1939.

173. Hagenmaier, H., et al., *Catalytic effects of fly ash from waste incineration facilities on the formation and decomposition of polychlorinated dibenzo-p-dioxins and polychlorinated dibenzofurans.* Environmental Science & Technology, 1987. **21**(11): p. 1080-1084.

174. Zhou, X., et al., *Size-Dependent Catalytic Activity and Dynamics of Gold Nanoparticles at the Single-Molecule Level.* Journal of the American Chemical Society, 2009. **132**(1): p. 138-146.

175. Fine, P.M., G.R. Cass, and B.R. Simoneit, *Chemical characterization of fine particle emissions from fireplace combustion of woods grown in the northeastern United States.* Environmental Science & Technology, 2001. **35**(13): p. 2665-2675.

176. Bonte, J.L., et al., *Catalytic destruction of PCDD/F in a fabric filter: experience at a municipal waste incinerator in Belgium.* Waste Management, 2002. **22**(4): p. 421-426.

177. Blumenstock, M., et al., *Estimation of the dioxin emission (PCDD/FI-TEQ) from the concentration of low chlorinated aromatic compounds in the flue and stack gas of a hazardous waste incinerator.* Journal of Analytical and Applied Pyrolysis, 1999. **49**(1): p. 179-190.

178. Fine, P.M., G.R. Cass, and B.R. Simoneit, *Chemical characterization of fine particle emissions from the fireplace combustion of wood types grown in the Midwestern and Western United States.* Environmental Engineering Science, 2004. **21**(3): p. 387-409.

179. Hays, M.D., et al., *Open burning of agricultural biomass: physical and chemical properties of particle-phase emissions.* Atmospheric Environment, 2005. **39**(36): p. 6747-6764.

180. Sheesley, R.J., et al., *Characterization of organic aerosols emitted from the combustion of biomass indigenous to South Asia.* Journal of Geophysical Research, 2003. **108**(D9): p. 4285.

181. Puxbaum, H., et al., *Levoglucosan levels at background sites in Europe for assessing the impact of biomass combustion on the European aerosol background.* Journal of Geophysical Research: Atmospheres (1984–2012), 2007. **112**(D23).

CHAPTER 2 - THEORETICAL METHODS

The major objective of a theoretical calculation is to determine molecular properties such as geometry, total energy, and vibrational modes, through the application of a model-independent set of mathematical relations. Among the many approaches that exist for doing this, an *ab initio* calculation is the most popular. *Ab initio* (which means "from first principles") defines the fundamental building blocks of a molecule as consisting of electrons, nuclei, and electrostatic forces by which they interact. In *ab initio* chemistry, the mathematical relation that is used to describe the interactions is the Schrodinger equation, for which a wavefunction is found that forms the basis for calculating all properties of a molecule [2].

2.1 The solution of the Schrödinger Equation

In this thesis, we are primarily concerned with the calculation of the ground state energy of a collection of atoms computed by solution of the time independent, non-relativistic Schrödinger equation. The solution starts by invoking the Born-Oppenheimer approximation, which states that the motion of the electrons and the nuclei can be completely de-coupled [3, 4].

$$H\Psi = E\Psi \tag{2.1}$$

The Hamiltonian operator, H, consists of a sum of three terms; the kinetic energy, the interaction with the external potential (V_{ext}) and the electron-electron interaction (V_{ee}). That is;

$$H = -\frac{1}{2}\sum_{i}^{N}\nabla_i^2 + V_{ext} + \sum_{i<j}^{N}\frac{1}{|\mathbf{r}_i - \mathbf{r}_j|} \tag{2.2}$$

This approximation has been shown to be quite accurate under many practical conditions. As a result of this, the calculations is simplified to one that calculates the optimum wave function for electrons in the presence of seemingly static, but oppositely charged, nuclei. For systems of more than one electron, this wave function cannot be calculated exactly, and numerous approximation

methods have been developed. The most difficult challenge in developing these methods is to account for the instantaneous interactions between electrons, so-called "electron correlation." Models that do not include electron correlation cannot be relied upon for consistently accurate results, but are generally less computationally intensive compared to models that include it. An exception is the semiempirical method, which attempts to improve upon the non-correlated wavefunction by adding parameters that are optimized using experimentally obtained values for molecular structure, enthalpy, and other physical properties. Since it is based upon this parameterization, the semiempirical method can only be considered as good as the database of experimental observations that are used in this parameterization; semiempirical methods cannot be reliably extended to molecular structures that are fundamentally different than those in the database. However, one area where semiempirical has enjoyed considerable popularity is in the calculation of molecular structure, especially for large compounds of biological interest where more rigorous methods are not practical due to computational requirements.

2.2 Hartree-Fock Theory

The average total energy for a state specified by a particular Ψ is the expectation value of H, given by;

$$E[\Psi] = \int \Psi^* \hat{H} \Psi dr \equiv \left\langle \Psi \middle| \hat{H} \middle| \Psi \right\rangle \tag{2.3}$$

The notation $[\Psi]$ emphasizes the fact that energy is a functional of the wavefunction. The energy is higher than that of the ground state unless Ψ corresponds to Ψ_0 (ground state wavefunction), which is the variational theorem;

$$E[\Psi] \geq E_0 \tag{2.4}$$

The ground state wavefunction and energy is found by searching all possible wavefunctions for the one that minimizes the total energy. Hartree-Fock theory consists of an ansatz for the structure of Ψ which is assumed to be an antisymmetric product of functions (ϕ_i) each of which depends in the coordinates of a single electron, that is;

$$\Psi_{HF} = \frac{1}{\sqrt{N!}} \det[\phi_1 \phi_2 \phi_3 .... \phi_N] \tag{2.5}$$

where $\det$ indicates a matrix determinant [3]. Substitution of this ansatz for Ψ into the Schrödinger equation results in an expression for the Hartree Fock energy;

$$\begin{aligned} E_{HF} &= \int \phi_i^*(\mathbf{r}) \left(-\frac{1}{2} \sum_i^N \nabla_i^2 + V_{ext} \right) \phi_i(\mathbf{r}) d\mathbf{r} \\ &+ \frac{1}{2} \sum_{i,j}^N \int \frac{\phi_i^*(\mathbf{r}_1) \phi_i(\mathbf{r}_1) \phi_j^*(\mathbf{r}_2) \phi_j(\mathbf{r}_2)}{|r_i - r_j|} d\mathbf{r}_1 d\mathbf{r}_2 \\ &- \frac{1}{2} \sum_{i,j}^N \int \frac{\phi_i^*(\mathbf{r}_1) \phi_i(\mathbf{r}_1) \phi_i(\mathbf{r}_2) \phi_j^*(\mathbf{r}_2)}{|\mathbf{r}_i - \mathbf{r}_j|} d\mathbf{r}_1 d\mathbf{r}_2 \end{aligned} \tag{2.6}$$

The second term is the classical Coulomb energy written in terms of the orbitals and the third term is the *exchange* energy. The ground state orbitals are determined by applying the variation theorem to this energy expression under the constraint that the orbitals are orthonormal. This leads to the Hartree-Fock (or SCF) equations;

$$\left[-\frac{1}{2} \nabla^2 + v_{ext}(\mathbf{r}) + \int \frac{\rho(\mathbf{r})}{|\mathbf{r} - \mathbf{r}'|} d\mathbf{r}' \right] \phi_i(\mathbf{r}) + \int v_X(\mathbf{r}, \mathbf{r}') \phi_i(\mathbf{r}') d\mathbf{r}' = \varepsilon_i \phi_i(\mathbf{r}) \tag{2.7}$$

where the non-local exchange potential, v_X, is such that:

$$\int v_X(\mathbf{r}, \mathbf{r}') \phi_i(\mathbf{r}') d\mathbf{r}' = -\sum_j^N \int \frac{\phi_j(\mathbf{r}') \phi_j^*(\mathbf{r}')}{|\mathbf{r} - \mathbf{r}'|} \phi_i(\mathbf{r}') \, d\mathbf{r}' \tag{2.8}$$

The Hartree-Fock equations describe *non-interacting* electrons under the influence of a mean field potential consisting of the classical Coulomb potential and a *non-local* exchange potential.

2.3 Density Functional Theory

In addition to Hartree-Fock and semiempirical methods, density functional theory (DFT) is gaining prominence. This can be attributed to development of new and accurate functionals as well as increases in versatility, availability, and efficiency of the codes [5]. DFT replaces the role of the wavefunction with the electron density and it can be used to determine the ground state energy as well as density of interacting particles. DFT was first developed independently by Thomas and Fermi in the 1920's although it gained prominence in the sixties.

2.3.1 The Hohenburg-Kohn Theorems

In 1964 Hohenburg and Kohn demonstrated that the ground state energy of a set of interacting electrons in an external potential is a unique functional of their density [6, 7], that is,

$$E[\rho] = \int V(\mathbf{r})\rho \mathrm{d}\mathbf{r} + F[\rho] \tag{2.9}$$

where $E[\rho]$ is the Hohenberg-Kohn energy functional, $[\rho]$ is the single electron charge density, $V(\mathbf{r})$ is the external potential and F is the unique functional. The total charge density must integrate over all space to give the number of electrons in the system. Subject to this constraint, the charge density ρ_t that minimizes equation (2.9) must be the exact ground state density for the system and the value of the functional for this density gives the exact ground state energy. Unfortunately, the precise form of $F[\rho]$ is unknown and an approximation is made.

The ground state charge density is that density which satisfies,

$$\delta\left\lfloor E[\rho] - \mu\left(\int \rho(\mathbf{r})dr - N\right)\right\rfloor = 0 \tag{2.10}$$

where μ is the Lagrange multiplier which enforces the constraint that the total integrated density must be equal to the number of particles. The Schrödinger equation consists of three terms of

energy functionals; the kinetic energy, the interaction with the potential and the electron-electron interaction which is given as,

$$E[\rho] = T[\rho] + V_{ext}[\rho] + V_{ee}[\rho] \tag{2.11}$$

The interaction with the external potential is trivial and the other two functionals (kinetic and electron-electron) are unknown.

2.3.2 The Kohn-Sham Formulation

The method for approximating $F[\rho]$ was developed by Kohn-Sham [8] for which Walter Kohn was awarded the Nobel Prize in 1998. They separated $F[\rho]$ into three parts,

$$F[\rho] = T[\rho] + E_H[\rho] + E_{xc}[\rho] \tag{2.12}$$

where $T[\rho]$ is the kinetic energy of the non-interacting system, $E_H[\rho]$ is the Hartree energy (the Coulomb energy of the charge density $[\rho]$ reacting with itself), and $E_{xc}[\rho]$ is the exchange-correlation energy. Kohn and Sham introduced a fictitious system of N *non-interacting* electrons described by a single determinant wavefunction in N orbitals ϕ_i [8].

$$\rho(\mathbf{r}) = \sum_i^N |\phi_i|^2 \tag{2.13}$$

This gives the kinetic energy and electron density as,

$$T_s[\rho] = -\frac{1}{2}\sum_i^N \langle \phi_i | \nabla^2 | \phi_i \rangle \tag{2.14}$$

However, this is not the true kinetic energy of the *interacting* system but the kinetic energy of a system of *non-interacting* electrons which reproduce the true ground state density. The difference between this energy and the true kinetic energy has been moved into the exchange-correlation energy. The density is constructed explicitly from a set of orbitals and is expressed as;

$$V_H[\rho] = \frac{1}{2}\int \frac{\rho(\mathbf{r}_1)\rho(\mathbf{r}_2)}{|\mathbf{r}_1 - \mathbf{r}_2|} d\mathbf{r}_1 d\mathbf{r}_2 \tag{2.15}$$

The energy functional is finally rearranged as;

$$E[\rho] = T_s[\rho] + V_{ext}[\rho] + V_H[\rho] + E_{xc}[\rho] \tag{2.16}$$

The exchange-correlational functional (E_{xc}) is the sum of the error made in using a non-interacting kinetic energy and the error made in treating the electron-electron interaction classically. Equation 2.16 may be expressed explicitly in terms of the density built from non-interacting orbitals (Equation 2.14) and upon applying the variational principle results in the following equation;

$$\left[-\frac{1}{2}\nabla^2 + v_{ext}(\mathbf{r}) + \int \frac{\rho(\mathbf{r}')}{|\mathbf{r} - \mathbf{r}'|} d\mathbf{r}' + v_{xc}(\mathbf{r})\right]\phi_i(\mathbf{r}) = \varepsilon_i \phi_i(\mathbf{r}) \tag{2.17}$$

where v_{xc} is expressed as;

$$v_{xc}(\mathbf{r}) = \frac{\delta E_{xc}[\rho]}{\delta \rho} \tag{2.18}$$

The computational cost of solving Kohn-Sham equation scales formally as N^3. The exact correspondence of the density and ground state energy of a system consisting of non-interacting Fermions and the "real" many body system as described by the Schrödinger equation is achieved by the Kohn-Sham approach. The approximations to DFT are also referred to as *ab initio* as they will involve excellent approximations to the universal functional to be developed and used in unbiased and thus predict studies of a wide range of materials [2].

The density function approach is inherently more efficient since it includes electron correlation. However, it has been shown to produce results that are comparable to high-level wave function-based *ab initio* methods, but requiring fewer computational resources. In practice,

the utility of the theory hinges on the approximations used for $E_{XC}[\rho]$ and major efforts have been made and continue to be expended in the construction of more useful approximations for this fundamental quantity.

2.3.3 The Local Density Approximation (LDA) method

Local density approximation is used where charge density is slowly varying and the exchange-correlation energy of an electronic system is constructed by assuming the exchange-correlation energy per electron at a point $\mathbf{r}$ in the electron gas [9]. In this case E_{XC} is given by,

$$E_{xc}^{LDA}[\rho] = \int \rho(\mathbf{r})\varepsilon_{xc}(\rho)d\mathbf{r} \qquad (2.19)$$

where $\varepsilon_{XC}(\rho)$ is the exchange plus correlation energy per electron in a homogenous electron gas with electron density ρ. In LDA, the exchange-correlation energy at any given point depends only on the electron density at that point.

2.3.4 The Generalized Gradient Approximation

Generalized gradient approximation (GGA) is amongst the successful functional which attempts to improve the LDA functional. GGA includes the so-called PW91 scheme of Perdew and Wang [10, 11], and the PBE scheme of Perdew, Burke and Ernzerhof [12]. The exchange-correlation energy in GGA scheme includes the gradient of the density to the LDA scheme,

$$E_{xc} \approx \int \rho(\mathbf{r})\varepsilon_{xc}(\rho,\nabla\rho)d\mathbf{r} \qquad . (2.20)$$

The GGA improves significantly on total energies, atomization energies, and structural energy differences.

2.3.5 Hybrid Exchange Functionals

An exact connection approach between the non-interacting density functional system and the fully interacting many-body system is formally written as,

$$E_{xc}[\rho] = \frac{1}{2} d\vec{\mathbf{r}} d\vec{\mathbf{r}}' \int_{\lambda=0}^{1} d\lambda \frac{\lambda e^2}{|\vec{\mathbf{r}} - \vec{\mathbf{r}}'|} \left[< \rho(\vec{\mathbf{r}}) \rho(\vec{\mathbf{r}}') >_{\rho,\lambda} - \rho(\vec{\mathbf{r}}) \rho(\vec{\mathbf{r}} - \vec{\mathbf{r}}') \right] \quad .(2.21)$$

where the expectation value $<...>_{\lambda,\rho}$ is the density-density correlation function and is computed at density $\rho(\mathbf{r})$ for a system described by the effective potential;

$$V_{eff} = V_{en} + \frac{1}{2} \sum_{i \neq j} \frac{\lambda e^2}{|\vec{\mathbf{r}}_\mathbf{i} - \vec{\mathbf{r}}'_\mathbf{j}|} \quad (2.22)$$

The exact energy can be computed if the variation density-density correlation function with the coupling constant, λ is known. An approximation of the integral over the λ as weighted sum may be set, with the coefficients determined by reference to a system for which exact result is known.

$$E_{xc} \approx a E_{Fock} + b E_{xc}^{GGA} \quad (2.23)$$

The resultant (three parameter) energy functional is,

$$E_{xc} = E_{xc}^{LDA} + 0.2\left(E_X^{Fock} - E_X^{LDA}\right) + 0.72 \Delta E_X^{B88} + 0.81 \Delta_c^{PW91} \quad (2.24)$$

Here ΔE_X^{B88} and ΔE_c^{PW91} are widely used GGA corrections [13-15] to the LDA exchange and correlation energies respectively. B3LYP has had considerable success in the calculation of the structure and energies of compounds similar to those in the current study. It's parameterization is as given as in equation 2.24 but with a different GGA treatment of correlation [16].

2.4 Basis Set

A basis set is a set of mathematical functions (basis functions), linear combinations of which yield molecular orbitals [2, 7]. The functions are usually centered on atomic nuclei. An individual molecular orbital is denoted by,

$$\phi_i = \sum_{\mu-1}^{N} c_{\mu i} \chi_\mu \quad (2.25)$$

Where ϕ_i is the i–th molecular orbital, $C_{\mu i}$ are the coefficients of linear combination, χ_μ is the μ–th atomic orbital, and N is the number of atomic orbitals. The Slater Type Orbitals (STO) were commonly used for atomic Hartree-Fock calculations. These are described by,

$$\phi_i(\zeta,n,l,m,r,\theta,\phi) = Nr^{n-1}e^{-\zeta r}Y_l^m(\theta,\phi) \tag{2.26}$$

where N is the normalization constant and ζ is called the orbital exponent. The parameters r, θ, and ϕ are the spherical coordinates and Y_l^m is the angular momentum part. The n, l, and m are quantum numbers: principal, angular momentum, and magnetic, respectively. The disadvantage with such functions are that they cannot be evaluated fast enough for efficient molecular integral evaluation. This led to Boys proposing the Gaussian-type orbitals (GTFs) for the atomic orbitals in an LCAO wave function. The GTFs are significantly simpler functions as r is squared, and are also called Gaussian primitives or Cartesian Gaussian;

$$g_{ijk} = Nx_b^i y_b^k z_b^k e^{-\alpha r_b^2} \tag{2.27}$$

where N is a normalization constant, i, j, and k are non-negative integers, α is a positive orbital exponent, and x_b, y_b, z_b are Cartesian coordinates with the origin at nucleus b. The Cartesian-Gaussian normalization constant is given by,

$$N = \left(\frac{2\alpha}{\pi}\right)^{3/4}\left[\frac{(8\alpha)^{i+j+k}\,i!\,j!\,k!}{(2i)!(2j)!(2k)!}\right]^{1/2} \tag{2.28}$$

Here the sum of exponents at Cartesian coordinates, $L = i + j + k$, is used analogously to the angular momentum quantum number for atoms, to mark functions as s-type (L=0), p-type (L=1), d-type (L=2) etc [7]. Although Gaussian functions are efficient and rapid enough to calculate two-electron integral, they do not represent the optimum basis functions as they have functions that are different from the known functional behavior of molecular orbitals [4].

Fortunately, this problem can be solved by fixing linear combinations of the primitive Gaussian function. These linear combinations, called contractions lead to contracted Gaussian-type function (CGTF),

$$\chi_r = \sum_u d_{ur} g_u \qquad (2.29)$$

where the g_u's are normalized Cartesian Gaussian (equation 2.29) centered on the same atom

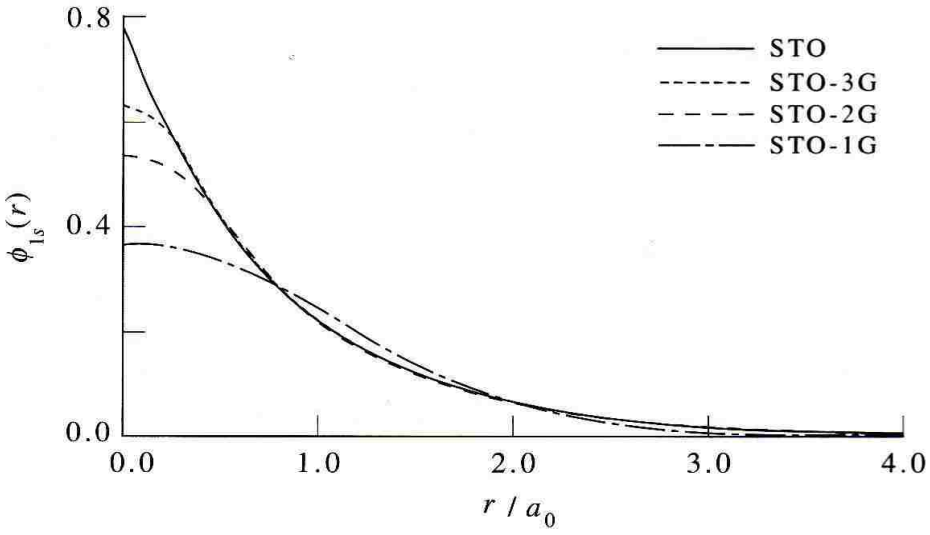

Figure 2.1 Comparison of the quality of the least-square fit of a 1s Slater function (ζ=1.0) obtained at the STO, STO-1G, STO-2G, and STO-3G levels.

and having the same i, j, k values as one another, but different α's. d_{ur} is the contraction coefficient and χ_r is the contracted Gaussian-type function (CGTF) [2].

In a single zeta (SZ), only one basis function (contraction) per Slater atomic orbital is used. The SZ set consists of one STO for each inner-shell and valence-shell AO of each atom. A double-zeta (DZ) basis set consist of two basis function that differ in their orbital exponents ζ (zeta), and a triple-zeta basis set that replaces each STO of a minimal basis set by 3-STOs that differ in their orbital exponents.

The split-valence basis set uses more contractions for each valence AO than core orbitals. The polarization functions are known to reproduce chemical bonding. They are usually added as uncontracted Gaussians. Higher angular momentum functions improves the description for anisotropic electron distribution. Here, p orbitals are added to hydrogen and helium atoms, d orbitals to first-row atoms, f orbitals to second-row atoms and so on. The augmented basis set are called diffuse functions [4]. These Gaussians have very small exponents and decay slowly with distance from the nucleus. They are used in systems with anions and hydrogen-bonded dimers as they possess a significant amount of electron density at a great distance from the nucleus.

2.4.1 Choice of a suitable functional for Copper oxide clusters

We used a series of DFT functionals and basis set to assess the ability of DFT. Specifically, the most popular and extensive hybrid GGA-B3LYP [5, 13, 16-19], hybrid GGA-PBE1PBE, and the recently developed meta-hybrid-GGA M06 [20, 21] were selected and applied in combination with LANL2DZ [22-24] and GEN (LANL2DZ for metals and aug-cc-pVDZ [25] for non-metals) basis sets. The B3LYP and PBE1PBE functionals have been parameterized to provide reliable structural parameters and energies for systems containing

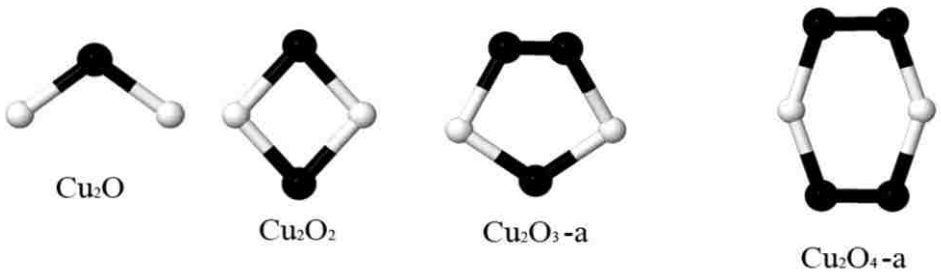

Figure 2.2 Lowest energy clusters for Cu_2O_n, n = 1−4. Different basis sets give different lowest energy isomers for n = 3 and 4.

transition metals [26-31]. In case of M06 functional, parameterization with training sets containing both metals and non-metals have been shown to provide reliable results for TM

containing systems [20]. While both B3LYP and PBE1PBE have the same percentage of exact Hartree-Fock exchange of 20%, M06 includes a higher portion (27%) of exact exchange. B3LYP has proved to be successful in assigning the bond lengths, ionization energies, and electron affinities (in comparison to experiment) of Cu systems [32]. Because our criterion for functional selection is to reproduce the experimental data, we first optimized known small CuO clusters with the three DFT functionals.

A comparison of the calculated (adiabatic) and experimental electron affinities are shown in Table 2.1. B3LYP and PBE1PBE have similar electron affinities, but M06 predicts a much higher energies. These differences are due to the fact that percentage of the exact Hartree-Fock exchange in M06 is larger than that of B3LYP and PBE1PBE. All our methods shows a good agreement with the experimental value and were used for copper oxide reactions with phenol, *o*-chlorophenol, and *p*-chlorophenol.

Table 2.1 Electron Affinity comparing different functionals and basis set with experimental values.

electron affinities (eV)				
	Cu_2O	Cu_2O_2	Cu_2O_3	Cu_2O_4
B3LYP/GEN	1.15	2.34	3.21	3.24
PBE1PBE/GEN	1.00	2.23	3.57	3.15
M06/GEN	1.02	2.42	3.78	3.29
B3LYP/LANL2DZ [33]	1.15	2.12	3.25	3.54
PBE1PBE/LANL2DZ	0.99	2.36	3.54	3.54
M06/LANL2DZ	1.08	2.55	3.77	3.62
WWD [34]	1.10	2.12	3.03	2.94
EXP [34]	1.10	2.46	3.54	3.50

2.4.2 Choice of a suitable functional for Aluminum Oxide clusters

Figure 2.3 shows the aluminum oxide structures that were studied in order to calibrate the basis sets. Preliminary studies were done using 6-31G* [35, 36], 6-31++G** [37-40], 6-311G**, 6-311++G** [39, 40], aug-cc-PVDZ [25], and DGDZVP [41, 42] basis set in order to choose the

best basis set for aluminum oxide clusters. A comparison of the electron affinities with the experimental values were made. 6-31G* consists of six 3d functions per atom: $3d_{xx}$, $3d_{yy}$, $3d_{zz}$, $3d_{xy}$, $3d_{xy}$, and $3d_{zx}$. These are Cartesian Gaussian which are a linear combination of the usual five 3d functions: $3d_{xy}$, $3d_{x^2-y^2}$, $3d_{zx}$, $3d_{z^2}$, and 3s function ($x^2+y^2+z^2$), including polarization

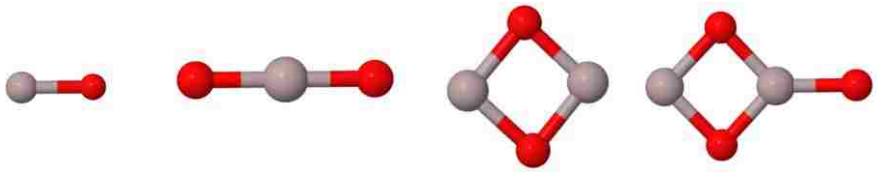

Figure 2.3 Lowest energy clusters for AlO, AlO_2, Al_2O_2, and Al_2O_3.
Aluminum/oxygen atoms are colored grey/red.

functions. Asterisk donates polarization, and 2 asterisks indicate that polarization is also added to light atoms such as hydrogen and helium [2]. A plus sign (+) is used to denote diffuse functions, which are expected to be more accurate for anions. Two plus (++) signs indicates that diffuse functions are also added to light atoms (hydrogen and helium).

DGDZVP basis sets are denoted by double-zeta valence plus polarization (DZVP) in DGauss. A comparison of the calculated and experimental electron affinities are shown in Table 2.2. The best agreement between calculated and experimental data [1] is found with the 6-311+G* basis set which is expected to be more accurate for anions. Based on the agreement with experimental electron affinities and the success of this model chemistry in previous study [1], the 6-311+G* was used in the remainder of this work.

Table 2.2 Electronic affinity comparing basis sets with experimental data.

	AlO	AlO_2	Al_2O_2	Al_2O_3
6-31G**	2.21	3.21	2.06	2.98
6-311+G*	2.55	4.02	2.32	3.41
6-31++G**	2.55	4.00	2.30	3.39
6-311G**	2.22	3.40	2.10	3.11
aug-cc-pVDZ	2.56	3.93	2.30	2.33
DGDZVP	2.36	3.80	2.23	2.33
EXP [1]	2.60	4.23	1.88	3.71

2.5 References

1. Desai, S.R., et al., *A study of the structure and bonding of small aluminum oxide clusters by photoelectron spectroscopy: AlO (x= 1–2, y= 1–5).* The Journal of chemical physics, 1997. **106**: p. 1309.

2. Lewars, E., *Introduction to the Theory and Application of Molecular and Quantum Mechanics*. 2003, Massachusetts: Kluwer Academic Publishers.

3. Szabo, A. and N.S. Ostlund, *Modern Quantum Chemistry: Introducton to Advanced Electronic Structure Theory*. 1996, New York: McGraw-Hill.

4. Hinchliffe, A., *Molecular Modelling for Beginners*. 2003, Chichester: John Wiley & Sons Ltd.

5. Stephens, P.J., et al., *Ab Initio Calculation of Vibrational Absorption and Circular Dichroism Spectra Using Density Functional Force Fields.* The Journal of Physical Chemistry, 1994. **98**(45): p. 11623-11627.

6. Hohenberg, P. and W. Kohn, *Inhomogeneous Electron Gas.* Physical Review, 1964. **136**(3B): p. B864-B871.

7. Foresman, J.B. and A. Frisch, *Exploring Chemistry with Electronic Structure Methods*. 1996, Pittsburgh: Gaussian, Inc.

8. Kohn, W. and L.J. Sham, *Self-Consistent Equations Including Exchange and Correlation Effects.* Physical Review, 1965. **140**(4A): p. A1133-A1138.

9. Perdew, J.P. and A. Zunger, *Self-interaction correction to density-functional approximations for many-electron systems.* Physical Review B, 1981. **23**(10): p. 5048-5079.

10. Perdew, J.P., K. Burke, and M. Ernzerhof, *Generalized Gradient Approximation Made Simple.* Physical Review Letters, 1996. **77**(18): p. 3865-3868.

11. Perdew, J.P. and Y. Wang, *Accurate and simple analytic representation of the electron-gas correlation energy.* Physical Review B, 1992. **45**(23): p. 13244-13249.

12. Perdew, J.P., K. Burke, and Y. Wang, *Generalized gradient approximation for the exchange-correlation hole of a many-electron system.* Physical Review B, 1996. **54**(23): p. 16533-16539.

13. Becke, A.D., *A new mixing of Hartree--Fock and local density-functional theories.* The Journal of Chemical Physics, 1993. **98**(2): p. 1372-1377.

14. Becke, A.D., *Correlation energy of an inhomogeneous electron gas: A coordinate-space model.* The Journal of Chemical Physics, 1988. **88**(2): p. 1053-1062.

15. Becke, A.D., *A multicenter numerical integration scheme for polyatomic molecules.* The Journal of Chemical Physics, 1988. **88**(4): p. 2547-2553.

16. Lee, C., W. Yang, and R.G. Parr, *Development of the Colle-Salvetti correlation-energy formula into a functional of the electron density.* Physical Review B, 1988. **37**(2): p. 785-789.

17. Becke, A.D., *Density-functional thermochemistry. III. The role of exact exchange.* The Journal of Chemical Physics, 1993. **98**(7): p. 5648-5652.

18. Handy, N.C. and A.J. Cohen, *Left-right correlation energy.* Molecular Physics, 2001. **99**(5): p. 403-412.

19. Vosko, S.H., L. Wilk, and M. Nusair, *Accurate spin-dependent electron liquid correlation energies for local spin density calculations: a critical analysis.* Canadian Journal of Physics, 1980. **58**(8): p. 1200-1211.

20. Zhao, Y. and D.G. Truhlar, *Density Functionals with Broad Applicability in Chemistry.* Accounts of Chemical Research, 2008. **41**(2): p. 157-167.

21. Zhao, Y. and D. Truhlar, *The M06 suite of density functionals for main group thermochemistry, thermochemical kinetics, noncovalent interactions, excited states, and transition elements: two new functionals and systematic testing of four M06-class*

functionals and 12 other functionals. Theoretical Chemistry Accounts, 2008. **120**(1-3): p. 215-241.

22. Hay, P.J. and W.R. Wadt, *Ab initio effective core potentials for molecular calculations. Potentials for the transition metal atoms Sc to Hg.* The Journal of Chemical Physics, 1985. **82**(1): p. 270-283.

23. Wadt, W.R. and P.J. Hay, *Ab initio effective core potentials for molecular calculations. Potentials for main group elements Na to Bi.* The Journal of Chemical Physics, 1985. **82**(1): p. 284-298.

24. Hay, P.J. and W.R. Wadt, *Ab initio effective core potentials for molecular calculations. Potentials for K to Au including the outermost core orbitals.* The Journal of Chemical Physics, 1985. **82**(1): p. 299-310.

25. Dunning, J.T.H., *Gaussian basis sets for use in correlated molecular calculations. I. The atoms boron through neon and hydrogen.* The Journal of Chemical Physics, 1989. **90**(2): p. 1007-1023.

26. Bühl, M. and H. Kabrede, *Geometries of Transition-Metal Complexes from Density-Functional Theory.* Journal of Chemical Theory and Computation, 2006. **2**(5): p. 1282-1290.

27. Furche, F. and J.P. Perdew, *The performance of semilocal and hybrid density functionals in 3d transition-metal chemistry.* The Journal of Chemical Physics, 2006. **124**(4): p. 044103-27.

28. Dai, B., K. Deng, and J. Yang, *A theoretical study of the Y4O cluster.* Chemical Physics Letters, 2002. **364**(1–2): p. 188-195.

29. Okumura, M., et al., *DFT studies of interaction between O2 and Au clusters. The role of anionic surface Au atoms on Au clusters for catalyzed oxygenation.* Chemical Physics Letters, 2001. **346**(1–2): p. 163-168.

30. Mukhopadhyay, S., et al., *Theoretical study of small clusters of indium oxide: InO.* Journal of Molecular Structure: THEOCHEM, 2010. **948**(1–3): p. 31-35.

31. David Jeba Singh, D.M., et al., *Closed-Cage Tungsten Oxide Clusters in the Gas Phase.* The Journal of Physical Chemistry A, 2010. **114**(17): p. 5445-5452.

32. Wang, M.Y. and Z.J. Wu, *Electronic Structures of 3d-Metal Monolithides.* Journal of Cluster Science, 2005. **16**(4): p. 547-558.

33. Bae, G.-T., B. Dellinger, and R.W. Hall, *Density Functional Calculation of the Structure and Electronic Properties of CunOn (n = 1−8) Clusters.* The Journal of Physical Chemistry A, 2011. **115**(11): p. 2087-2095.

34. Wang, L.-S., et al., *Electronic structure of small copper oxide clusters: From Cu_{2}O to Cu_{2}O_{4}.* Physical Review B, 1996. **53**(12): p. 8028-8031.

35. Francl, M.M., et al., *Self-consistent molecular orbital methods. XXIII. A polarization-type basis set for second-row elements.* The Journal of Chemical Physics, 1982. **77**(7): p. 3654-3665.

36. Rassolov, V.A., et al., *6-31G* basis set for atoms K through Zn.* The Journal of Chemical Physics, 1998. **109**(4): p. 1223-1229.

37. Hehre, W.J., R. Ditchfield, and J.A. Pople, *Self-Consistent Molecular Orbital Methods. XII. Further Extensions of Gaussian---Type Basis Sets for Use in Molecular Orbital Studies of Organic Molecules.* The Journal of Chemical Physics, 1972. **56**(5): p. 2257-2261.

38. Dill, J.D. and J.A. Pople, *Self-consistent molecular orbital methods. XV. Extended Gaussian-type basis sets for lithium, beryllium, and boron.* The Journal of Chemical Physics, 1975. **62**(7): p. 2921-2923.

39. Clark, T., et al., *Efficient diffuse function-augmented basis sets for anion calculations. III. The 3-21+G basis set for first-row elements, Li–F.* Journal of Computational Chemistry, 1983. **4**(3): p. 294-301.

40. Krishnan, R., et al., *Self-consistent molecular orbital methods. XX. A basis set for correlated wave functions.* The Journal of Chemical Physics, 1980. **72**(1): p. 650-654.

41. Godbout, N., et al., *Optimization of Gaussian-type basis sets for local spin density functional calculations. Part I. Boron through neon, optimization technique and validation.* Canadian Journal of Chemistry, 1992. **70**(2): p. 560-571.

42. Sosa, C., et al., *A local density functional study of the structure and vibrational frequencies of molecular transition-metal compounds.* The Journal of Physical Chemistry, 1992. **96**(16): p. 6630-6636.

CHAPTER 3 - EXPERIMENTAL

3.1 Tar Balls Site Sampling

The tar balls used for this study were collected from the Gulf of Mexico shores at four different times after the Deep Horizon (DH) oil spill. The DH incident of April 20, 2010 resulted in 4.4 - 4.9 x 10^6 barrels of crude oil being released into the waters of the Gulf of Mexico [1]. Particularly affected were the shores of Louisiana, Mississippi, Alabama, and Florida [2]. The samples were labeled as TB_0, TB_{60}, TB_{90}, and TB_{450}, the subscript representing the number of days from the incident when collected (cf. Table 3.1).

Table 3.1 Tar ball samples, collection location, and designation.

Sample designation	Collection Location	Collection date	# of Days since DH incident	Post ageing in air	# of days Post-aged
TB_0	Gulf shores, Al	05/01/2010	12	--	
TB_{60}	Gulf shores, Al	06/15/2010	56	--	
TB_{90}	Gulf shores, Al	07/21/2010	92	--	
TB_{450}	Pensacola Beach, Fl	07/14/2011	450	--	
$TBA1_{60}$	Gulf shores, Al	06/15/2010	56	yes	232
$TBA2_{60}$	Gulf shores, Al	06/15/2010	56	yes	409
$TBA1_{90}$	Gulf shores, Al	07/21/2010	92	yes	196
$TBA2_{90}$	Gulf shores, Al	07/21/2010	92	yes	373

Each sample was analyzed primarily for the presence of paramagnetic signal, either from metal centers or organic radicals using electron paramagnetic resonance (EPR) spectroscopy without prior treatment. In order to study the origin of the components of complex paramagnetic

signals, tar ball samples were extracted from the matrix using polar and non-polar solvents, *iso*propyl alcohol and *tert*-butyl benzene, respectively. A small quantity of each sample was placed in extracting vials and sonicated with 2 mL of solvent for 1 h. The extract and the residue were separated by centrifuging for 10 min, upon which the solids were dried in the oven for 2 h at 37 ^{0}C. The liquid part was introduced into capillary tubes, sealed with critoseal and then placed in high purity quartz EPR tube for EPR analysis.

3.2 Metals Analysis of Tar ball Samples

The metal content of the four tar ball samples from the shores of Louisiana, Mississippi, Alabama, and Florida was determined using Inductively Coupled Plasma Atomic Emission Spectroscopy (ICP-AES). The samples were digested in a cocktail mixture of acids; 3mL 70% HNO3, 3mL 35% HCl, and 4mL 50% HF acid. Approximately, 0.1 g of each tar ball sample was digested by placing it in a conical plastic centrifuge tube and then added 10.0 mL of the cocktail mixture. The digestion was done in the CEM Mars 5 Microwave Reaction system. The system was programmed to ramp to 400 W over 5 minutes and then to hold for 10 minutes. The system program was ran two times. The samples were then submitted for metal analyses by ICP-AES, particularly transition metals that included Fe, Cu, V, Mn, as well as heavy metals like Pb.

3.3 Surface-Associated Radical Matrix Preparation

Flyash from combustion system is characterized by a various amounts of components such as silica, alumina and transition metals (Cu and Fe) which are catalytically and highly redox-active [3, 4]. Due to these properties, the components are expected to induce the formation of environmentally persistent free radicals (EPFRs) through adsorption of substituted aromatic molecular precursors on the surface of metal oxide particles at cool zone conditions. Different concentrations of copper oxides were used to facilitate in the formation of EPFRs. Cab-OSil

which was purchased from CABOT Corporation is a high purity, fumed silica (SiO_2) powder (>99.8%) with high surface area (380 m^2/g, EH-5) and a particle size of about 0.1 μm. Cab-O-Sil was used as the supporting matrix for the copper oxide particles.

3.4 Preparation of Cu(II)O Nanoparticles

Flyash "surrogates" were prepared to mimic a real environmental flyash by adsorbing transition metals on silica powder (Cab-O-Sil) as a substrate [5, 6]. Particulate matter samples of copper oxide were supported on silica through incipient wetness with different copper loading (0.25, 0.5, 0.75, 1, 2, and 3%) on mass basis [7]. The first step in this preparation was to determine the amount of water needed to achieve incipient wetness for a given amount of silica. Incipient wetness is the term used when the water added to the silica is either contained within the pore structure and/or bound to adsorption sites on the surface, i.e. no bulk water is present. In this method, metal clusters adsorbed on the surface have a large size distribution which resembles the metal distribution in fly ash. Once the correct volume of water had been determined, an aqueous solution of copper(II) nitrate hemipentahydrate ($Cu(NO_3)_2 \cdot 2.5H_2O$, 99+%) purchased from Sigma Aldrich, of the concentration necessary to yield 0.25, 0.5, 0.75, 1, 2, and 3% Cu in the CuO/silica substrate were mixed with the correct amount of silica powder. For instance, 0.60 g ($Cu(NO_3)_2 \cdot 2.5H_2O$) requires 10.0 g of silica to yield 2% Cu(II)O/silica. The mixture was stirred occasionally for 2 h and the resulting blue paste allowed to gel for 12 h at room temperature before being oven-dried for 6 h at 120 ^0C to remove water. The blue-green rock was thoroughly ground with a mortar and pestle, then transferred into a crucible and calcined at 450 ^0C for 5 h to convert all $Cu(NO_3)_2 \cdot 2.5\ H_2O$ to Cu(II)O. The resulting grey black powder was sieved with a 230 nm sieve and stored in a vial for use.

3.5 Gas Phase Dosing

The particles of Cu(II)O/silica were exposed to the vapors of selected organic precursors that had been implicated in forming PCDD/Fs using a custom-made vacuum exposure system.

3.5.1 Custom-Made Vacuum Exposure System

The vacuum and thermoelectric furnace system is a custom designed for studying the formation and stabilization of EPFRs [5, 8]. The entire system consists of five main parts namely; high power vacuum pumps, a high temperature thermoelectric ceramic heater, a vacuum exposure chamber, an EPR-extraction cell, and a dosing vial port displayed in Figure 3.1. The vacuum part of the dosing system is crucial in the initial and final preparations of EPFRs. The flyash surrogates are initially dried and cleaned of organic contaminants prior to adsorption experiment. The vacuum system consists of two main pumps: a roughing vacuum pump (Edwards, model E2MO.7) which is used entirely during the experiment and the second high power turbo-molecular pump (Edwards, model EXT70) which is used after dosing to remove physisorbed molecular species. This turbo pump is a high power vacuum pump and it can evacuate to lower pressure down to 10^{-2} torr. The roughing pump is connected to a carbon capsule filter (Pall, model 12011) in order to remove the toxic organic precursors (2-CP, PH, and DCBz). The end of the carbon capsule filter (Pall, model 12011) is connected to the fume hood in order to vent.

The vacuum exposure glass chamber hosts the dosing pot and the two EPR extraction cells. The dosing pot can easily be detached for addition of more adsorbate and cleaning. The EPR extraction cell can easily be detached from the system after dosing. The vacuum exposure glass chamber is covered with rope heaters (Omegalux®, model FGR) connected to a variable AC temperature controller (Electrothermal, model MC240X1) that control the temperature of the

whole chamber to about 80 ^{0}C. In addition, the vacuum exposure glass chamber is covered with aluminum foil in order to prevent the organic precursor from condensing.

The digital pressure gauge (Varian, eyesys convector, model L973633200220) which is used to monitor the pressure of the whole system is mounted on the upper side of the vacuum

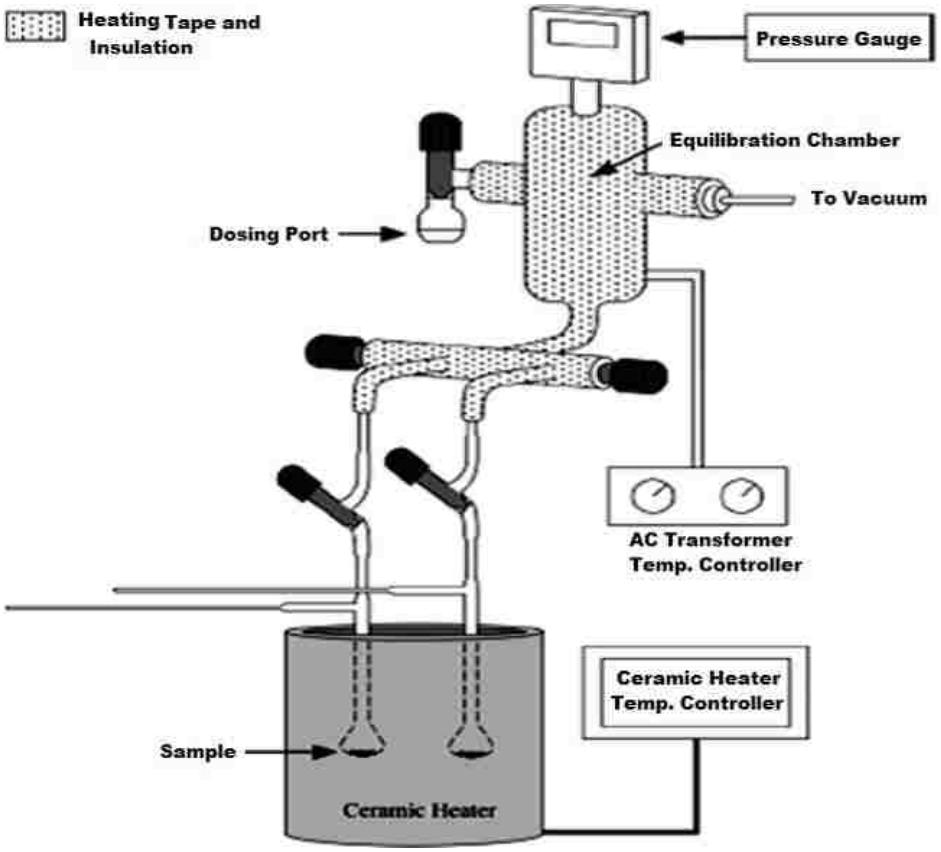

Figure 3.1 Vacuum and thermoelectric furnace system apparatus.

exposure chamber. The L-shaped dosing pot which is made of glass is equipped with a double o-ring PTFE valve and is connected to the vacuum system on the side. A liquid nitrogen cold finger is placed in-between the vacuum pumps and the vacuum exposure chamber to trap excess physisorbed species so as to prevent excess physisorbed species from reaching the vacuum pumps.

3.5.2 High Temperature Cylindrical Ceramic Heater

The two reactor bulbs are placed inside a high-temperature cylindrical ceramic heater (Omegalux®, model CRFC) which has a maximum operating temperature of 950 ºC. The temperature inside the heater is controlled by a relay temperature controller (Omegalux®, model SSRL240DC25) connected to a relay (Tyco, model SSR-240D25R) and equipped with a high temperature K thermocouple sensor (Omega, model XCIB-K-2-3-3) which controls the temperature of the ceramic heater. Both ends of the cylinder are covered with thermal blanket in order to keep the temperature constant inside the heater.

3.5.3 EPR Extraction Cell

The EPR extraction cell has a multipurpose function; adsorption, extraction, and EPR measurement. The EPR extraction cell is 12-inch quartz tube with a detachable 9-inch Suprasil™ EPR side arm and a reactor bulb at the button which holds the sample for adsorption of organic precursor at temperature 150 - 400 ^{0}C. The 9-inch Suprasil™ tube is attached to the EPR extraction cell by a high vacuum adapter fitted with a PTFE o-ring and a plastic nut. The reactor bulb has a round bottom with an i.d. of 1.5-inch so as to increase the surface of the sample matrix during adsorption or extraction. After being assembled, the EPR extraction cell and the suprasil™ EPR side are attached to the vacuum chamber using a stainless steel ultrahigh vacuum adapter (Swagelok, SS-4-UT-6). The sample is introduced to the EPR extraction cell through the opening on the side where the suprasil™ EPR tube is later attached. The EPR extraction cell (cf. Figure 3.2) design is suitable for adsorption and transfer of the sample matrix from the reactor bulb to the suprasil™ EPR tube.

3.6 Surface-Bound Radical Adsorption Procedure

In this work, three precursors without further purification were chosen for the study of

surface-bound free radicals: phenol—PH (Aldrich, 99+%), 2-chlorophenol—2-CP (Aldrich,

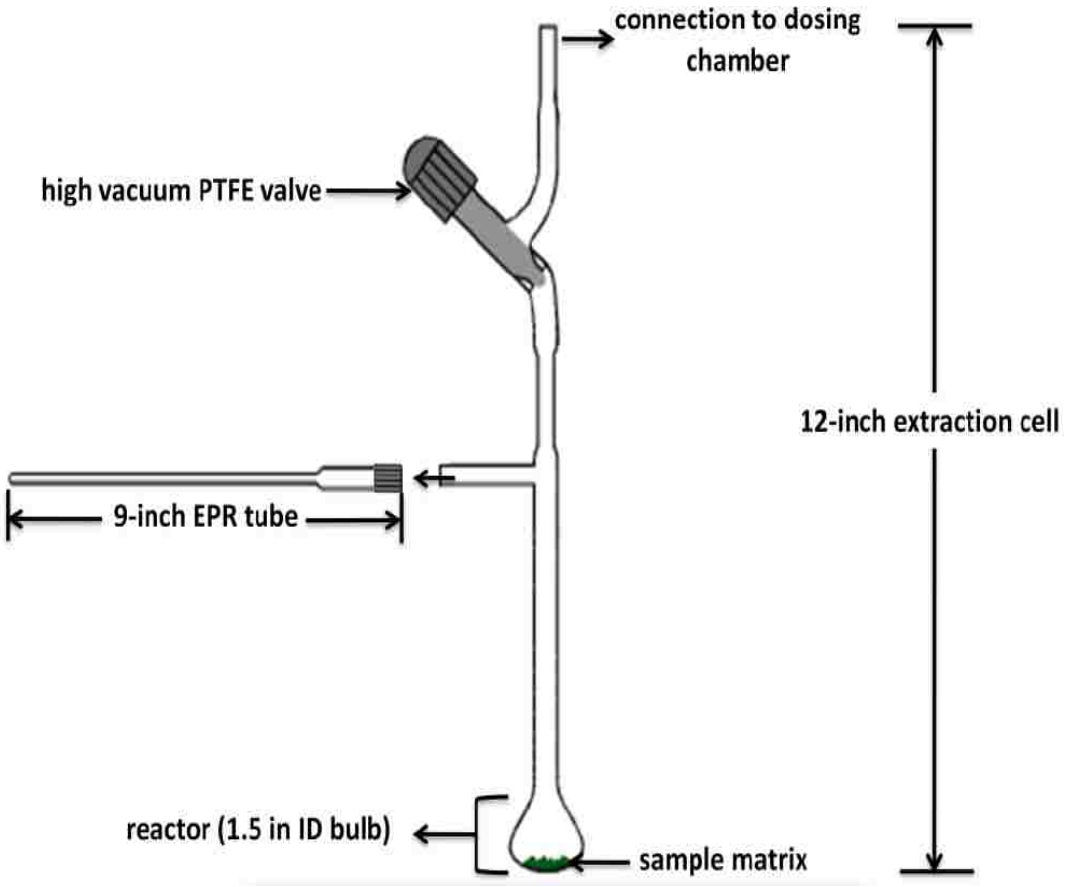

Figure 3.2 Custom-designed EPR-extraction cells.

99+%), and 1,2-dichlorobenzene—1, 2-DCBz (Aldrich, 99+% HPLC grade). All the precursors selected had been reported previously in a series of experiments to catalyze formation of EPFRs and PCDD/Fs [6, 9, 10]. Phenol is the most common partial oxidation product of aromatic species in the combustion system. Chlorinated aromatics (2-chlorophenol and 1,2-dichlorobenzene) are known precursors of dioxins.

Approximately, 100 mg of metal oxide particulate matter was weighed and introduced into an extraction EPR cell via the side arm opening before attaching the EPR tube with a high

vacuum plastic threaded screw nut equipped with o-ring. The extraction EPR cell was closed with the PTFE vacuum valve. The two EPR extraction cells were mounted on the exposure vacuum chamber using Swagelok^{TM} stainless steel adapter with the bottom part (reactor-bulb) inside the cylindrical high temperature furnace. The roughing pump was switched on before the main valve to the vacuum exposure was opened. After ensuring that there are no leaks in the system, the temperature was increased to 120 ^{0}C for 10 min in order to remove water from the sample. The temperature was then increased to 450 ^{0}C and maintained for 1 h to clean, pretreat, and remove any surface organic contaminants. The temperature was brought to reaction temperature of 230 ^{0}C and the dosing port opened to evacuate air. The water line was then opened, turbomolecular pump turned on and the system evacuated until the pressure stabilized at 10^{-2} Torr before turning off the roughing pump. The system was heated up by turning on the AC heater for 5 min followed by the introduction of the dosant vapor to the EPR extraction cell. The heat gun was used to heat the adsorbate, metal parts, and the EPR tubes to avoid decomposition of the adsorbate molecules. After dosing for 5 min, the dosing pot was closed and the main valve opened to evacuate physisorbed adsorbates out of the system at 10^{-2} Torr for 1 h at 120 ^{0}C. The EPR extraction cell valves were then detached for EPR analysis.

3.7 Electron Paramagnetic Resonance Analysis

The samples were analyzed for the presence of EPFRs at room temperature by placing them into 4mm ID, suprasil^{TM} EPR tubes. The spectra were measured using a Bruker model EMX 2.0/2.7 EPR spectrometer with dual cavities, X-band at room temperature. The typical operating parameters were as follows: microwave frequency (9.5 GHz), microwave power of 2 mW, center field at 3450 G, sweep width of 200 or 1000 G, resolution 1024 points, receiver gain of 3.56×10^{4}, modulation frequency of 100 kHz, time constants of 40 ms, and sweep width of 167

s. A di(phenyl)-(2,4,6-trinitrophenyl)iminoazanium (DPPH) standard was used to calibrate both the field position and radical concentration [11].

3.7.1 Analysis and Calculation

The g-value and the $\Delta H_{p\text{-}p}$ were measured and then calculated with the Bruker WINEPR data processing software. The assignment of the spectral components in the resulting EPR spectra was preformed based on the spectral deconvolution using the Origin 7E Peak Fitting module to obtain a best fit (0.999 or higher with minimal number of peaks). The fitted absorption spectrum was compared with the original first-derivative and absorption spectra. The radical concentrations were calculated using the formula in equation 3.1 using a double integration method of the first derivative signal and then compared with DPPH) as the standard;

$$C = \frac{Spins \times A \times RG_{DPPH}}{A_{DPPH} \times RG_A \times m} \tag{3.1}$$

where C (spins/g) is the radical concentration of the sample; A is the area count of the sample; RG_{DPPH} is the receiver gain used to acquire the DPPH signal; A_{DPPH} is the area count of DPPH; RG_A is the receiver gain used to acquire the sample; and m is the mass of the sample analyzed.

3.7.2 Calibration Curve

The quantitative radical concentration was determined using a calibration curve. 5 mg of DPPH was weighed using a microbalance with 1 μg readability. The DPPH was then dissolved in 100mL of benzene to make a stock solution of 50 μg/mL. 1 mL aliquot was removed and subsequently diluted to 10 mL with benzene. The concentration of the diluted standard was analyzed using a UV-Vis-NIR spectrophotometer (Shimadzu, model UV-3101PC, double beam) with the following parameters: λmax at 520 nm and a molar extinction coefficient (ε) of 12,800 M^{-1} cm^{-1} [11]. This confirmed the concentration of the original stock solution, after accounting

for dilution, as 1.37×10^{-4} M. Four different aliquots of the DPPH solution were taken (20 μL, 60 μL, 80 μL, and 100 μL) and then placed in a high purity quartz EPR tube. This range was compared with the normal concentration range of all radicals measured. The samples were dried in an inert environment by flowing nitrogen gas slowly. The tubes were sealed in vacuum and EPR spectra were acquired. The area counts were determined using the double integration of the first-derivative signal and a calibration curve by plotting the area counts vs. the amount of DPPH.

3.7.3 Determination of EPFRs' 1/e Lifetime

The kinetic studies were performed to determine the persistency and stability of the radicals in air. The samples were exposed to air by opening the PTFE valve on the EPR extraction cells at room temperature. The samples were exposed to ambient air and EPR spectra obtained regularly to determine the concentration of radicals as a function of time until the sample had decayed and acquisition of the EPR spectra was at the noise level of the instrument. The decay of the relative radical concentration was plotted vs. time, and the lifetimes (1/e) calculated from the fitted data as first-order decay.

Radical decay kinetic experiments in air are based on an assumed reaction with molecular oxygen,

$$R^* \times O_2 = S$$

where R^* is the radical and S is the molecular product. Then the rate equation for the decay of radical R^* can be written as,

$$-\frac{dR^*}{dt} = K[O_2][R^*] \qquad (3.2)$$

Since the concentration of oxygen is higher than the concentration of the radical, the change of concentration in oxygen is negligible (i.e., we assume a steady-state), that is

$$-\frac{d[O_2]}{dt} = 0$$

Then equation 3.2 integrates to,

$$d\ln[R^*] = kdt \quad \text{where } k = K[O_2]$$

$$\int_{R_0^*}^{R_f^*} d\ln[R^*] = \int_0^t kdt$$

$$\ln R_f^* - \ln R_0^* = -kt$$

$$\ln \frac{R_f^*}{R_0^*} = -kt$$

$$R_f^* = R_0^* e^{-kt}$$

The 1/e half-life is the time taken for the original concentration to decay to $1/e$, that is

$$R_f^* = {}^{1}\!/_{e}\, R_0^*$$

Substituting this to the above equation yields,

$${}^{1}\!/_{e}\, R_0^* = R_0^* e^{-kt}$$

Which for a first order reaction, the $1/e$ half-life is the reciprocal of the rate constant.

$$t_{1/e} = {}^{1}\!/_{k} \tag{3.3}$$

3.8 Hydroxyl Radical Generation Studies

High purity 5,5-dimethyl-1-pyrroline-N-oxide (DMPO, 99 %+, GLC) was obtained from ENZO Life Sciences International and used as received; 2-chlorophenol (2-CP, 99+%); copper nitrate hemipentahydrate (99.9+%); 0.01M phosphate buffered saline (PBS, NaCl 0.138M: KCl 0.0027M) were all obtained from Sigma-Aldrich. Particles containing EPFRs were synthesized from the method described in section 3.4. The control sample was undosed Cu(II)O/silica which did not contain surface-associated EPFRs.

A phosphate buffer saline solution (PBS, 0.01M) was prepared by dissolving 100 mg of PBS in 10 ml deionized water which was then aerated for 10 minutes. The PBS was used to

maintain the pH at 7.4 and also balance the final volume at 200 μL. 1 mg of undosed CuO/silica and the sample (CuO-EPFRs) were weighted and then placed in a vials where 1 mL of PBS was added. The treatment of particle was either centrifuged or non-centrifuged. The particles were [1] suspended in PBS (pH 7.4) and ultrasonicated for 5 min (Fisher Scientific FS20, 40 W) in a 5 ml glass vial (as non-centrifuged) and [2] centrifuged (ultrasonicated + centrifugation for 5 min). The particle suspensions were then introduced into vials; (10 μL from solution of 1 mg/mL), DMPO (10 μL from a freshly prepared solution of 3 M), and PBS (180 μL from solution of 0.01M). Solutions were shaken for 30 s using a Vortex Genie 2 (Scientific Industries) and then kept under kitchen foil for 1 h prior to the EPR analysis. It was found out that this concentration of DMPO (150 mM) prevents secondary reactions, such as dimerization and decomposition reactions with molecular oxygen [12, 13]. A 10 μL of fleshly made 3M DMPO (150 mM), 10 μL of sample or control, and 180 μL were placed in an eppendorf vial and shaken with vortex Genie 2 for 30s. The final particle concentration was approximately 50 μg/mL. The eppendorf vials were covered using aluminum foil for all experiments in order to prevent DMPO photo-oxidation from the light [14]. Samples of approximately 20 μL were periodically withdrawn using an EPR capillary tube (i.d. ~1mm, o.d. 1.55mm) and then sealed on one end with sealant (Fisher brand). The capillary tube was inserted in a 4 mm EPR tube and EPR spectra recorded at 1, 3, 5, 7, and 12 h.

The EPR parameters for the DMPO-OH experiment were: scan range of 100 G, time constant of 40.96 msec corresponding to a conversion of 163.84 msec, sweep time of 167.77 seconds, receiver gain 3.56×10^4 modulation amplitude of 0.80 G, a power of 10.25 mW, and two scans. Each experiment was performed at least twice, and the final EPR spectrum represents an average of all spectra obtained for each experiment. The calculated area was then plotted

against the time, i.e., $\left(\Delta H_{p-p}\right)^2$ multiplied by the intensity of the spectrum. Only the two-inner lines were considered.

3.9 Basics Theory of Electron Paramagnetic Spectroscopy

EPR is a spectroscopic technique that detects the transitions of unpaired electrons in an applied magnetic field [15]. The angular motion of this charged particle generates a magnetic field because an electron is charged. The energy differences studied in EPR spectroscopy are due to interaction of unpaired electrons in the sample with the EPR magnets. This effect is called the Zeeman Effect (cf. Figure 3.3) [16]. The field of resonance is described by the equation:

$$h\nu = g_e \beta B_0 \qquad (3.4)$$

where h is a Planck's constant ($h = 6.63 \times 10^{-34}\,\mathrm{J \cdot s}$), ν (Hz) is the frequency of the incident microwave, β is the Bohr magneton ($\beta = 9.27 \times 10^{-24}\,\mathrm{J\,T^{-1}}$), and B_0 (Tesla) is the magnetic field. The magnetic field, B_0, produces two energy levels for the magnetic moment μ of the electron. The unpaired electron will have a state of lowest energy when the moment of the electron is aligned with the magnetic field and a state of highest energy when μ is aligned against the magnetic field. The two states are labeled by the projection of the electron spin, *ms*, on the direction of the magnetic field. Because the electron is a spin ½ particle, the parallel state is designated as ms = -½ and the antiparallel state is ms = +½. The first derivative EPR spectrum is given in Figure 3.4.

3.9.1 EPR Instrumentation

The Bruker EMX-2.02/2.7 EPR spectrometer in Dr. Dellinger's laboratory consists of four parts: a microwave bridge, a cavity, sample holder, and two large magnets. It also has a cooling unit, a console and a computer. The schematics set-up of the EPR instrumentation is illustrated in Figure 3.5 (Images of EPR are from;

http://www.chemistry.jhu.edu/NMR/WhatsEPR.pdf).

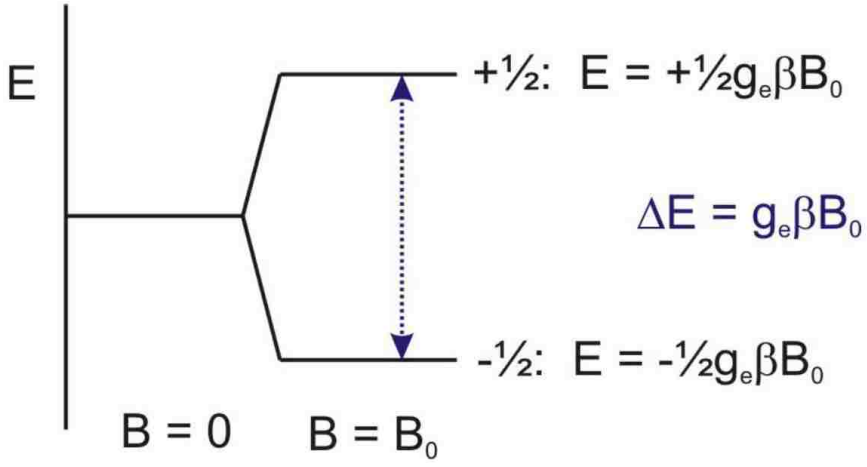

Figure 3.3 The Zeeman Effect.

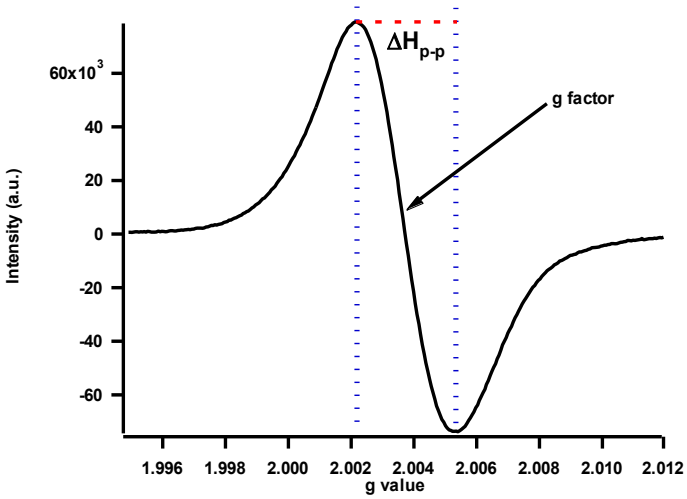

Figure 3.4 First-derivative EPR spectrum.

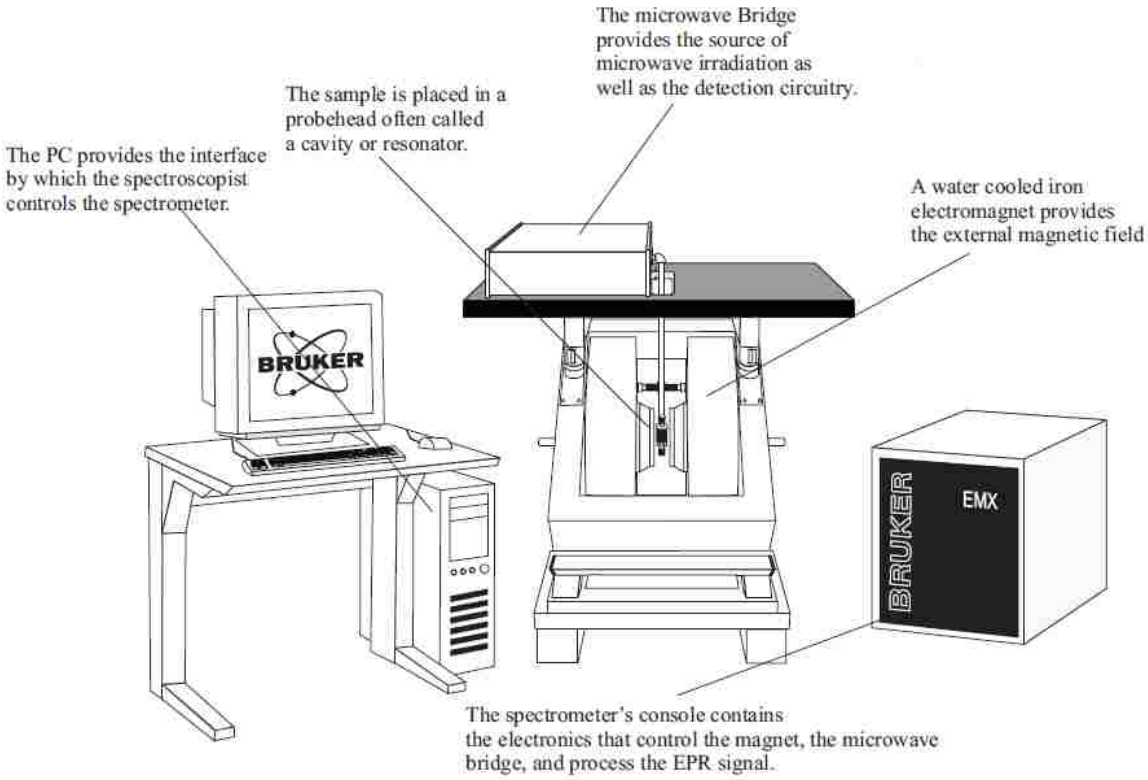

Figure 3.5 Instrument set-up of the Bruker EPR spectrometer.

3.10 References

1. Crone, T.J. and M. Tolstoy, *Magnitude of the 2010 Gulf of Mexico Oil Leak.* Science, 2010. **330**(6004): p. 634.

2. Owens, E.H., et al., *Tar ball frequency data and analytical results from a long-term beach monitoring program.* Marine Pollution Bulletin, 2002. **44**(8): p. 770-780.

3. Goodarzi, F., *Characteristics and composition of fly ash from Canadian coal-fired power plants.* Fuel, 2006. **85**(10–11): p. 1418-1427.

4. Lomnicki, S. and B. Dellinger, *Formation of PCDD/F from the pyrolysis of 2-chlorophenol on the surface of dispersed copper oxide particles.* Proceedings of the Combustion Institute, 2002. **29**(2): p. 2463-2468.

5. Lomnicki, S., et al., *Copper Oxide-Based Model of Persistent Free Radical Formation on Combustion-Derived Particulate Matter.* Environmental Science & Technology, 2008. **42**(13): p. 4982-4988.

6. Vejerano, E., S. Lomnicki, and B. Dellinger, *Formation and Stabilization of Combustion-Generated Environmentally Persistent Free Radicals on an Fe(III)2O3/Silica Surface.* Environmental Science & Technology, 2010. **45**(2): p. 589-594.

7. Alderman, S.L., et al., *An Infrared and X-ray Spectroscopic Study of the Reactions of 2-Chlorophenol, 1,2-Dichlorobenzene, and Chlorobenzene with Model CuO/Silica Fly Ash Surfaces.* Environmental Science & Technology, 2005. **39**(19): p. 7396-7401.

8. dela Cruz, A.L.N., et al., *Detection of Environmentally Persistent Free Radicals at a Superfund Wood Treating Site.* Environmental Science & Technology, 2011. **45**(15): p. 6356-6365.

9. Vejerano, E., S.M. Lomnicki, and B. Dellinger, *Formation and Stabilization of Combustion-Generated, Environmentally Persistent Radicals on Ni(II)O Supported on a Silica Surface.* Environmental Science & Technology, 2012. **46**(17): p. 9406-9411.

10. Lomnicki, S., H. Truong, and B. Dellinger, *Mechanisms of product formation from the pyrolytic thermal degradation of catechol.* Chemosphere, 2008. **73**(4): p. 629 - 633.

11. Yordanov, N.D. and A. Christova, *DPPH as a primary standard for quantitative EPR spectrometry.* Applied Magnetic Resonance, 1994. **6**(1-2): p. 341-345.

12. Janzen, E.G., et al., *Detection of alkyl, alkoxyl, and alkyperoxyl radicals from the thermolysis of azobis(isobutyronitrile) by ESR/spin trapping. Evidence for double spin adducts from liquid-phase chromatography and mass spectroscopy.* Journal Name: Journal of the American Chemical Society; (United States); Journal Volume: 112:23, 1990: p. Medium: X; Size: Pages: 8279-8284.

13. Khachatryan, L., et al., *Environmentally Persistent Free Radicals (EPFRs). 1. Generation of Reactive Oxygen Species in Aqueous Solutions.* Environmental Science & Technology, 2011. **45**(19): p. 8559-8566.

14. Kim, J.K. and I.S. Metcalfe, *Investigation of the generation of hydroxyl radicals and their oxidative role in the presence of heterogeneous copper catalysts.* Chemosphere, 2007. **69**(5): p. 689-696.

15. Bramley, R. and S.J. Strach, *Electron paramagnetic resonance spectroscopy at zero magnetic field.* Chemical Reviews, 1983. **83**(1): p. 49-82.

16. Weil, J.A. and J.R. Bolton, *Basic Principles of Paramagnetic Resonance*, in *Electron Paramagnetic Resonance*. 2006, John Wiley & Sons, Inc. p. 1-35.

CHAPTER 4 - DFT STUDY OF REACTION OF PHENOL AND CHLORINATED PHENOLS WITH COPPER OXIDE CLUSTERS

The EPFRs are formed by the multistep process initiated by physisorption, which is followed by chemisorption on the metal oxide surface and electron transfer as described in our previous experimental studies which involved Cu(II)O, $Fe(III)O_3$, and Ni(II)O surfaces through elimination of (i) H_2O, (ii) HCl or (iii) both [1-4]. The cluster models of $(CuO)_n$ with $n = 1-8$ used in this study were previously reported elsewhere [5]. The first step in the surface-mediated process involves addition of water to a copper atom which is followed by a hydrogen transfer to the adjacent oxygen leading hydroxyl group formation on the surface (cf. Scheme 4.1).

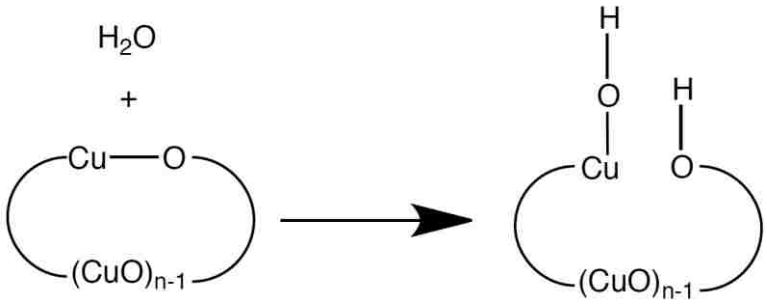

Scheme 4.1 Hydroxylation of Cu(II)O surface leading to the formation of Cu-hydroxyl groups.

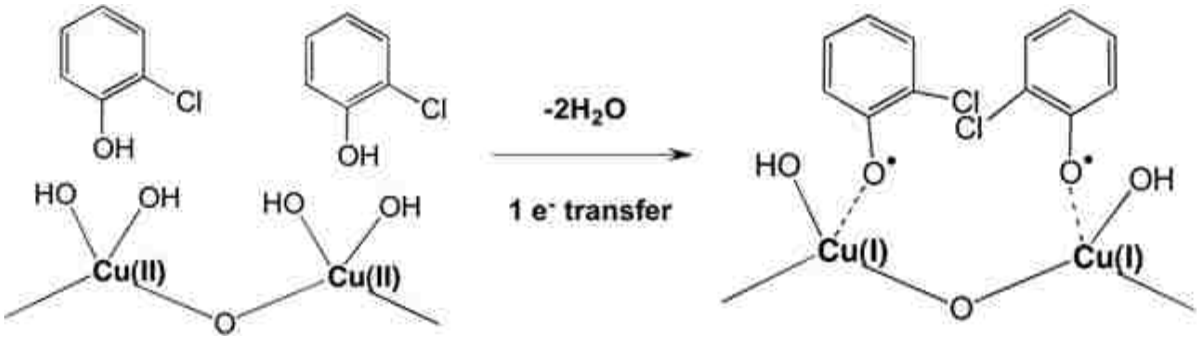

Scheme 4.2 Model for the formation and stabilization of environmentally persistent free radicals.

A phenolic/or chlorophenolic compound then reacts with hydroxylated metal surfaces and upon electron-transfer forms surface-stabilized EPFRs complexes (cf. Scheme 4.2) [3, 4, 6-10]. The electron transfer is a key stabilizing feature of the radicals on metal surfaces. The reaction of small hydroxylated copper oxide clusters with PCCD/Fs precursors provides a useful model for the surface reactions expected in ultrafine particulate matter [11, 12]. Therefore, we have calculated the reaction energies and change in charge distribution for reactions of hydroxlated copper oxide clusters with phenol, *o*-chlorophenol, and *p*-chlorophenol.

4.1 Computational Details

The structures of copper oxide clusters from previous work [5] were taken as the starting point for this work. We employed two basis sets and three density functionals (a total of six model chemistries) for the purpose of validation. All the calculation were conducted using Gaussian 09 package [13]. The functionals used were; B3LYP [14, 15], newly developed M06 [16, 17], and hybrid GGA PBE1PBE [18, 19]. The two basis set employed are; (i) LANL2DZ [20-22] as basis set 1 (BS1) and (ii) 'mixed basis set' consisting of LANL2DZ for copper atoms and aug-cc-pVDZ [23] basis set for all other non-metal atoms as basis set 2 (BS2). The mixed basis set (BS2) was created by the use of GEN keyword. The LANL2DZ basis set for copper represents the Los Alamos nonrelativistic effective core potential (ECP) developed by Hay and Wadt. The valence shell, including the 3d orbitals is described by a basis set of essentially double-ζ quality including a diffuse 3d function. For the rest of the atoms, LANL2DZ implies the Dunning-Huzinaga full double- ζ basis set. With the chemically inactive core electrons represented by an ECP, the computational cost is decreased, since the cost formally increases as $\sim N^4$ where N is the number of explicitly treated electrons [24].

The Dunning style basis set aug-cc-pVDZ (Dunning, 1989) was utilized, its small size allows calculations on the cluster of interest and is large enough to produce accurate results [25].

For evaluating the amount of electron charge transfer from the O atom of the organic adsorbate to the metal cation center, Bader analysis [26-28] was performed. The method is also known as the Atoms-In-Molecules approach [29] and is well suited with the electronic structure calculations method since the required input is the electronic density and nuclear coordinates [30]. The method has been demonstrated to work well both in charged system [31] and water containing systems [32]. The atomic charge is an ill-defined property and therefore charge assignation may be ambiguous. We are however interested to see the changes in the amount of partial charge in Cu before and after reaction with an organic compound.

4.2 Hydroxylation of $(CuO)_{1-8}$ Clusters

The $(CuO)_{1-8}$ clusters shown in Chapter 1 (cf. Figure 1.5) were re-optimized using BS1 and BS2 basis sets and three density functionals (a total of six model chemistries). Further examination of the spin states for each cluster was conducted to determine the most stable structures. The lowest spin state are given in Table 4.1. All the model chemistries agreed on the

Table 4.1 Lowest energy spin states of (CuO)n clusters

Cluster	Spin State
CuO	doublet
Cu_2O_2	singlet
Cu_3O_3	quartet
Cu_4O_4	triplet
Cu_5O_5	quartet
Cu_6O_6	triplet
Cu_7O_7	quartet
Cu_8O_8	triplet

geometries obtained and on the lowest energy spin state. We however noted that the bond length of Cu-O using BS1 were larger in comparison to those obtained by BS2. For example, the

average bond length of Cu-O is 1.80 Å with BS1 and 1.77 Å with BS2. The experimental bond length of Cu-O is 1.72 Å [33].

As aforementioned, the adsorption of EPFRs precursors to $(CuO)_{1-8}$ clusters is initiated by addition of a water molecule. Preliminary studies were done where a single water molecule was added to each unique copper atom to determine the most reactive site for addition of phenolic compound. The addition of the single water molecule to the most reactive copper atom was then taken as a model for the hydroxylated nanocluster. We noted that the addition of water targeted the Cu atom with the largest positive partial Bader charge except for Cu_6O_6 and Cu_8O_8 clusters where the Cu atom with the largest Bader charge is one of the atoms forming the 4-

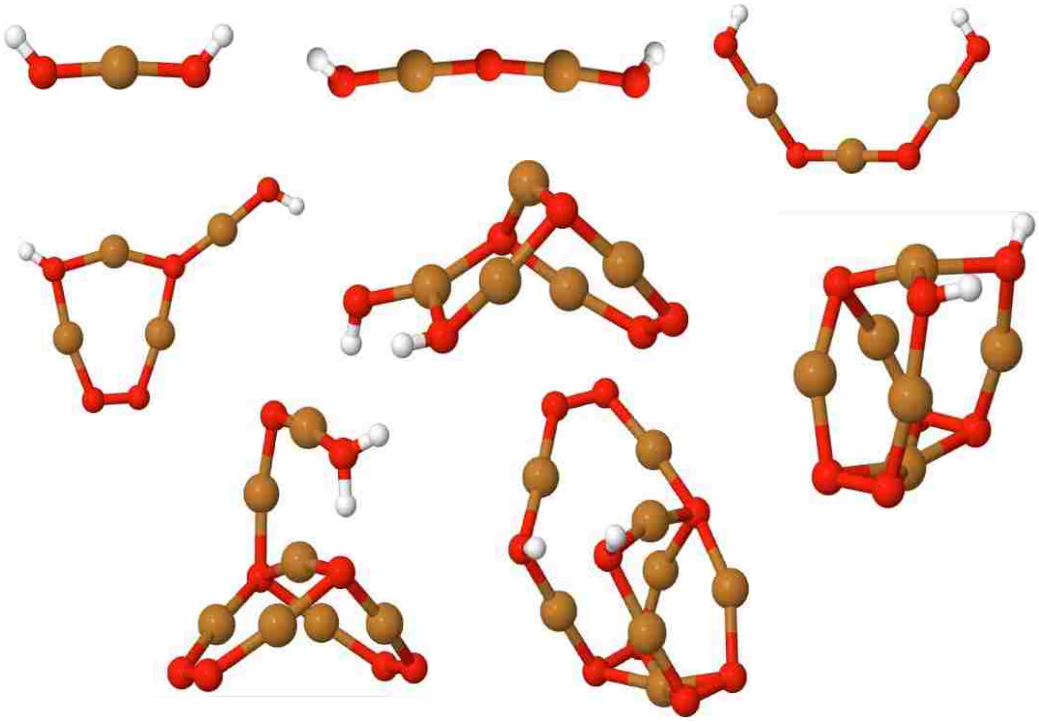

Figure 4.1 Optimized structures of hydroxylated $(CuO)_{1-8}$ clusters. Copper/oxygen/hydrogen are colored gold/red/white.

coordinate and nearly square planar, which particularly is a stable local structure. The Bader charges help to understand the reaction site between copper oxide cluster and water molecule.

Figure 4.2 displays the lowest energy of hydroxylated clusters using the B3LYP/BS2. The first insight is that the structures for all model chemistries were qualitatively similar except the Cu_3O_3-H_2O using BS1 which was linear rather than bent. Briefly, the addition of water resulted in either rupture of a Cu-O bond, formation of an –OH bond to the target Cu atom or migration of a hydrogen atom from water molecule to the adjacent oxygen atom. For CuO, the Cu-O bond remains intact for lack of additional Cu-O bond in the cluster. Using B3LYP/BS2, the H atom of the water molecule in Cu_7O_7 cluster is not completely migrated but forms a hydrogen bonding with the nearby O atom and this H-O distance is measured to be 1.43 Å. Addition of water to CuO and Cu_2O_2 resulted in linear or near linear structures. For Cu_3O_3, the BS1 resulted in linear structures while the BS2 resulted in bent structures. Examination of the Cu-O bonds that were broken leads to some observation: (1) small, strained Cu-O-Cu bond angles ranging from 77^0 to 92^0 for BS2, (2) preservation of Cu-O bonds involving a Cu-O-O moiety, and (3) preservation of Cu-O bonds involved in distorted square planar geometries. The reaction energies for the hydroxylation reaction were similar for all the DFT methods as displayed in the Appendix I. Figure 4.2 displays the ΔE_{rxn} for the 2 basis set averaged over the 3 density functionals. For all the eight clusters, the BS1 ΔE_{rxn} are systematically more negative than the corresponding values using BS2. We note that, $n = 3$ cluster is the least reactive and $n = 4$ cluster is particularly exoergic due to the strained four membered ring.

The change in oxidation state of the copper atom adjacent to the added water was calculated using the Bader charge and all the 6 model chemistries resulted in similar Bader charges. Figure 4.3 displays the Bader charges for each cluster averaged over the 6 model chemistries. In all cases, the addition of water lead to an increase in the Bader charge (partial oxidation) of the copper atom.

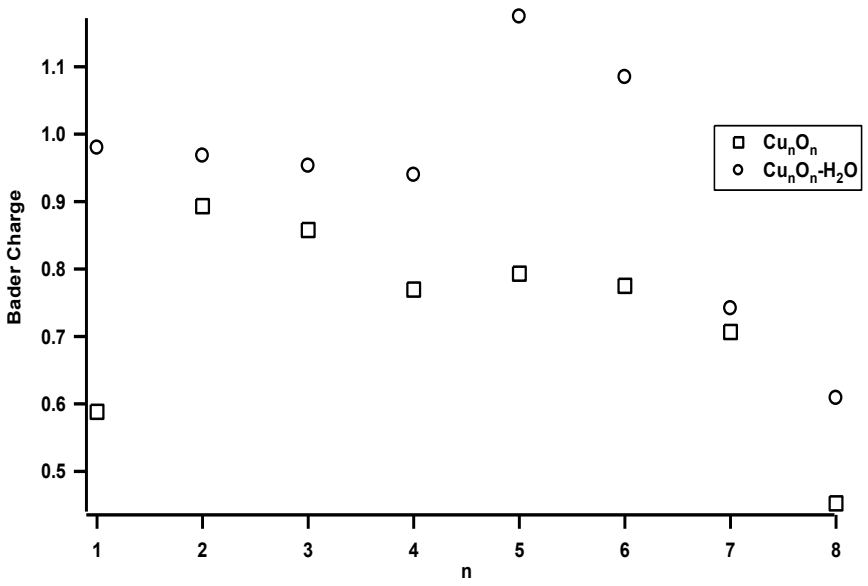

Figure 4.2 Bader charges on the copper atom to which oxygen of the water is attached, after and before hydroxylation on the $(CuO)_{1-8}$ clusters. The results were averaged over the 6 model chemistries.

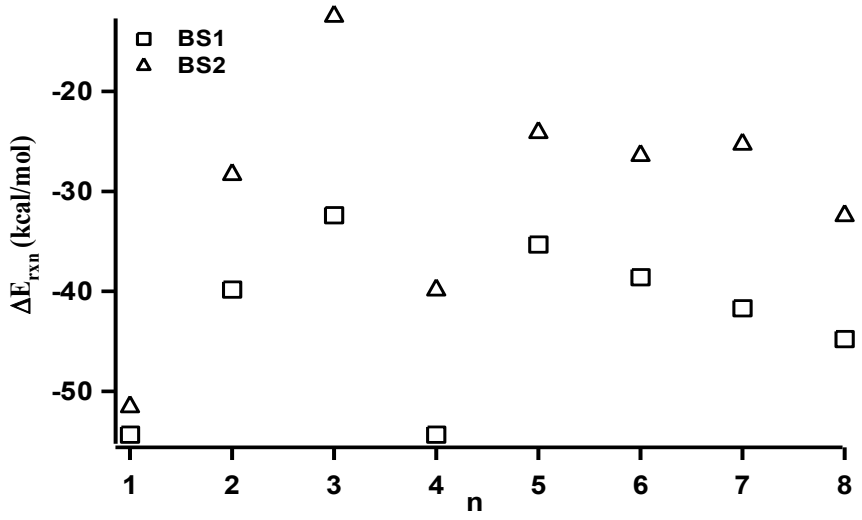

Figure 4.3 Reaction energies (kcal/mol) for the hydroxylation reactions of the copper oxide clusters.

4.3 Adsorption of Phenolic and Chlorophenolic Compounds on $(CuO)_{1-8}$ clusters

The formation of phenolate and chlorophenolate occurs via elimination of water are

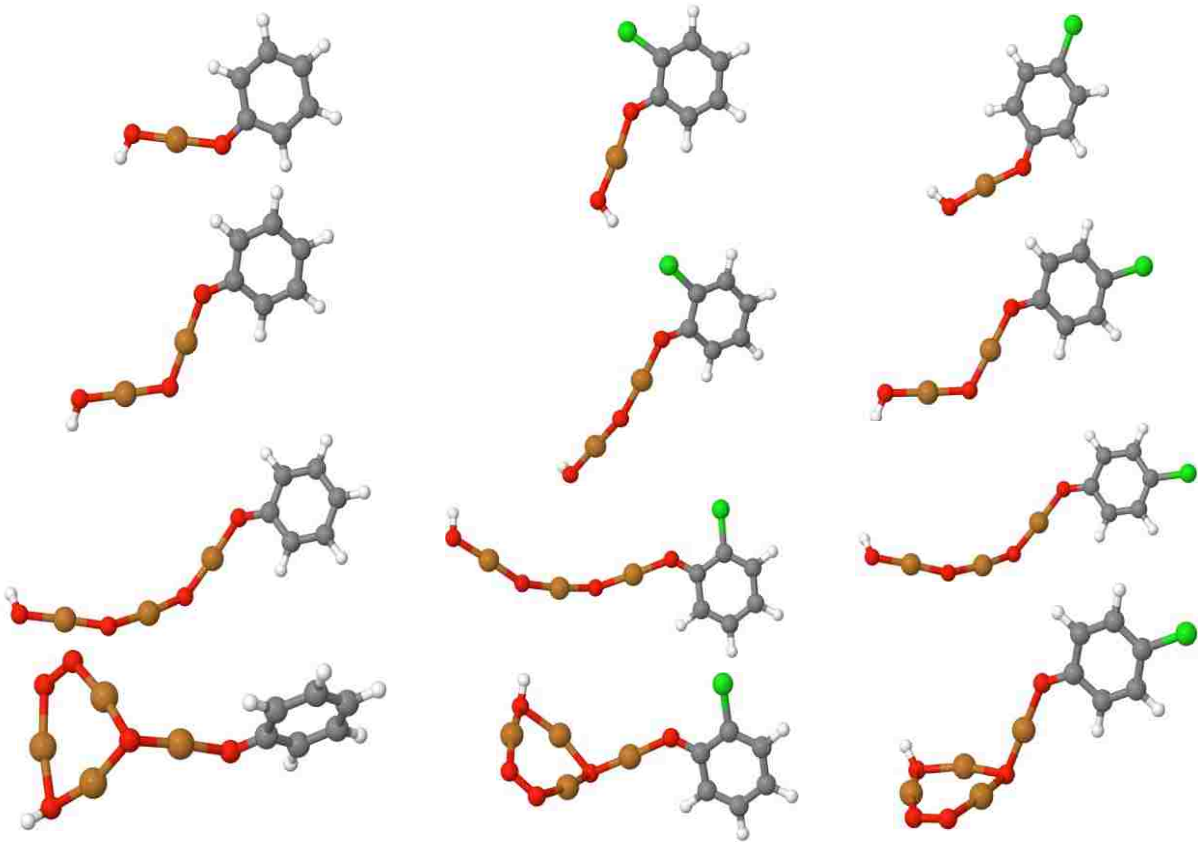

Figure 4.4 Optimized structures of CuO)n-phenol, -*o*-chlorophenol, and –*p*-chlorophenol with $n = 1-4$. Copper/oxygen/hydrogen/chlorine are colored gold/red/white/green.

considered as models for the initial step in the formation of PCCD/Fs. Figure 4.4 and Figure 4.5 displays the geometric structures of (CuO)n-phenol and chlorinated phenols, with $n = 1-8$ using the B3LYP/BS2 model chemistry. Qualitatively, the structures were similar across all the model chemistry except for few cases. For example, for the $n = 3$ copper oxide cluster, the product was bent using BS2 and linear using BS1. For $n \geq 4$ there is no fundamental discrepancies between structures over the 6 model chemistries that could be determined visually.

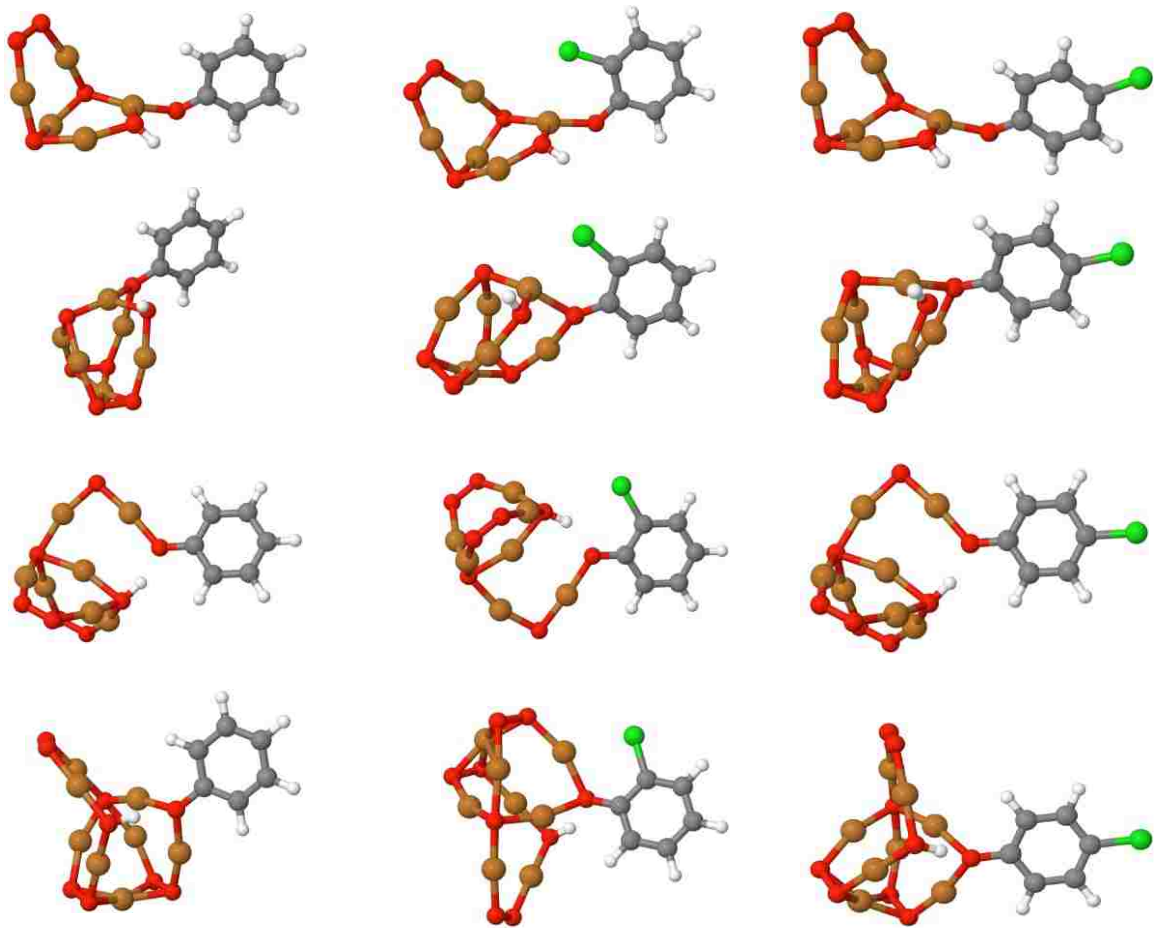

Figure 4.5 Optimized structures of CuO)n-phenol, -*o*-chlorophenol, and –*p*-chlorophenol with $n = 5-8$. Copper/oxygen/hydrogen/chlorine are colored gold/red/white/green.

The reaction energetics of resulting hydroxylated clusters with phenol and substituted phenols averaged over the density functionals are displayed in Figure 4.6, Figure 4.7, and Figure 4.8. The reaction is given by,

$$E_{rxn} = E\left(Cu_nO_n - Organic\ Compound\right) - \left(E\left(Cu_nO_n - H_2O\right) + \left(Organic\ Compound\right)\right) \quad (4.0)$$

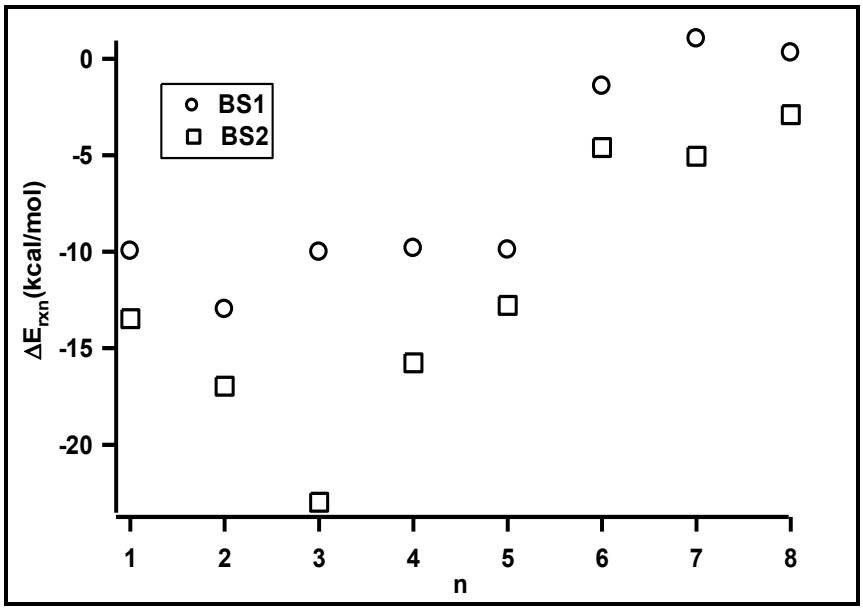

Figure 4.6 ΔE_{rxn} for the reaction of hydroxylated clusters with phenol.

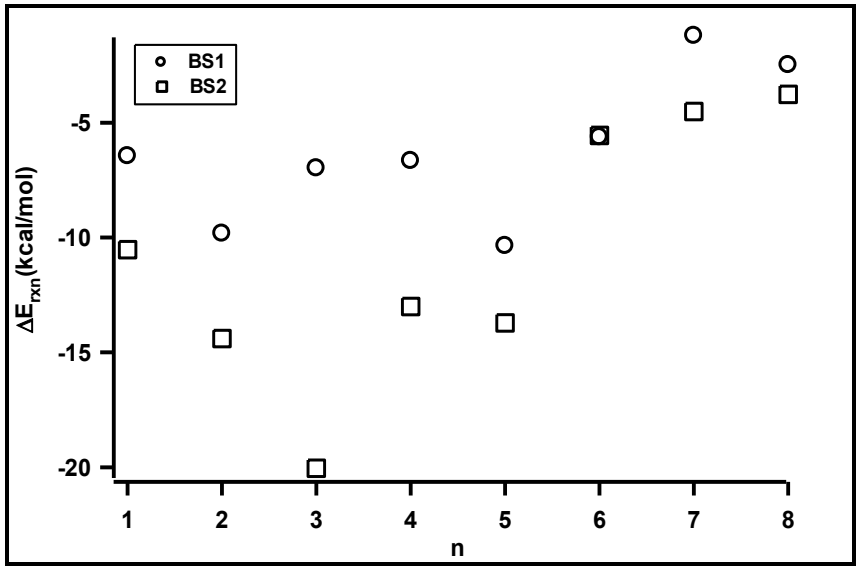

Figure 4.7 ΔE_{rxn} for the reaction of hydroxylated clusters with *o*-chlorophenol.

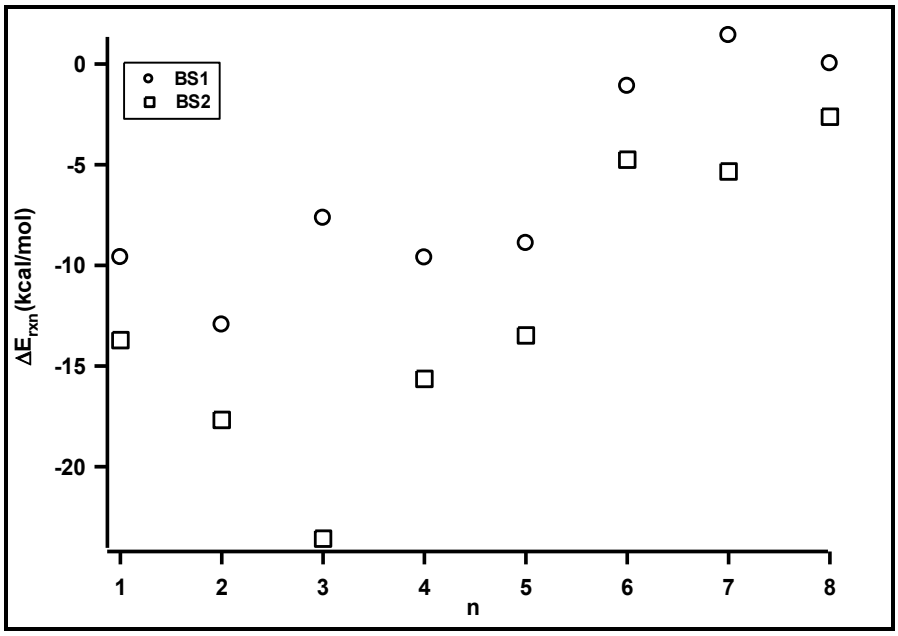

Figure 4.8 ΔE_{rxn} for the reaction of hydroxylated clusters with *p*-chlorophenol.

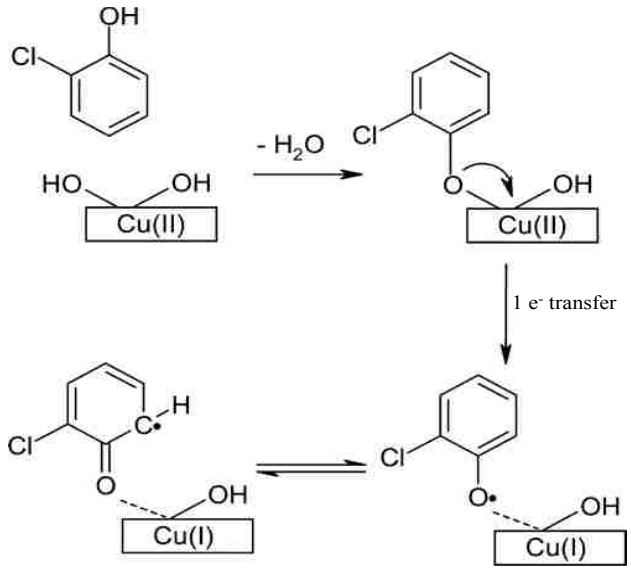

Scheme 4.3 Chemisorption of 2-chlorophenol on hydroxylated CuO and formation of the chlorophenoxyl radical. Since the radical is resonance stabilized, electron density is located at both the carbon and oxygen atoms.

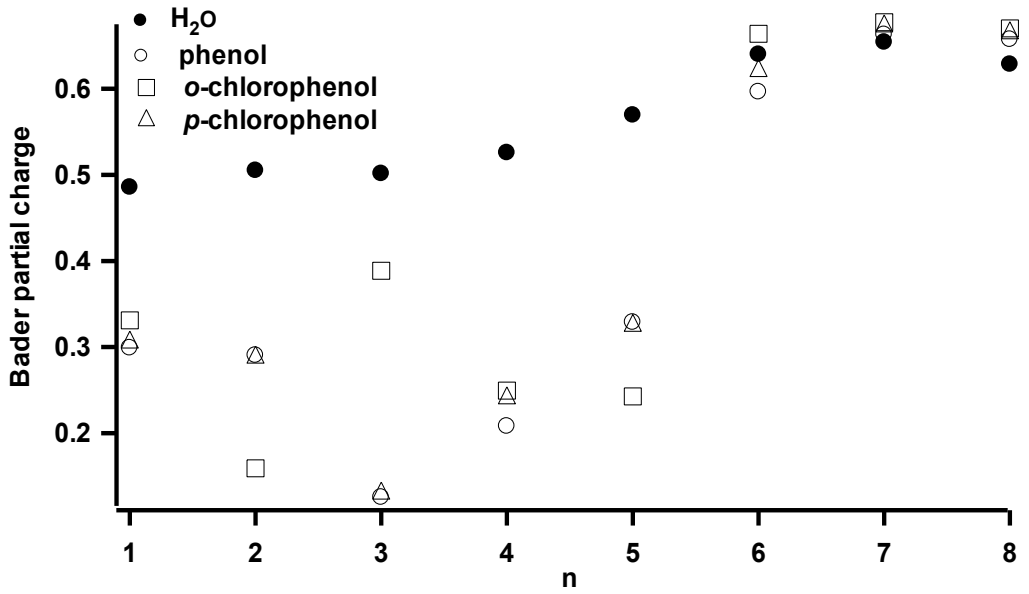

Figure 4.9 Change in Bader charge of the copper cluster fragment upon reaction of the hydroxylated cluster and clusters with phenol, *o*-chlorophenol, or *p*-chlorophenol.

The values of ΔE_{rxn} using BS1 show a little dependence on $n = 1-5$ whereas there is more variation with n for BS2. In all cases, the energies of $n \geq 6$ show significantly positive values suggesting the smaller clusters to be reactive than larger clusters. Overall, the BS2 gives lower reaction energies than those of BS1. Using BS2, Cu_3O_3 has the lowest reaction energies.

4.4 Bader Charge Analysis

Figure 4.9 and Figure 4.10 shows the change in Bader charges for the copper atom at which reaction occurs and the change in fragment, respectively. The fragment is defined as the portion of the hydroxylated portion except the OH group, which is the reaction site for phenol and chlorinated phenol. The Bader charges were averaged over 6 model chemistries. The change in oxidation state of the copper atom was calculated by first generating cube files of the optimized geometries, which were then used by the Texas Bader software package to calculate the charge densities. As observed, the addition of water to bare clusters led to an increase in Bader charge (partial oxidation) of copper atom (*vide infra*). The partial charge of the target Cu

atom reduced by ~0.2e for clusters $n = 1-5$. For $n = 6$, a slight reduction was noted for *o*-chlorophenol complex. However, there was no reduction observed for clusters $n = 7-8$. The partial changes of fragments is displayed in Figure 4.10. In small clusters ($n = 1-5$) there is significant reduction in charge on the copper atom which is more pronounced when the entire fragment is taken into account. A small or non-copper reduction is noted for $n = 6-8$ clusters.

4.5 Molecular Orbitals of Surface-Bound Radicals

A detailed dosing studies were conducted at Dellinger laboratory using PCDD/Fs precursors and CuO supported on silica as a model fly ash [8]. The results suggested that EPFRs are formed through 1- electron transfer from the adsorbate to metal cation center, thus reducing Cu(II) to Cu(I) as illustrated in Scheme 4.3 (*vide infra*). Using EPR spectroscopy, convincing

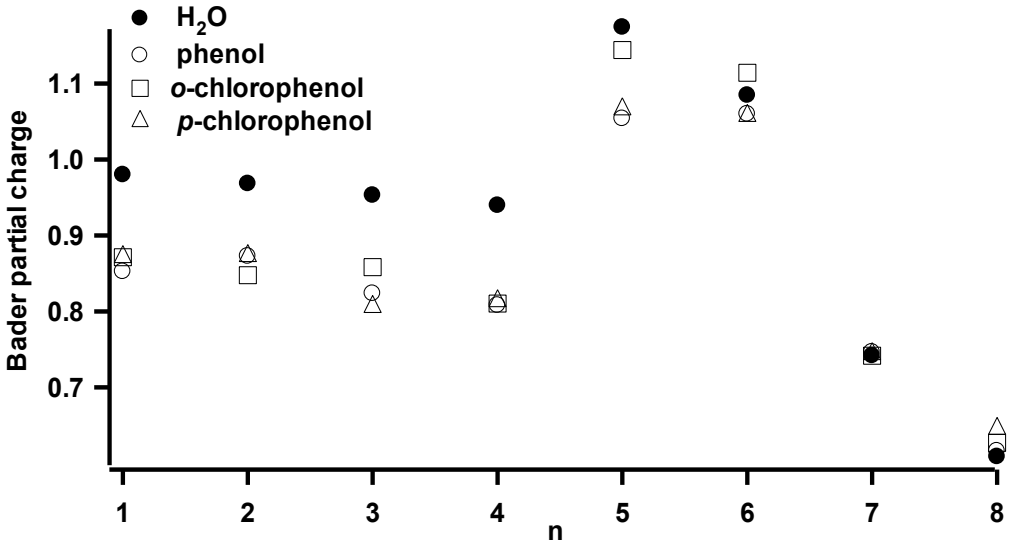

Figure 4.10 Change in Bader charge of the Cu atom to which phenol, *o*-chlorophenol, or p-chlorophenol adsorbs.

evidence have been found for the existence of a carbon-centered and oxygen-centered phenoxyl radicals when PCDD/Fs precursor is adsorbed onto CuO/SiO_2 particles. The reaction products of the $(CuO)_{1-8}$ with phenol and chlorinated phenols showing the highest occupied molecular orbitals (HOMO) where a single unpaired electron is located are displayed in Appendix I. In all

cases, except $n = 4$, this orbital was the HOMO. In addition, a similar orbital occupied by an opposite spin does not exist. Thus, the phenolic entity has free radical character, a key point in the proposed mechanism of dioxin formation.

4.6 Reaction of 1,2-Dichlorobenzene and Chlorobenzene with $(CuO)_{1-8}$ Clusters

4.6.1 Comparison of Adsorption Products

To further explore the nature of adsorption on copper oxide clusters, 1,2-dichlorobenzene (1,2-DCBz) and monochlorobenzene (MCBz) precursors were studied and their reaction energies compared to those of 2-CP and phenol precursors. Phenol and MCBz adsorb in a manner analogous to that of 2-CP and 1,2-DCBz (cf. Figure 4.11 via H_2O and HCl elimination, respectively).

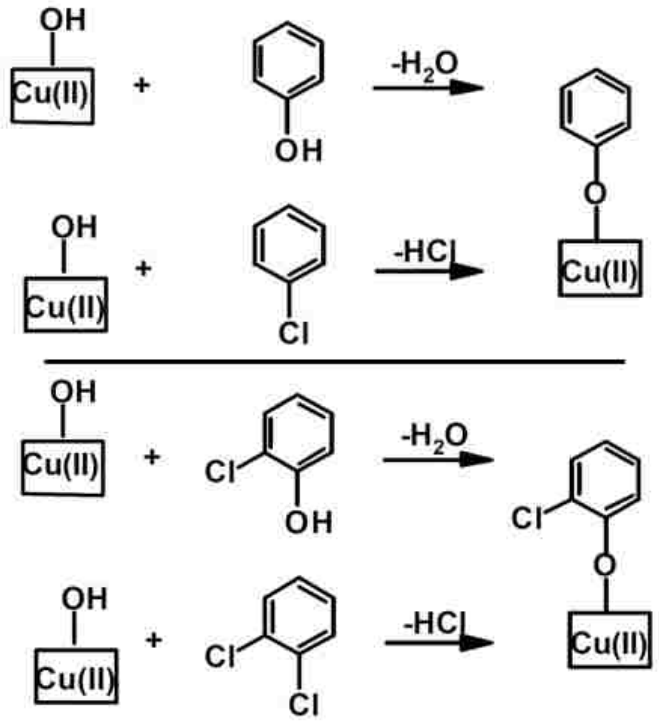

Figure 4.11 Adsorption of PCDD/Fs precursors to yield the same Surface-stabilized radicals; Upper drawing Adsorption of 2-chlorophenol and monochlorobenzene, Lower drawing is Adsorption of 2-chlorophenol and 1,2-dichlorobenzene.

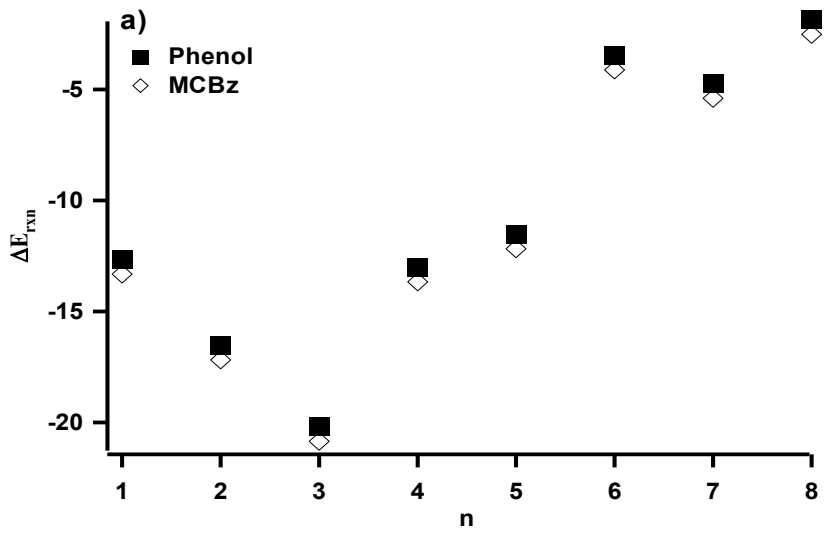

Figure 4.12 Reaction energies of phenol and monochlorobenzene adsorbed on copper oxide clusters to yield same surface-bound radicals.

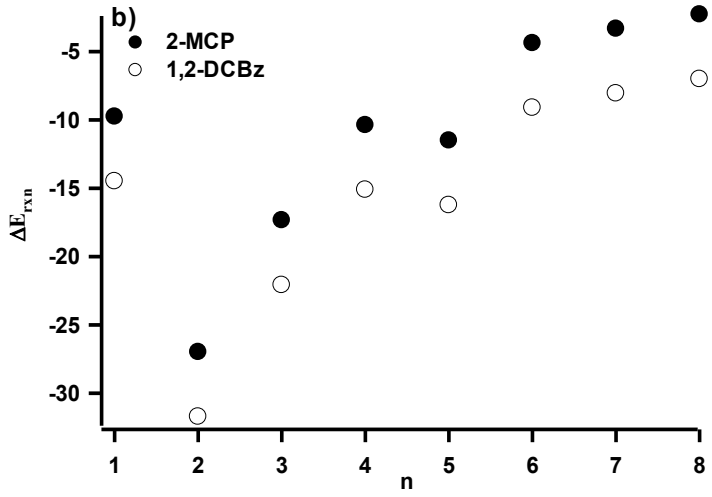

Figure 4.13 Reaction energies of 2-chlorophenol and 1,2-dichlorobenzene adsorbed on copper oxide clusters to yield same surface-bound radicals.

Figure 4.12 and Figure 4.13 displays the reaction energies comparing the adsorption of phenol and MCBz, and 2-CP and 1,2-DCBz using BS2. The reaction energies for the MCBz and 1,2-DCBz are lower than those of phenol and 2-CP. The adsorption of MCBz and 1,2-DCBz was shown to occur at a slower rate in comparison to that involving phenol and 2-CP. The chemisorption of 2-CP occurs 11 times faster than that of a DCBz [9]. This is expected since

chemisorption of 2-CP requires breaking of the phenolic O-H bond, which has a bond dissociation energy of 82 kcal/mol [34] compared to a dissociation of 97 kcal/mol for the C-Cl bond in 1,2-DCBz [35].

4.7 Summary and Relevance to EPFRs Formation

In this chapter, we used three density functionals (B3LYP, PBE1PBE, and M06) and two-sets of basis set (BS1 and BS2) to calculate the reaction energies of EPFRs formation. It was demonstrated that phenolic compounds chemisorbs on surface hydroxyl groups of copper oxide to form surface-bound radicals. First, a water molecule was added to a topological Cu atom, followed by a hydrogen transfer. This resulted in formation of hydroxyl groups and rupture of a bond in $(CuO)_{2\text{-}4}$. The formation of EPFRs was accomplished by adsorption of an organic precursors (phenol, 2-chlorophenol, and 4-chlorophenol) with the hydroxylated clusters. The reaction energies of CuO - Cu_5O_5 EPFRs complexes are more exergonic than Cu_6O_6 - Cu_8O_8 EPFRs complexes. The small clusters are therefore more stable and reactive toward EPFRs formation. The reaction energies of EPFRs formation are similar. However, we note that the reaction energies of 2-chlorophenol adsorption over copper oxide clusters were higher for CuO – Cu_4O_4 compared with energies of phenol and 4-chlorophenol. The instability of CuO – Cu_4O_4-2-chlorophenoxyl complexes is attributed to the interaction of chlorine atom and the oxygen of the copper oxide clusters (cf. Figure 4.4). We also note that the complexes, Cu_6O_6 – Cu_8O_8 of 2-chlorophenoxl are more stable than those of phenoxyl and 4-chlorophenoxyl. The stability is attributed to the interaction of chlorine and Cu or O atom of the cluster (cf. Figure 4.5). An additional Bader charge analysis showed that there was a reduction in Cu atom for small clusters (CuO - Cu_5O_5) and none in large clusters (Cu_6O_6 - Cu_8O_8). This indicates that the catalytic part of the clusters is a small “islands” of the metal oxide clusters.

4.8 References

1. Lomnicki, S., et al., *Copper oxide-based model of persistent free radical formation on combustion-derived particulate matter.* Environmental science & technology, 2008. **42**(13): p. 4982-4988.

2. Vejerano, E., S. Lomnicki, and B. Dellinger, *Formation and Stabilization of Combustion-Generated Environmentally Persistent Free Radicals on an Fe(III)2O3/Silica Surface.* Environmental Science & Technology, 2010. **45**(2): p. 589-594.

3. Vejerano, E., S.M. Lomnicki, and B. Dellinger, *Formation and Stabilization of Combustion-Generated, Environmentally Persistent Radicals on Ni(II)O Supported on a Silica Surface.* Environmental Science & Technology, 2012. **46**(17): p. 9406-9411.

4. Vejerano, E., S. Lomnicki, and B. Dellinger, *Lifetime of combustion-generated environmentally persistent free radicals on Zn(ii)O and other transition metal oxides.* Journal of Environmental Monitoring, 2012. **14**(10): p. 2803-2806.

5. Bae, G.-T., B. Dellinger, and R.W. Hall, *Density Functional Calculation of the Structure and Electronic Properties of CunOn (n = 1−8) Clusters.* The Journal of Physical Chemistry A, 2011. **115**(11): p. 2087-2095.

6. Lomnicki, S. and B. Dellinger, *Formation of PCDD/F from the pyrolysis of 2-chlorophenol on the surface of dispersed copper oxide particles.* Proceedings of the Combustion Institute, 2002. **29**(2): p. 2463-2468.

7. Farquar, G.R., et al., *X-ray Spectroscopic Studies of the High Temperature Reduction of Cu(II)O by 2-Chlorophenol on a Simulated Fly Ash Surface.* Environmental Science & Technology, 2003. **37**(5): p. 931-935.

8. Lomnicki, S. and B. Dellinger, *A Detailed Mechanism of the Surface-Mediated Formation of PCDD/F from the Oxidation of 2-Chlorophenol on a CuO/Silica Surface.* The Journal of Physical Chemistry A, 2003. **107**(22): p. 4387-4395.

9. Alderman, S.L., et al., *An Infrared and X-ray Spectroscopic Study of the Reactions of 2-Chlorophenol, 1,2-Dichlorobenzene, and Chlorobenzene with Model CuO/Silica Fly Ash Surfaces.* Environmental Science & Technology, 2005. **39**(19): p. 7396-7401.

10. Lomnicki, S., et al., *Copper oxide-based model of persistent free radical formation on combustion-derived particulate matter.* Environ Sci Technol, 2008. **42**: p. 4982 - 4988.

11. Altarawneh, M., et al., *A first-principles density functional study of chlorophenol adsorption on CuO (110): CuO.* The Journal of chemical physics, 2009. **130**: p. 184505.

12. Altarawneh, M., et al., *Adsorption of 2-chlorophenol on Cu2O(1 1 1)–CuCUS: A first-principles density functional study.* Applied Surface Science, 2010. **256**(15): p. 4764-4770.

13. Frisch, M.J., et al., *Gaussian 09, Revision B.01*, 2009: Wallingford CT.

14. Becke, A.D., *A new mixing of Hartree--Fock and local density-functional theories.* The Journal of Chemical Physics, 1993. **98**(2): p. 1372-1377.

15. Becke, A.D., *Density-functional thermochemistry. III. The role of exact exchange.* The Journal of Chemical Physics, 1993. **98**(7): p. 5648-5652.

16. Zhao, Y. and D. Truhlar, *The M06 suite of density functionals for main group thermochemistry, thermochemical kinetics, noncovalent interactions, excited states, and transition elements: two new functionals and systematic testing of four M06-class functionals and 12 other functionals.* Theoretical Chemistry Accounts, 2008. **120**(1-3): p. 215-241.

17. Zhao, Y. and D.G. Truhlar, *Density Functional for Spectroscopy: No Long-Range Self-Interaction Error, Good Performance for Rydberg and Charge-Transfer States, and Better Performance on Average than B3LYP for Ground States.* The Journal of Physical Chemistry A, 2006. **110**(49): p. 13126-13130.

18. Perdew, J.P., M. Ernzerhof, and K. Burke, *Rationale for mixing exact exchange with density functional approximations.* The Journal of Chemical Physics, 1996. **105**(22): p. 9982-9985.

19. Perdew, J.P., K. Burke, and M. Ernzerhof, *Generalized Gradient Approximation Made Simple.* Physical Review Letters, 1996. **77**(18): p. 3865-3868.

20. Hay, P.J. and W.R. Wadt, *Ab initio effective core potentials for molecular calculations. Potentials for the transition metal atoms Sc to Hg.* The Journal of Chemical Physics, 1985. **82**(1): p. 270-283.

21. Wadt, W.R. and P.J. Hay, *Ab initio effective core potentials for molecular calculations. Potentials for main group elements Na to Bi.* The Journal of Chemical Physics, 1985. **82**(1): p. 284-298.

22. Hay, P.J. and W.R. Wadt, *Ab initio effective core potentials for molecular calculations. Potentials for K to Au including the outermost core orbitals.* The Journal of Chemical Physics, 1985. **82**(1): p. 299-310.

23. Dunning, J.T.H., *Gaussian basis sets for use in correlated molecular calculations. I. The atoms boron through neon and hydrogen.* The Journal of Chemical Physics, 1989. **90**(2): p. 1007-1023.

24. Yang, Y., M.N. Weaver, and K.M. Merz Jr, *Assessment of the "6-31+ G**+ LANL2DZ" Mixed Basis Set Coupled with Density Functional Theory Methods and the Effective Core Potential: Prediction of Heats of Formation and Ionization Potentials for First-Row-Transition-Metal Complexes.* The Journal of Physical Chemistry A, 2009. **113**(36): p. 9843-9851.

25. Seta, T., et al., *Structures of Hydrated Oxygen Anion Clusters: DFT Calculations for O-(H2O)n, O2-(H2O)n, and O3-(H2O)n (n = 0−4).* The Journal of Physical Chemistry A, 2003. **107**(7): p. 962-967.

26. *Improved grid-based algorithm for bader charge allocation.* J. Comput. Chem., 2007. **28**(5): p. 899.

27. *A fast and robust algorithm for bader decomposition of charge density.* Comput. Mater. Sci., 2006. **36**(3): p. 354.

28. *A fast algorithm to compute atomic charges based on the topology of the electron density.* Theor. Chem. Acc., 2001. **105**(4-5): p. 393.

29. Bader, R.F.W., *Atoms in molecules: a quantum theory*. 1990, USA: Clarendon Press Oxford.

30. *Aim2000-a program to analyze and visualize atoms in molecules.* J. Comput. Chem., 2001. **36**: p. 65.

31. Bork, N., et al., *Ab initio charge analysis of pure and hydrogenated perovskites.* Journal of Applied Physics, 2011. **109**(3): p. 033702-033702-4.

32. Tang, W., E. Sanville, and G. Henkelman, *A grid-based Bader analysis algorithm without lattice bias.* Journal of Physics: Condensed Matter, 2009. **21**(8): p. 084204.

33. Polak, M.L., et al., *Photoelectron spectroscopy of copper oxide (CuO-).* The Journal of Physical Chemistry, 1991. **95**(9): p. 3460-3463.

34. Khachatryan, L., R. Asatryan, and B. Dellinger, *Development of expanded and core kinetic models for the gas phase formation of dioxins from chlorinated phenols.* Chemosphere, 2003. **52**(4): p. 695-708.

35. Tsang, W., *Mechanisms for the Formation and Destruction of Chlorinated Organic Products of Incomplete Combustion.* Combustion Science and Technology, 1990. **74**(1-6): p. 99-116.

CHAPTER 5 - EPFR FORMATION OVER ALUMINUM OXIDE CLUSTERS: A THEORETICAL STUDY

Alumina is second in abundance to silica in combustion and thermal systems, making it significant along with the copper oxides and other transition metals in catalyzing the formation of polychlorinated-*p*-dioxins and polychlorinated dibenzofurans (PCDD/Fs). A recent *ab initio* study of the reactions of 2-chlorophenol (2-CP) over dehydrated and hydroxylated silica structures established the formation of highly stable 2-chlorophenolate [1].

In this study, we used density functional method to investigate the formation of EPFRs from phenol, *o*-chlorophenol, and *p*-chlorophenol on the surface of hydroxylated Al_2O_3 and Al_4O_6 clusters. The study aims to provide insight on a precise molecular basis of surface mediated reactions of physisorption, chemisorption, and electron transfer. The interaction of substituted benzene precursor is the initial and fundamental step in dioxin formation. In addition, we examined frontier molecular orbitals to determine whether radical formation has occurred and, if so, to establish the location of the single electron.

5.1 Computational Details

Equilibrium structures (EQ) of Al_2O_3 and Al_4O_6 clusters were located by *ab initio* automated searches using Global Reaction Route Mapping [2] on potential energy surface (PES) of alumina clusters (GRRM combined with Gaussian 09). GRRM is based on scaled hypersphere search (SHS) developed by Ohno and Maeda [3, 4] which makes it possible to discover reaction networks such as equilibrium structure (EQ), transition structure (TS), and dissociation channel (DC) along the PES connecting various isomers with the same chemical formula, starting from an arbitrary isomer structure [3]. Only EQ structures were searched because of the cost of SHS procedure for GRRM.

Geometry optimization was then carried out on all EQ geometries found by GRRM method using Gaussian 09 program with B3LYP [5] (Becke's 3-parameter exchange functional [6] with Lee-Yarr-Parr correlation energy functional [7] and 6-311+G* basis set [8-11]. The model chemistry, B3LYP/ 6-311+G* basis set was chosen from a pool of several basis sets evaluated for our studies: 6-31G* [12, 13], 6-31++G** [8-11], 6-311G**, 6-311++G** [10, 11], aug-cc-PVDZ [14], and DGDZVP [15, 16]. The EQ0 and EQ0′ elucidated as global minima structures were then used as starting geometry for reactions leading to formation of EPFRs. The geometries of the reactants, transition states, and products involving the reaction of Al_2O_3 and Al_4O_6 with phenol, *o*-chlorophenol, and *p*-chlorophenol were optimized without any symmetric restriction. True minima structures were verified by lack of imaginary frequency. The transition states (TS) were verified through the presence of a one negative frequency. In addition, intrinsic reaction coordinate (IRC) calculations confirm that each TSs is linked to correct reactants and products.

5.2 Geometry Optimization

Figures 5.1 and 5.2 illustrates the topographic map of all the EQ structures obtained relating to Al_2O_3 and Al_4O_6 clusters. For each EQ structure, the spin state is in parentheses and the relative energy with respect to the most stable isomer (EQ0) is as well indicated. Obtained EQs were numbered in the order of increasing energy.

Since full optimization considered several multiplicities, we only report the lowest multiplicity for each isomer. Through our calculations, the D_{2h} rhombus (EQ0, triplet) with non-bridging oxygen atom is found to be the most stable, and this is consistent with other reports [17-19]. The linear geometry (EQ1, singlet) is higher in energy than EQ0 by only 2.4 kcal/mol. However, all the other local minima identified are significantly higher in energy with respect to

EQ0. Chang et al. found out that the energy difference between EQ0 and EQ1 to be ~1.8 kcal/mol using MP2/6-31G(d) model chemistry [20]. The structure of anionic Al_2O_3 has been studied using photoelectron spectroscopy [21]. The rhombus-like with attached oxygen atom was observed to be the true minima. In addition, matrix isolation experiments [22] have been used to identify the structures of Al_2O_3 by comparing their observed IR and Raman bands with the values obtained through calculations [23]. From these experiments, the linear OAlOAlO molecule was found to be the most stable and this was later confirmed to be the case on a singlet potential surface calculation [23].

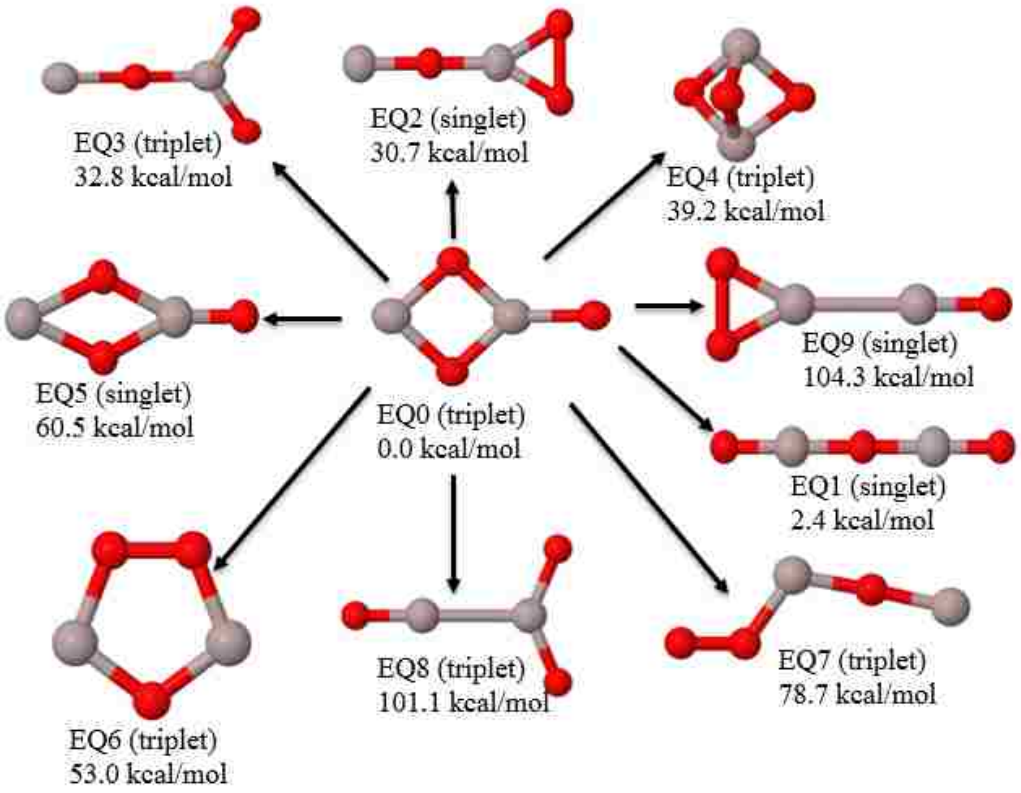

Figure 5.1 Possible isomers of the Al_2O_3 clusters as generated by GRRM. Energies are calculated with respect to EQ0.

In the present work, the linear structure (EQ1) has the lowest energy structure for singlet spin states. However, a comparison of the total energies of the two isomers (linear and rhombus)

shows that the rhombus isomer in the triplet state is the most stable. For Al_4O_6 isomers displayed in Figure 5.2, our minima (EQ0′) agree with other researchers [17, 24]. The EQ1′ is 8.7 kcal/mol higher in energy than EQ0′ where four O and two Al atoms form a planar linking two AlO units. EQ0′ and EQ1′ are in agreement with Ref. [17] with energy difference of 11.3 kcal/mol. The spin states, adiabatic ionization energies, adiabatic electron affinities, and binding energies of the neutral EQ0 and EQ0′ are displayed in Appendix I.

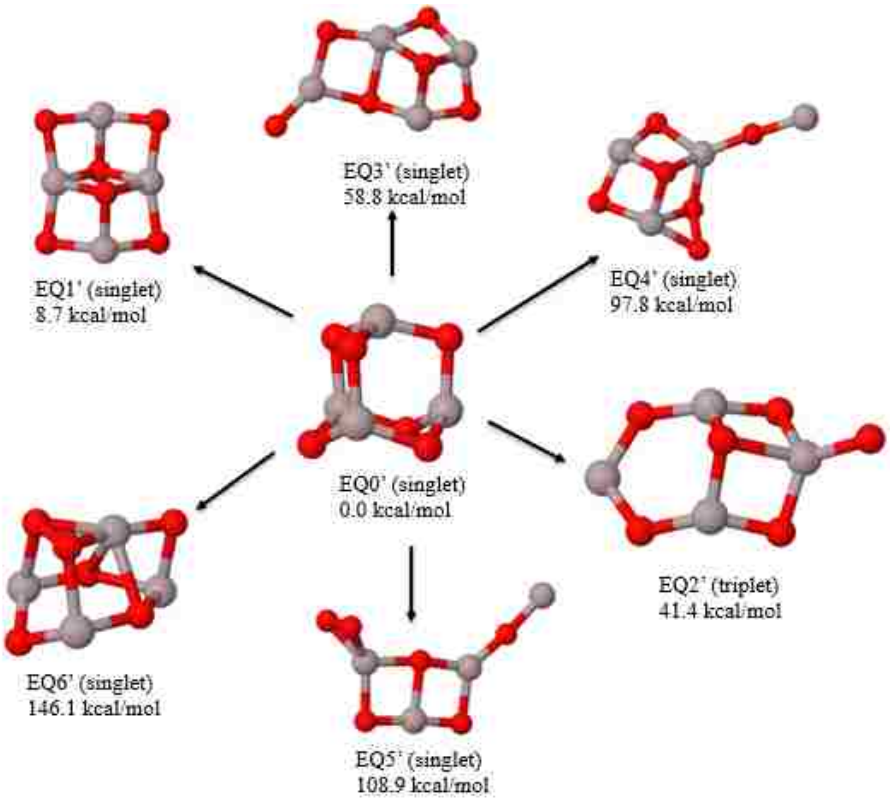

Figure 5.2 Possible isomers of the Al_4O_6 clusters as generated by GRRM. Energies are calculated with respect to EQ0′.

For Al_2O_3 cluster, the spin states for the optimized structures are triplet, doublet, and doublet for the neutral, cation, and anion, respectively. For Al_4O_6 cluster, the spin states for the neutral, cation, and anion are singlet, doublet, and doublet, respectively. The valence configuration of aluminum atom is $3s^2\,3p^1$ and that of the oxygen atom is $2s^2\,2p^4$. Aluminum has 3 valence electrons meaning that it has typical oxidation state of +3, which is commonly found in

all Al compounds including Al_2O_3. The Al-O chemical bond is dominated by ionic character. In both the alumina clusters considered, the valences of both Al and O atoms are saturated and it is expected to result in closed shell configuration. The calculated band gap between the highest occupied molecular orbital (HOMO) and the lowest unoccupied molecular orbital (LUMO) using B3LYP/6-311+G* is 4.31 eV for Al_2O_3 and 5.36 eV for Al_4O_6.

The first step in the formation of EPFRs involved the reaction of the oxide with water followed by a hydrogen transfer to an adjacent oxygen atom resulting in formation of hydroxylated alumina surface. The EPFRs precursor's physisorbs on the hydroxylated surface through hydrogen bonding, followed by chemisorption resulting in the formation of surface-bound radical. The optimized structures of positively charged and negatively charged alumina clusters (EQ0 and EQ0´) are very similar to the corresponding neutral molecule with subtle bond lengths differences. The neutral and cation clusters have identical bond lengths of 1.74 Å and 1.76 Å, respectively.

5.3 Adsorption of Phenolic Compounds with Alumina Clusters

The optimized structures for Al_2O_3 and Al_4O_6 with EPFRs precursors and their respective energies at 298.15 K are shown in Figure 5.3 and Figure 5.4, respectively. The addition of H_2O and subsequent H-transfer did not disrupt the Al_2O_2 rhombus structure (cf. Figure 5.4). Our results are consistent with Gianotto et al. [25] who observed that addition of one or two molecules of H_2O to Al_2O_4H- could not rupture the rhombus structure of an Al_2O_2 [26].

The average bond length of the rhombus structure increased from 1.77 Å to 1.81 Å after reacting with water. The structure of Al_4O_6 was found to undergo ring opening after reacting with water and subsequent hydrogen transfer to an adjacent oxygen atom. The changes in reaction energies, enthalpies, and Gibbs free energies are indicated alongside each pathway. The reaction energy of hydroxylation of Al_4O_6 cluster is more exoergic than that of Al_2O_3 cluster which can be attributed to

the ring strain.

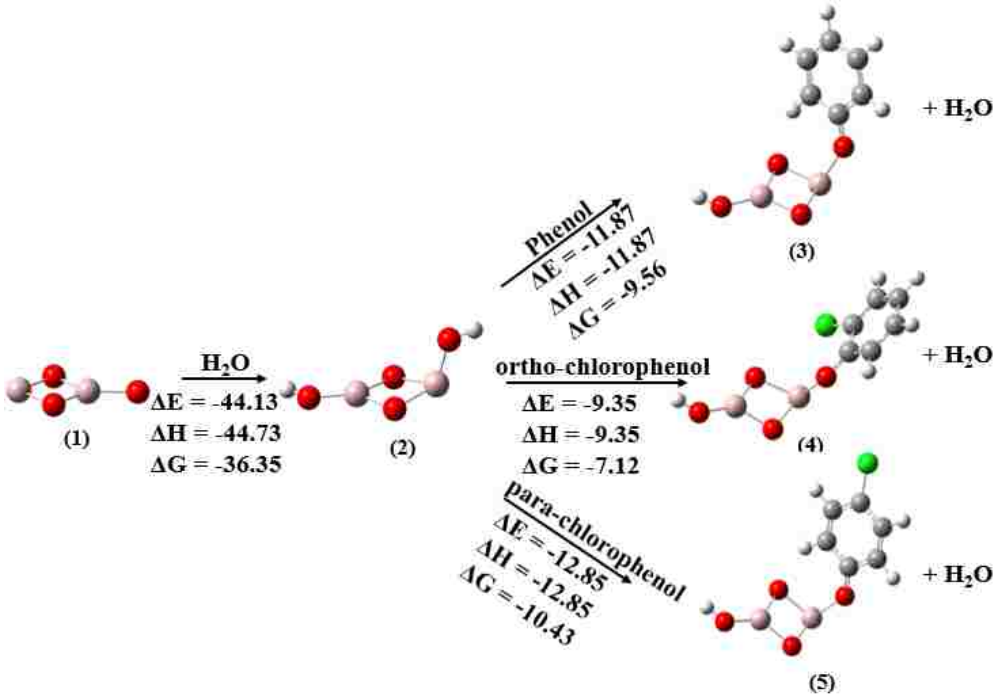

Figure 5.3 Reaction pathway of Al_2O_3 cluster. Atom colors are as follows: Aluminum : pink, oxygen: red, carbon: gray, hydrogen: white, and chlorine: green.

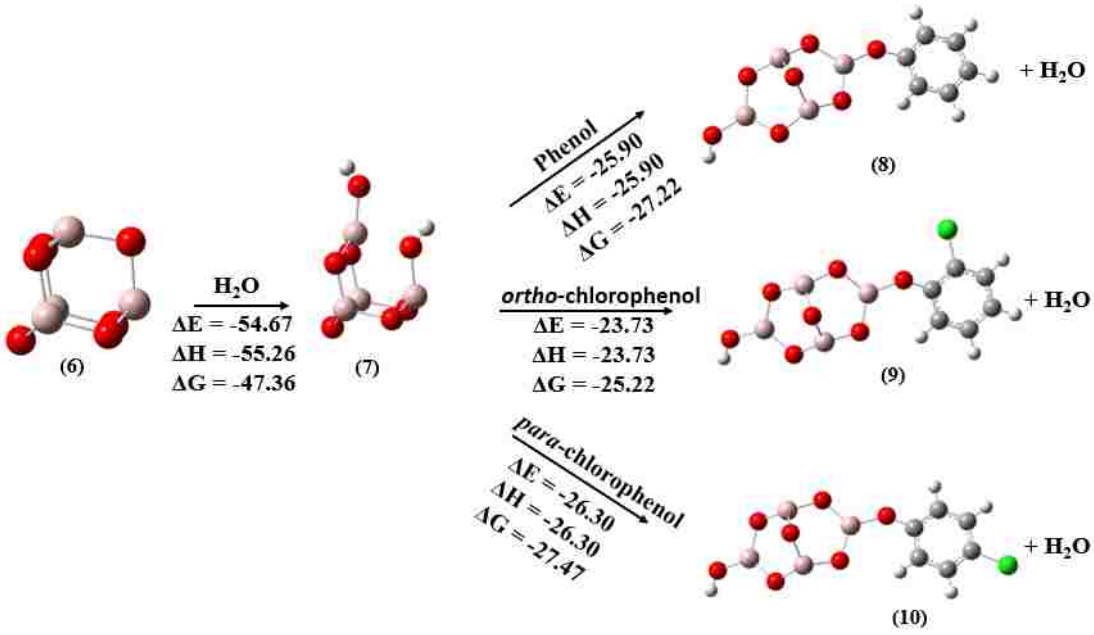

Figure 5.4 Reaction pathway of Al_4O_6 cluster. Atom colors are the same as in Figure 5.3.

We further note that the energies and enthalpies of the aluminum oxide- chlorinated

phenols are similar while Gibbs energies are slightly different from the reaction energies and enthalpies. The aluminum oxide *o*-chlorophenol complexes are slightly unstable compared with their counterparts (EPFRs of phenol and *p*-chlorophenol), which can be attributed to inductive, electrostatic repulsion as well as steric effects. Figures 5.5 and 5.6 displays optimized structures of reactants, transition states, and products involved in formation of different EPFRs. In both cases, phenol, *o*-chlorophenol, and *p*-chlorophenol physisorbed on Al-O bridge through hydrogen bonding between the O atom of the EPFRs precursor and Al atom to form the reactant complex 1, 2, 3, 7, 8, and 9 respectively.

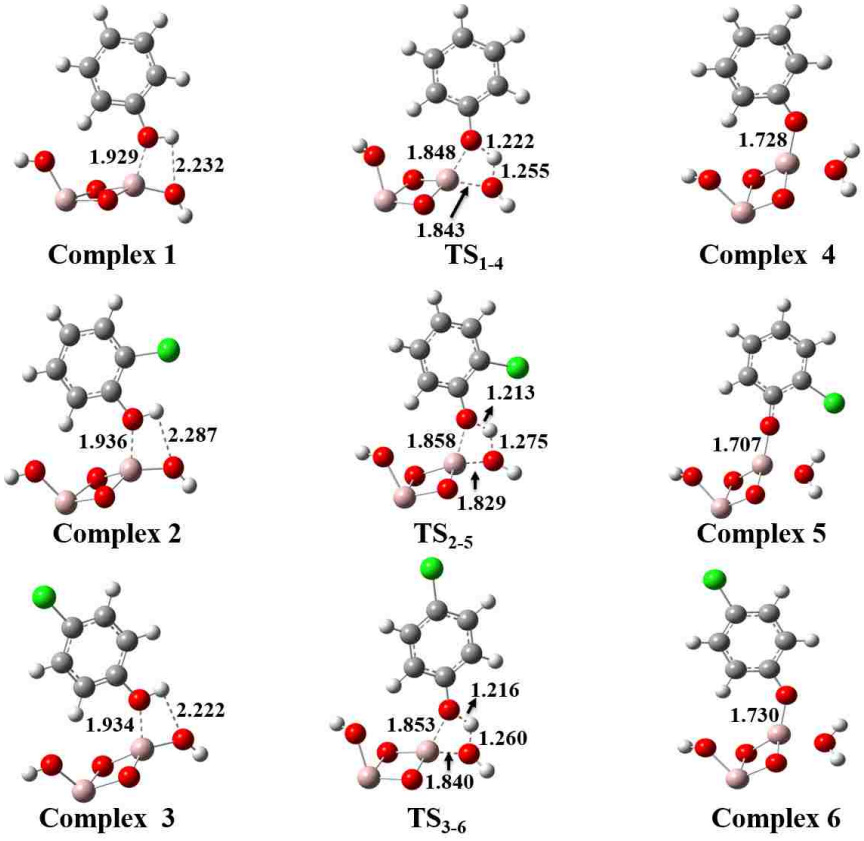

Figure 5.5 Optimized geometries involved in the reaction of phenol, o-chlorophenol, and p-chlorophenol with Al_2O_3 cluster. The values in parentheses at the bottom of the geometries denote the relative energies with respect to the isolated reactants and the bond lengths in angstrom.

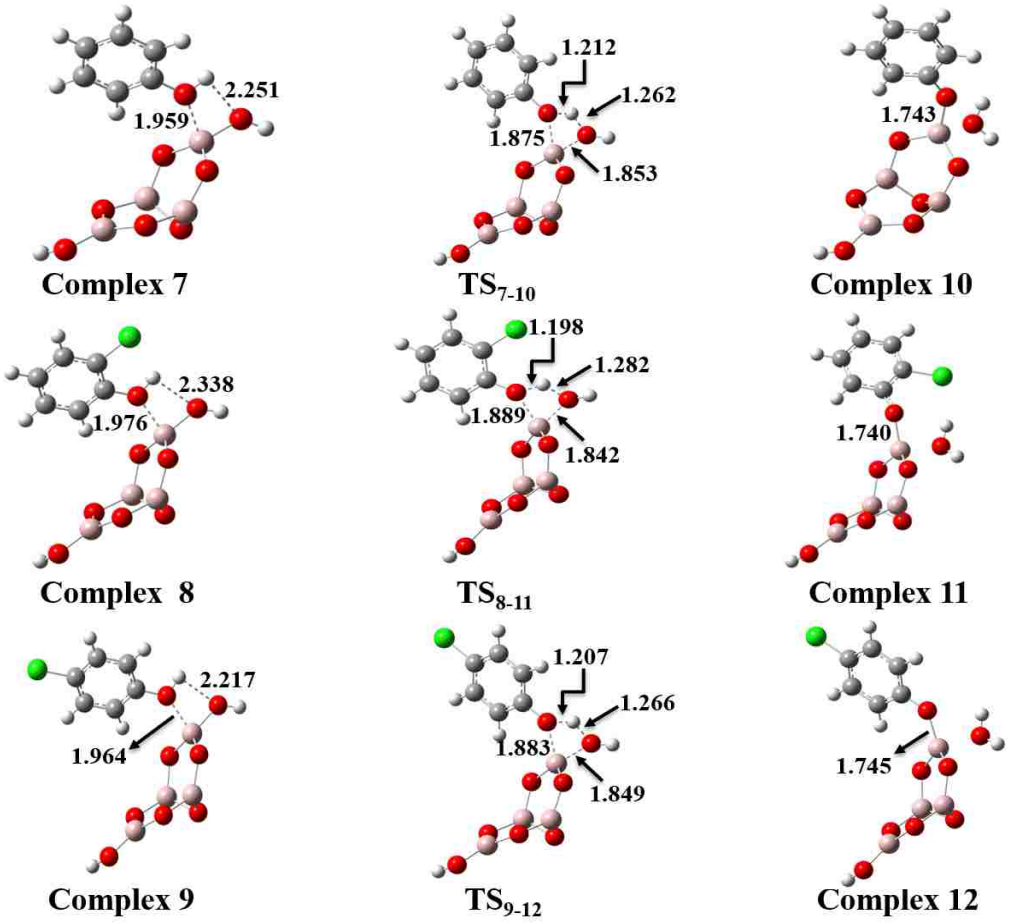

Figure 5.6 Optimized geometries involved in the reaction of phenol, o-chlorophenol, and p-chlorophenol with Al_4O_6 cluster. The values in parentheses at the bottom of the geometries denote the relative energies with respect to the isolated reactants and the bond lengths in angstrom.

This physisorption step is identified to be exothermic by -14.3, -12.7, and -13.4 kcal/mol for complexes 1, 2, and 3, respectively. The complexes are then chemisorbed on the surface through a four-membered ring ($TS_{1\text{-}4}$, $TS_{2\text{-}5}$, and $TS_{3\text{-}6}$) characterized by Gibbs free energies of activation, $\Delta G^{\ddagger}$, of 7.8, 9.1, and 7.9 kcal/mol with respect to isolated reactants. In all the transition states, the distance between the phenolic oxygen of the adsorbates approaching the Al atom of the cluster decreases dramatically from the physisorbed structures to the transition state complexes. For instance, while moving from Complex 1 → $TS_{1\text{-}4}$ the bond length changes from 1.929 Å to 1.848 Å. At the same time, the hydroxyl H atom of the organic compound approaches

the O atom of the alumina cluster. For example, in the case of Complex 1 → $TS_{1\text{-}4}$, the H-O bond length goes from 2.232 Å → 1.222 Å. In the final product (Complex 4, 5, and 6) the bond length between the phenolic O atom of the organic compound and the Al atom shortens to 1.728 Å, 1.707 Å, and 1.730 Å, respectively. We note that the O-Al bond of Al_2O_3-*o*-chlorophenoxyl is shorter by ~0.3 Å compared with Al_2O_3-phenoxyl and Al_2O_3-*p*-chlorophenoxyl complexes. The forward IRC calculations show the final products to be adsorbed phenoxyl (complex 4), *o*-chlorophenoxyl (complex 5), and *p*-chlorophenoxyl (complex 6) radicals along with departing water molecule. The details of reactions' mechanism depicted in Figure 5.6 are similar to that discussed above. However, it is interesting to note that the phenolic O-Al bond length of the products (Complex 10, 11, and 12) is approximately similar. The Complexes are characterized by Gibbs free energies of activation, $\Delta G^{\ddagger}$, of 28.5, 27.2, and 28.4 kcal/mol with respect to isolated reactants. The reactions of Al_4O_6 produce relatively stable complexes 10 – 12 than those of Al_2O_3 (complexes 4-6) (cf. Figures 5.5 and 5.6). This is a clear indication that the reactions of EPFRs precursors depend relatively on the size of the cluster.

5.4 The Potential Energy Surface Profiles

The potential energy surface depicting the connections of the investigated pathways are shown in Figures 5.7 and 5.8 where the reactants and products connected via TSs are obtained by optimizing the structures from IRC calculations. The optimized geometries of the various reactants, transition states, and products were illustrated previously (*vide infra*). As depicted in Figure 5.7, the activation energies relative to the pre-reactive complexes for Al_2O_3 cluster with phenol, *o*-chlorophenol, and *p*-chlorophenol are 22.1, 21.8, and 21.3 kcal/mol, respectively. Similarly, the activation energies relative to the pre-reactive complexes for Al_4O_6 cluster with phenol, *o*-chlorophenol, and *p*-chlorophenol are 8.7, 7.9, and 8.1 kcal/mol, respectively (cf.

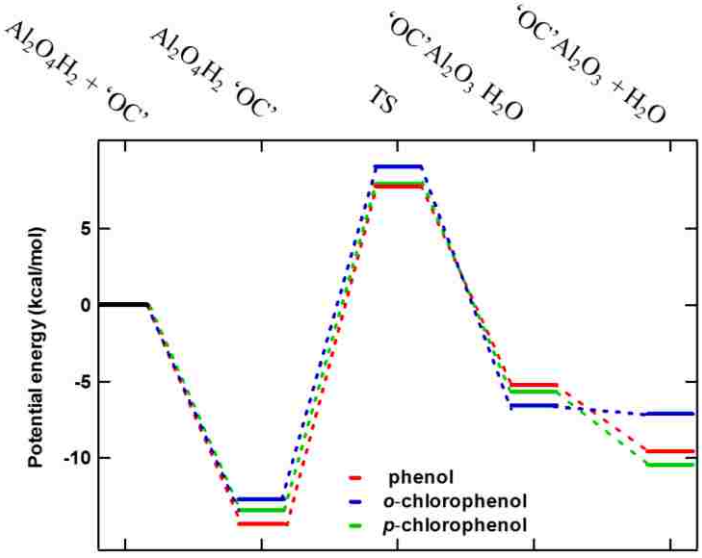

Figure 5.7 Relative potential energy of the reactions of phenol, *o*-chlorophenol, and *p*-chlorophenol over Al_2O_3 cluster. 'OC' is shorthand for organic compound'.

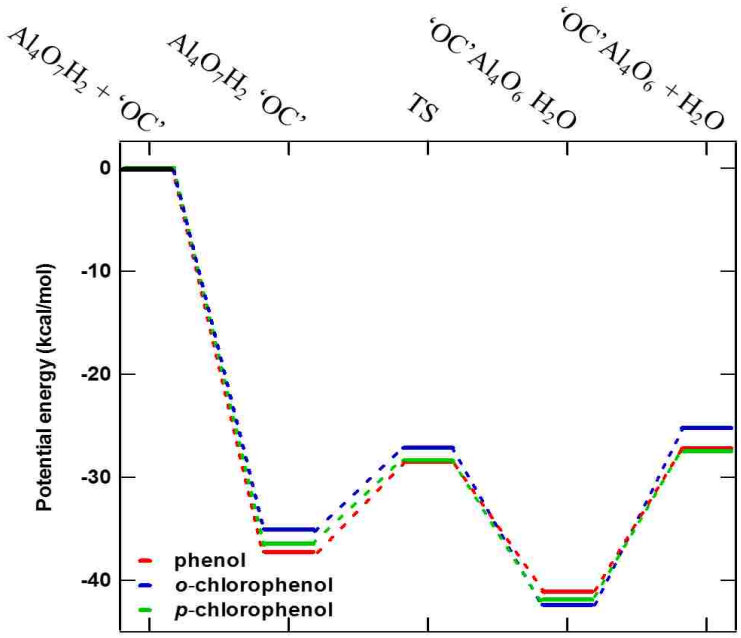

Figure 5.8 Relative potential energy of the reactions of phenol, o-chlorophenol, and p-chlorophenol over Al_4O_6 cluster. 'OC' is shorthand for organic compound'.

Figure 5.8). The Gibbs free energies and the entropies for all the reactants, transition states, and products are depicted in the Appendix I. From the above results, it is clear that Figure 5.8 is the

most dynamically favorable and hence results in formation of most thermodynamically stable EPFRs. This fact indicates that cluster size of alumina plays a crucial role in PCDD/Fs formation. The reaction energies of Al_2O_3 and Al_4O_6 clusters in the formation of EPFRs lead to exoergic reactions. This is in agreement with the experimental observations that aluminum oxide catalyze PCDD formation from structurally related precursors [27, 28].

5.5 EPFRs Molecular Orbital

We also investigated the frontier molecular orbitals to establish the location of the unpaired electron in the alumina-EPFR complex. Figure 5.9 shows that the highest occupied molecular orbital (HOMO), which is the singly occupied orbital, is located at the phenoxyl part of the system. Our calculated results are consistent with the electron paramagnetic resonance (EPR) experiments [28].

5.6 Summary and Relevance to EPFRs Formation

We carried out density functional study of formation of EPFRs over aluminum oxide clusters. The mechanism involves physisorption, chemisorption, and an electron transfer from

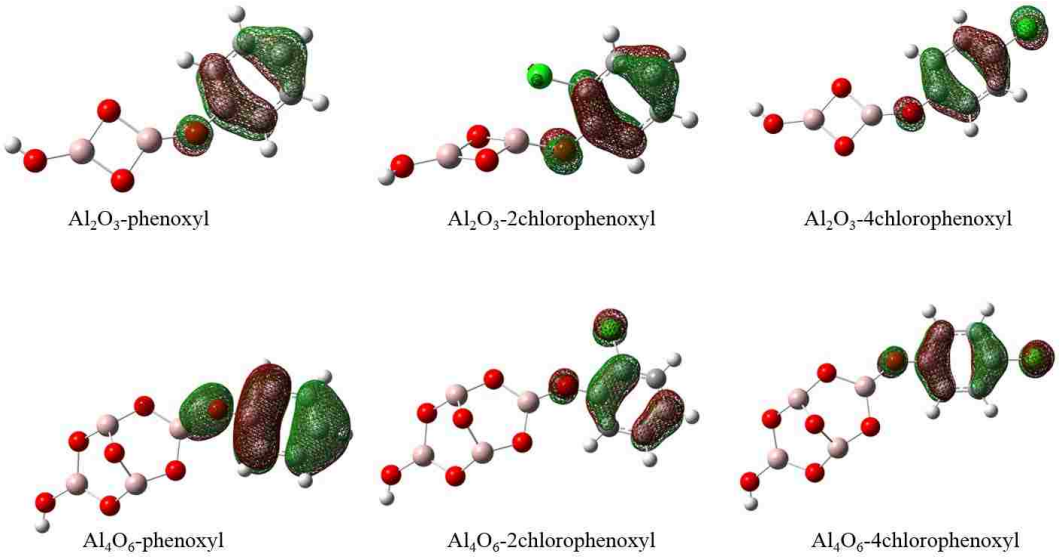

Figure 5.9 Frontier Molecular orbitals of optimized geometries of EPFRs-complexes showing the location of the unpaired electron.

the adsorbate to the metal cationic center. The overall reaction of aluminum oxide with the EPFRs precusors (phenol, 2-chlorophenol, and 4-chlorophenol) are significantly exergonic indicating that alumina is a likely catalyst in EPFRs formation. The hydroxylated Al_4O_6 cluster is more exergonic and hence, more reactive than the Al_2O_3 cluster. 2-chlorophenol adsorbs weakly to the surface due to the displacement of both the oxygen of the aluminum oxide cluster and the chlorine atom of the phenolic compound.

In additional study of frontier molecular orbitals, the unpaired electron was shown to be located in the phenoxly part of the complex. This was in good agreement with the experimental findings of electron paramagnetic resonance (EPR) spectroscopy. The results clearly indicates the alumina important in EPFRs formation and also significant in PCDD/Fs formation.

5.7 References

1. Pan, W., et al., *Theoretical Study of the Reactions of 2-Chlorophenol over the Dehydrated and Hydroxylated Silica Clusters.* The Journal of Physical Chemistry A, 2011. **116**(1): p. 430-436.

2. Inc., H.S. *Automated Exploration of Chemical Reaction Pathways GRRM ~Global Reaction Route Mapping~.* [cited 2013 8/31/2013]; Available from: http://www.hpc.co.jp/eng/product_grrm.html.

3. Ohno, K. and S. Maeda, *A scaled hypersphere search method for the topography of reaction pathways on the potential energy surface.* Chemical Physics Letters, 2004. **384**(4–6): p. 277-282.

4. Maeda, S. and K. Ohno, *Global mapping of equilibrium and transition structures on potential energy surfaces by the scaled hypersphere search method: applications to ab initio surfaces of formaldehyde and propyne molecules.* The Journal of Physical Chemistry A, 2005. **109**(25): p. 5742-5753.

5. Stephens, P.J., et al., *Ab Initio Calculation of Vibrational Absorption and Circular Dichroism Spectra Using Density Functional Force Fields.* The Journal of Physical Chemistry, 1994. **98**(45): p. 11623-11627.

6. Becke, A.D., *A new mixing of Hartree–Fock and local density-functional theories.* The Journal of Chemical Physics, 1993. **98**: p. 1372.

7. Lee, C., W. Yang, and R.G. Parr, *Development of the Colle-Salvetti correlation-energy formula into a functional of the electron density.* Physical Review B, 1988. **37**(2): p. 785.

8. Hehre, W.J., R. Ditchfield, and J.A. Pople, *Self---Consistent Molecular Orbital Methods. XII. Further Extensions of Gaussian---Type Basis Sets for Use in Molecular Orbital Studies of Organic Molecules.* The Journal of Chemical Physics, 1972. **56**(5): p. 2257-2261.

9. Dill, J.D. and J.A. Pople, *Self-consistent molecular orbital methods. XV. Extended Gaussian-type basis sets for lithium, beryllium, and boron.* The Journal of Chemical Physics, 1975. **62**(7): p. 2921-2923.

10. Clark, T., et al., *Efficient diffuse function-augmented basis sets for anion calculations. III. The 3-21+G basis set for first-row elements, Li–F.* Journal of Computational Chemistry, 1983. **4**(3): p. 294-301.

11. Krishnan, R., et al., *Self-consistent molecular orbital methods. XX. A basis set for correlated wave functions.* The Journal of Chemical Physics, 1980. **72**(1): p. 650-654.

12. Francl, M.M., et al., *Self-consistent molecular orbital methods. XXIII. A polarization-type basis set for second-row elements.* The Journal of Chemical Physics, 1982. **77**(7): p. 3654-3665.

13. Rassolov, V.A., et al., *6-31G[sup *] basis set for atoms K through Zn.* The Journal of Chemical Physics, 1998. **109**(4): p. 1223-1229.

14. Dunning, J.T.H., *Gaussian basis sets for use in correlated molecular calculations. I. The atoms boron through neon and hydrogen.* The Journal of Chemical Physics, 1989. **90**(2): p. 1007-1023.

15. Godbout, N., et al., *Optimization of Gaussian-type basis sets for local spin density functional calculations. Part I. Boron through neon, optimization technique and validation.* Canadian Journal of Chemistry, 1992. **70**(2): p. 560-571.

16. Sosa, C., et al., *A local density functional study of the structure and vibrational frequencies of molecular transition-metal compounds.* The Journal of Physical Chemistry, 1992. **96**(16): p. 6630-6636.

17. Li, R. and L. Cheng, *Structural determination of (Al2O3)n (n=1–7) clusters based on density functional calculation.* Computational and Theoretical Chemistry, 2012. **996**(0): p. 125-131.

18. Woodley, S.M., *Atomistic and electronic structure of (X2O3) n nanoclusters; n= 1–5, X= B, Al, Ga, In and Tl.* Proceedings of the Royal Society A: Mathematical, Physical and Engineering Science, 2011. **467**(2131): p. 2020-2042.

19. Rahane, A.B., M.D. Deshpande, and V. Kumar, *Structural and Electronic Properties of (Al2O3)n Clusters with n = 1–10 from First Principles Calculations.* The Journal of Physical Chemistry C, 2011. **115**(37): p. 18111-18121.

20. Chang, C., et al., *Ab initio studies of stationary points of the AlO molecule.* The European Physical Journal D-Atomic, Molecular, Optical and Plasma Physics, 1998. **2**(1): p. 57-62.

21. Desai, S.R., et al., *A study of the structure and bonding of small aluminum oxide clusters by photoelectron spectroscopy: AlO (x= 1–2, y= 1–5).* The Journal of chemical physics, 1997. **106**: p. 1309.

22. Andrews, L., T.R. Burkholder, and J.T. Yustein, *Reactions of pulsed-laser evaporated aluminum atoms with oxygen: infrared spectra of the reaction products in solid argon.* The Journal of Physical Chemistry, 1992. **96**(25): p. 10182-10189.

23. Nemukhin, A.V. and F. Weinhold, *Structures of the aluminum oxides studied by ab initio methods with natural bond orbital analysis.* The Journal of Chemical Physics, 1992. **97**(5): p. 3420-3430.

24. Sun, J., et al., *Theoretical Study on (Al2O3)n (n = 1–10 and 30) Fullerenes and H2 Adsorption Properties.* Inorganic Chemistry, 2008. **47**(7): p. 2274-2279.

25. Gianotto, A.K., et al., *Hydration of Alumina Cluster Anions in the Gas Phase.* Journal of the American Chemical Society, 2004. **126**(26): p. 8275-8283.

26. Scott, J.R., et al., *Experimental and Computational Study of Hydration Reactions of Aluminum Oxide Anion Clusters.* The Journal of Physical Chemistry A, 2000. **104**(30): p. 7079-7090.

27. Vončina, E. and T. Šolmajer, *Thermolysis of 2, 4, 6-trichlorophenol chemisorbed on aluminium oxides as example of fly ash mediated surface catalysis reaction in PCDD/PCDF formation.* Chemosphere, 2002. **46**(9): p. 1279-1286.

28. Patterson, M.C., et al., *EPFR formation from phenol adsorption on Al2O3 and TiO2: EPR and EELS studies.* Chemical Physics, (0).

CHAPTER 6 - EPFR YIELD DEPENDENCE ON COPPER CONCENTRATION

The concentration of metals in particulate matter may vary a lot. In ambient particulate matter (aerodynamic diameter < 2.5μm, PM2.5), 1-5*10^3, 0.1-0.3, ~2.0, and 0.5-20*10^3 μg/g of Fe, Ni, Cu, and Zn has been reported [1-5]. Previous studies of EPFRs that used the same concentrations of metals (5% by weight as oxide) in particulates indicated that almost any transition metal that was under study yielded EPFRs on particle surfaces [6-9]. Large distribution of metal concentration in particulate matter raises a question of how the metal concentration affects yield, lifetime, and chemical reactivity of the EPFRs. One can anticipate that changing concentration of metal in particulate will affect the metal oxide clusters' size and reactivity. In fact, the size of metal/metal oxide clusters has been reported to be a pivotal property in the catalytic activity [10-15]. Changing catalytic properties may affect the propensity of the metal oxides to form EPFRs and contribute to different chemical behavior of EPFRs. In this chapter we are attempting to answer the above question using copper oxide clusters as an example. Silica (Cabosil) based synthetic particulates containing varying concentrations of CuO (0.25-5% by weight) were tested for EPFRs yield and persistence.

6.1 Transition Metal Assisted Formation of Stable Organic Radicals

The chemisorption and catalytic mechanism have been reported to result in the formation of particle-bound radicals. Our recent studies on the surrogates of metal oxide particles have shown that metal ions can interact with the functionalized aromatic molecules to produce surface stabilized EPFR [16]. Chemisorption of the organic molecules on the surface of metal oxides leads to the formation of surface-molecule complexes that undergoes electron transfer to form surface-associated EPFRs. (cf. Scheme 6.1). Depending on the structure and

nature of the adsorbate, the radical may be a phenoxyl or semiquinone-type EPFR with characteristic EPR g-values of 2.0035-2.0045 (as g2-type) and 2.006-2.007 (as g3-type), respectively. The electron transferred from the adsorbate to the metal ion center can be trapped in the solid matrix forming an F-center that is also a source of an EPR signal with a low g-value of

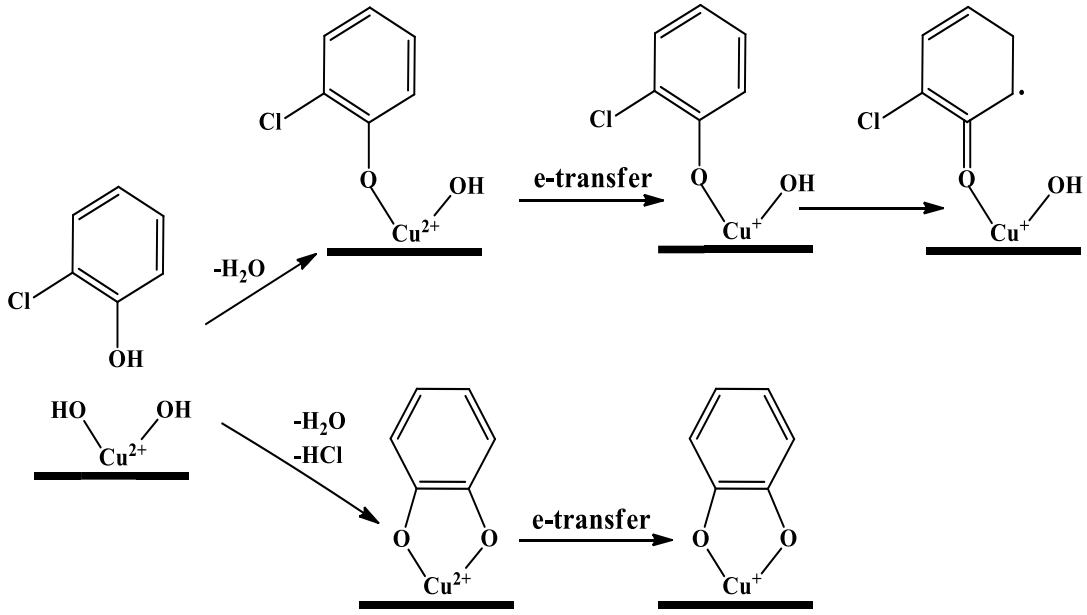

Scheme 6.1 General mechanism of EPFRs formation from 2-chlorophenol at Cu^{2+} sites on a CuO/silica Particle.

2.001-2.002.

6.2 EPFRs Formation on Different CuO/SiO_2 Concentrations

Adsorption of aromatic precursors on the CuO supported on silica at 230 ^{0}C resulted in appearance of EPR signal centered at ~3400 G with a narrow line width ΔH_{p-p} ~ 5-7 G for phenol and 2-chlorophenol, and a broader line width ΔH_{p-p} ~ 8-16 G of 1,2-dichlorobenzene. Figure 6.1 shows the EPR spectra with complex features and unresolved hyperfine splitting for phenol, 2-CP, and 1,2-DCBz adsorbates.

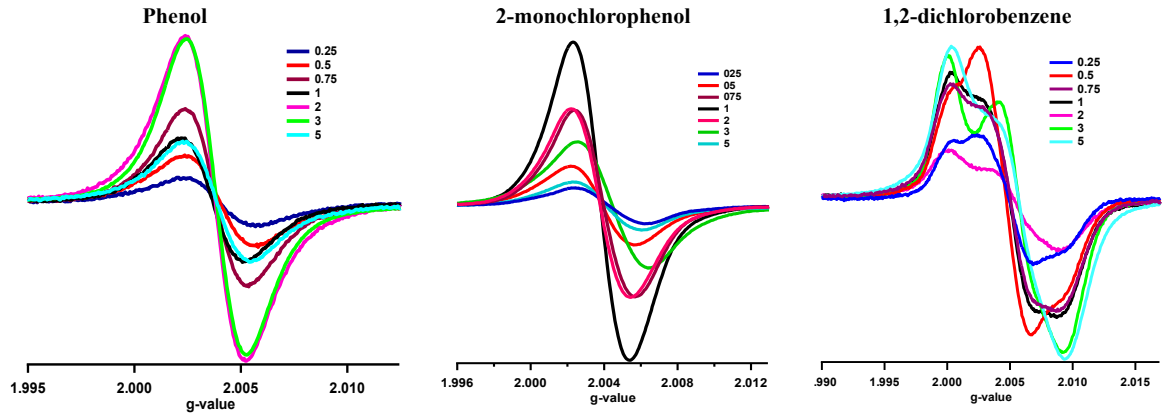

Figure 6.1 Concentration dependence of the EPR spectra of phenol, 2-CP, and 1,2-DCBz dosed at 230 ^{0}C on different concentrations of CuO/SiO_2.

Table 6.1 Spectral characteristics of EPFRs formed on different Cu(II)O loading on silica matrix from different adsorbates at 230 ^{0}C.

% CuO	g-value			ΔH_{p-p}		
	2-CP	DCBz	PH	2-CP	DCBz	PH
5	2.0042	2.0060	2.0039	6.7	16.0	5.2
3	2.0044	2.0057	2.0039	6.9	15.9	4.8
2	2.0039	2.0053	2.0039	5.5	15.3	5.4
1	2.0038	2.0050	2.0037	5.3	15.2	5.3
0.75	2.0040	2.0051	2.0039	5.6	14.2	5.2
0.5	2.0040	2.0048	2.0040	6.1	7.4	5.4
0.25	2.0040	2.0050	2.0038	6.0	7.7	4.6

Table 6.1 presents the spectral parameters of each adsorbate. These paramagnetic signals arise due to the interaction of hydroxyl- and chlorine substituted molecules with metal oxide surface. The general mechanism of EPFRs formation has been established and confirmed in our previous studies of copper, iron, nickel, zinc oxides, titania, and alumina [7, 9, 17, 18]. The molecular precursors react with the surface-hydroxyl groups and chemisorbs via elimination of H_2O/HCl resulting in surface-bound EPFR. This interaction results in a 1-electron transfer to the

metal cationic center. The general scheme for the reaction is presented for substituted 2-chlorophenol with Cu^{2+} on a particle surface (cf. Scheme 6.1).

6.2.1 Radical Speciation

Precursor - metal oxide interaction may result in more than one type of EPFR depending on the number and position of the substituent in the aromatic precursor [17] with the overall EPR spectrum being a superposition of those species [6-9]. Depending on the relative concentration of g2 and g3 type of radicals, an overall shift of g-value of the EPR signal is observed. In the current study, the overall g-values for the EPFRs species for phenol and 2-CP were similar (~2.0037 – 2.0044) with a shift towards lower g-values for phenol (cf. Figure 6.2) [7, 9].

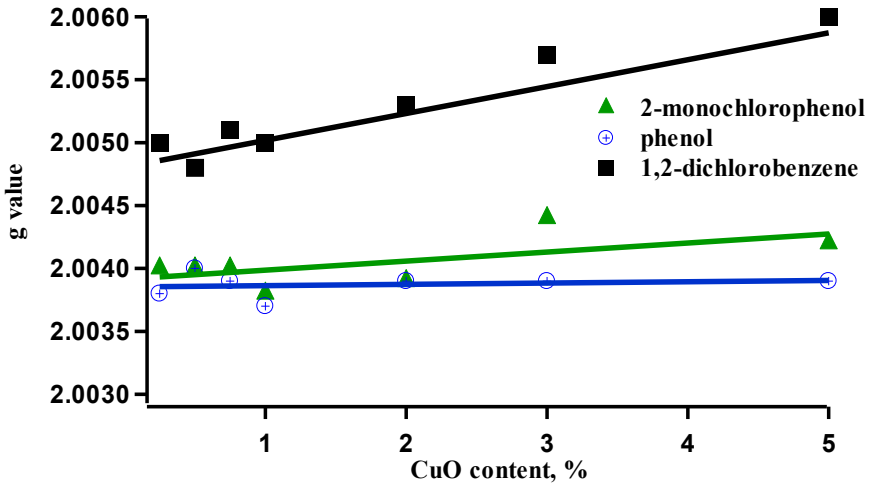

Figure 6.2 Overall g values of radical signal with changing CuO content in particles.

For phenol adsorption, the resulting radical signals did not change either the position or the line width with respect to concentration of copper oxide on silica (cf. Figures 6.2, 6.3, Table 6.1). Thus, it is evident that no change of radical speciation occurred with decreasing CuO content. Based on the spectral parameters from previous studies of silica supported on 5% CuO,

Fe_2O_3, and NiO, as well as the current results, formation of a phenoxyl type radical on the surface of all copper concentrations can be concluded [7, 9, 17, 19]. The narrower spectrum width indicates a rather vertical orientation of the phenol adsorption which is typical in metal oxide and metallic surfaces [20, 21].

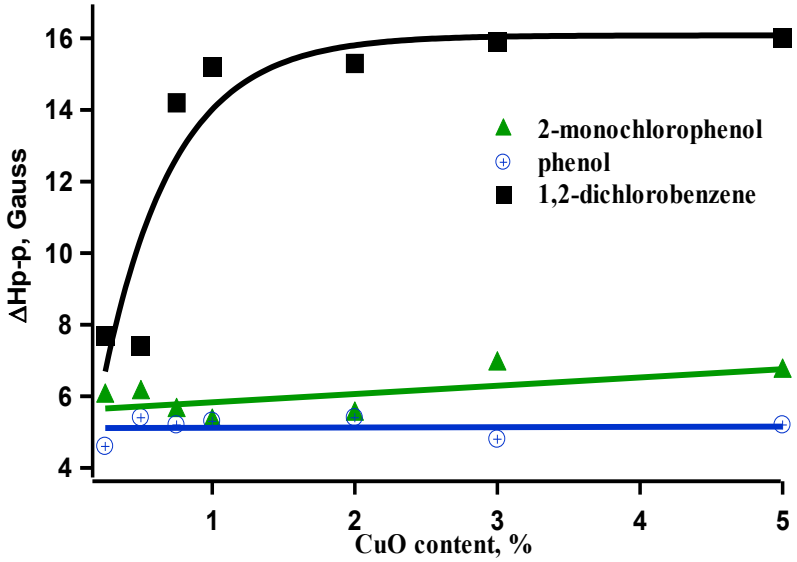

Figure 6.3 Change of $\Delta H_{p\text{-}p}$ of EPR spectra with changing CuO content.

For adsorption of 2-CP, the overall g-value of spectra for all CuO concentrations changed only slightly with copper content and oscillates within the range of 2.0038 - 2.0044. Based on the above finding, we conclude that majority of radicals are of chlorophenoxyl type [22]. Thus, the overall peak width, $\Delta H_{p\text{-}p}$, was larger on average by 1 gauss for the radical species resulting from adsorption of 2-chlorophenol compared with phenol adsorption (*vide infra*). This indicates contribution of another radical species in the spectrum of 2-chlorophenol exposed samples and it is believed to originate from semiquinone radicals that are formed by interaction of both chlorine and hydroxyl groups with the surface (cf. scheme 6.1). This is similar to the results obtained

from other metal oxides [7, 9, 17, 18]. Interestingly, unlike in the case of phenol, the peak width broadens with increase in g-value (*vide infra*).

1,2-Dichlorobenzene chemisorption on copper oxide-containing particles resulted in highly asymmetric EPR spectra and high g-values (>2.0048) and line-width (~7.7 – 16 G) compared with those resulting from adsorption of phenol and 2-chlorophenol (*vide infra*). A high contribution of the *o*-semiquinone radicals to the overall spectrum is anticipated for 1,2-dichlorobenzene as observed in other metals. Indeed, 1,2-dichlorobenzene adsorption has been reported to proceed with simultaneous displacement of both chlorine atoms, resulting in

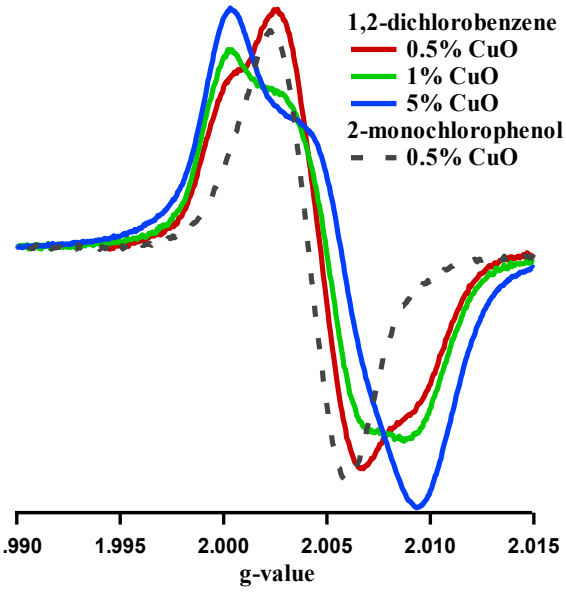

Figure 6.4 EPR spectra from the adsorption of 1,2-dichlorobenzene and 2-chlorophenol on the particles containing different copper oxide concentration**.**

formation of predominantly *o*-semiquinone radicals [23]. However, there can be seen a distinct spectral change with decreasing copper content (cf. Figure 6.1) when the overall g-values of the spectra is decreasing (cf. Figure 6.2). Observed dramatic spectral changes result from changing speciation of the formed radicals from predominantly *o*-semiquinone species to a more balanced ratio of chlorophenoxyl to *o*-semiquinone radicals. Decreasing spectral width also supports this

conclusion (cf. Figure 6.4). For 0.5% CuO adsorption of 1,2-dichlorobenzene produces a spectrum that resembles more the spectrum that results from adsorption of 2-chlorophenol than the one that results from higher concentrations of CuO exposed to 1,2-dichlorobenzene (cf. Figure 6.4).

6.2.2 Surface Radical Density

Surface concentration of radicals formed upon adsorption of precursors on CuO/silica samples is dependent on the concentration of copper oxide (cf. Figures 6.5 and 6.6). In general, adsorption of 2-chlorophenol resulted in the highest concentration of radicals on the surface, with the maximum yield at ~1% CuO content.

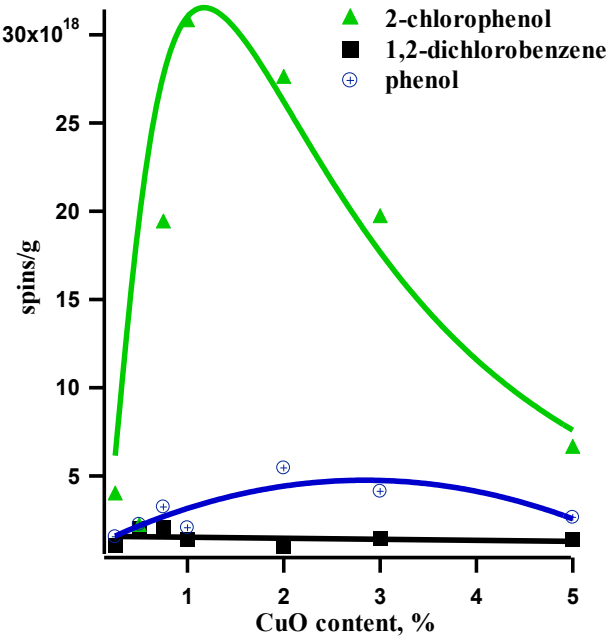

Figure 6.5 Concentrations of organic EPFR adsorbed at 230 ^{0}C for different CuO content based on a sample mass.

Above that concentration, the yield drops rapidly (cf. Figure 6.5). The adsorption of 2-CP occurs 11 times faster than that of a DCBz [23]. This is expected since chemisorption of 2-CP requires

breaking of the phenolic O-H bond, which has a bond dissociation energy of 82 kcal/mol [24] compared with 97 kcal/mol for the C-Cl bond in 1,2-DCBz [25].

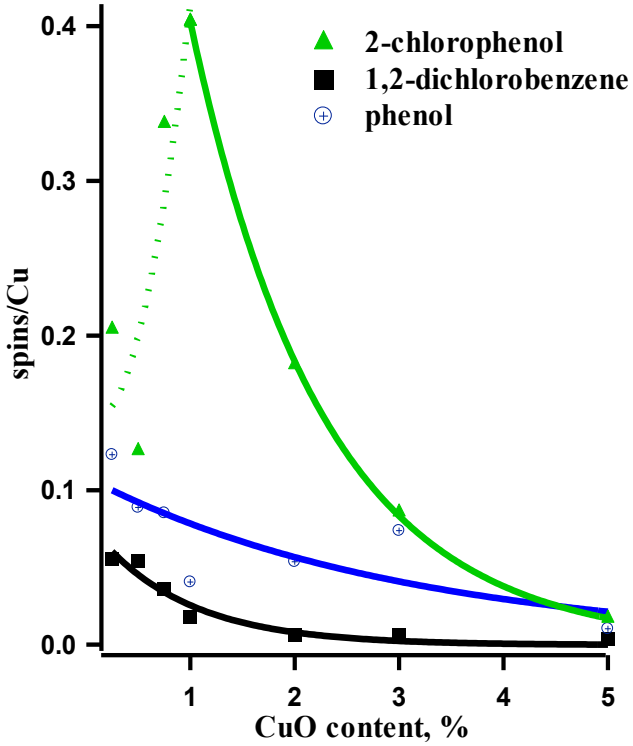

Figure 6.6 Dependence of EPFR density with metal concentration dosed with 1, 2-Dichlorobenzene, 2-chlorophenol, and phenol on different CuO concentrations on silica.

Since only copper sites are active in the formation of radicals, a linear correlation between the radical yield and copper content should be expected. However, as presented in Figure 6.6, this is not the case. An exponential increase in radical density per copper atom was observed between 5 and 1% CuO content, with radical density drop-off below 1%. The exponential increase in radical density can be as a result of the non-uniform size distribution of CuO clusters on the surface. This suggests that as CuO concentration decreases, the average size of the CuO cluster also decreases but the number of surface available (copper sites) increases. In fact, at the maximum surface radical density (1% CuO for CP), 1 radical is formed for every ~2

copper atoms in the samples. Considering the fact that once a copper site is occupied by an adsorbed radical the surface access to all neighboring sites is hindered, we can assume a close to complete saturation of the surface sites with adsorbate at 1% CuO. Below 1% CuO content, a small drop of radical density from 2-CP precursor can be observed (cf. Figure 6.6). We speculate that all copper sites are surface available on the 1% CuO content and further decrease in copper oxide concentration results in smaller CuO clusters. At this point, two explanations of the lower radical density are plausible: i) for very small clusters, electron transfer from adsorbate to metal center is unfavorable and radical stabilization is unlikely or ii) with decreasing cluster size steric constrictions are more significant.

Phenol adsorption over CuO containing particles results in both lower EPFR yield and radical density, when compared with 2-chlorophenol (*vide infra*). In this case, a maximum yield of radicals is detected between 2-3 % CuO content. The differences in the radical yield of 2-chlorophenol and phenol result from the effect of *ortho* group substituent [7, 9]. On the other hand, the surface radical density increase exponentially with decreasing copper oxide content. Increase in radical density below 1% copper oxide content indicates a higher reactivity of small clusters. Thus, steric effects are responsible for obstruction of radical formation for the smallest clusters of 2-chlorophenol. The same conclusion is supported by exponential increase in radical density by decreasing the copper oxide content after 1,2-dichlorobenzene adsorption (cf. Figure 6.6). As discussed earlier, by decreasing the copper oxide content, radical species are gradually changing from bidentate semiquinone to monodentate phenoxyl radicals. This results in a "more closely" packed species on the surface. Indeed, adsorption of 1,2-dichlorobenzene is the only case where a linear increase of EPFR yield is detected with decreasing copper oxide content (cf. Figure 6.5).

6.2.3 Relative Persistence of the Radicals

One of the most important characteristics of EPFR from environmental perspective is their persistency in the environment. EPFR have been reported to have much longer lifetime compared with other short-lived radicals such as acyl, hydroxyl, or superoxide [26, 27], which makes them environmentally hazardous when emitted from combustion sources. As mentioned previously, particulate matter may contain a varying concentration of metal oxides and therefore decay times have to be evaluated relative to the metal concentration. The EPFR lifetime in ambient air which is associated with CuO is depicted in Figure 6.7. It is evident that by decreasing copper oxide content, and as discussed earlier, EPFR lifetime increase with to a maximum at ~0.5-0.75% CuO. Interestingly, for 1,2-dichlorobenzene and 2-chlorophenol precursors, the maximum lifetimes observed are very similar (22-23h) indicating again similar species dominating the surface at CuO content – chlorophenoxyl species. At higher copper oxide

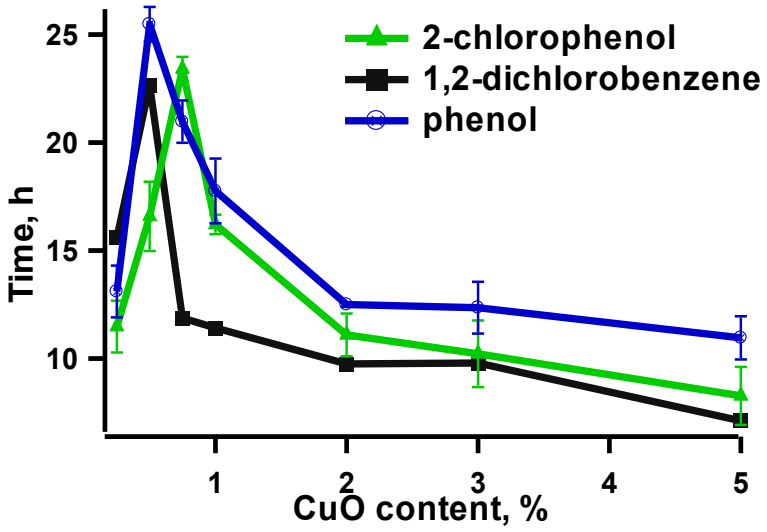

Figure 6.7 EFPRs 1/e lifetimes in ambient air at room temperatures formed on different Cu(II)O loading on silica formed from three adsorbates dosed at 230 ^{0}C.

content, a difference between lifetimes of those 2 samples is notable. This is in line with the

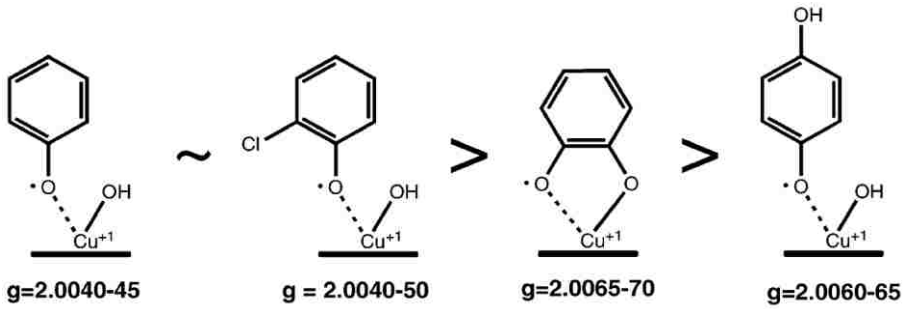

Figure 6.8 Order of lifetimes and persistence of the radicals.

previous studies that showed longer lifetimes of phenoxyl compared with semiquinone type EPFRs (cf. Figure 6.8). *Ab initio* calculations of the reactivities of gas-phase radicals with O_2 follows similar trend [28].

It is also worth to note that small clusters do not stabilize radicals as efficiently as indicated by the drop in 1/e lifetime of EPFRs below 0.5% concentration. A word of caution is therefore necessary - 0.5% CuO should not be taken as a limit for the highest stability of radicals in environmental samples – in real life a cluster size distribution may not correlate with the concentration as in the case of those synthetic samples.

6.3 Hydroxyl Radical Generation

Our previous research on the reactivity of EPFRs in aprotic media have showed a significant production of hydroxyl radicals [29, 30]. The presence of EPFR-associated with a redox-metal ion may result in a cycling chain reaction that generates ROS [31]. The steps involved in this cycle [31] are already known in biological media and are adapted to the radical-particle system. Studies of hydroxyl group were accomplished using the spin trapping abilities of 5,5-dimethylpyrroline-N-oxide (DMPO) and electron paramagnetic resonance spectroscopy (EPR) [32] as described in Chapter 3. A 4-line EPR spectra characteristic of DMPO-OH adducts

was detected in solutions containing both EPFR and Cu(II)O/silica particles with DMPO in PBS

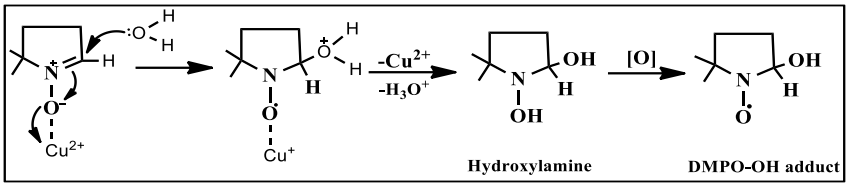

Scheme 6.2 Nucleophilic addition of H_2O to DMPO in the presence of Cu(II).

media (cf. Figure 6.9). On average, the EPFRs particles produced more DMPO-OH adducts than the control particles. In addition, DMPO-OH adduct increased with increase in incubation time to 3 h. A significant difference between DMPO-OH adducts of EPFRs particles and control particles, was registered using centrifuged particles (cf. Figure 6.10B). The net output of the hydroxyl radical considered is the difference between DMPO-OH adduct of EPFR-containing particles and control particles (Cu(II)O/silica). According to literature, generation of DMPO-OH adduct in presence of Fe(III) or Cu(II) is as a result of nucleophilic addition of H_2O to DMPO (cf. Scheme 6.2). The nucleophilic addition of water to DMPO accounts for 96% of the DMPO-OH adduct formed in the presence of Cu^{2+} and H_2O_2 [33]. This pathway, although an artifact, produces a 4-line spectrum like that of EPFR-containing particles [33, 34]. The difference between the DMPO-OH adduct of the EPFR-containing particles and control particles could therefore be attributed to hydroxyl radicals in Cu(I)-EPFR particles in solutions.

6.3.1 Mass Loading Dependence of CuO

When the suspensions were centrifuged for 5 min, their ability to generate hydroxyl radical increased significantly (cf. Figure 6.10). The mass loading dependence of hydroxyl radical formation was studied using centrifuged and non-centrifuged (only sonicated). Figures 6.10 and 6.11 shows that non-centrifuged particles resulted in higher hydroxyl generation than

centrifuged particles, and that DMPO-OH generation has different relationship with mass concentration for each sample.

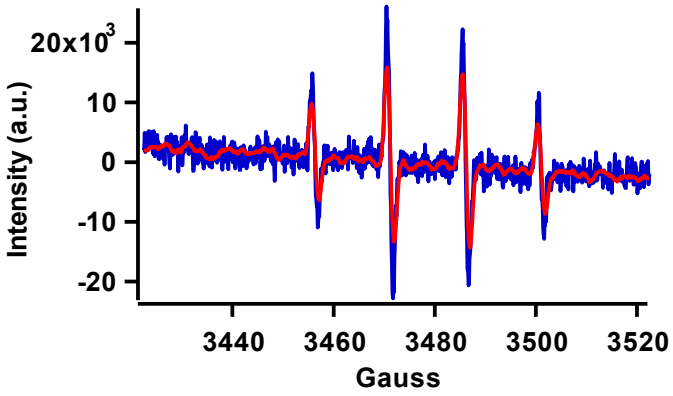

Figure 6.9 Comparison of EPR intensity signal of the DMPO-OH adduct in the presence of EPFR-containing particles (blue) and the control (Cu(II)O/silica) particles (red).

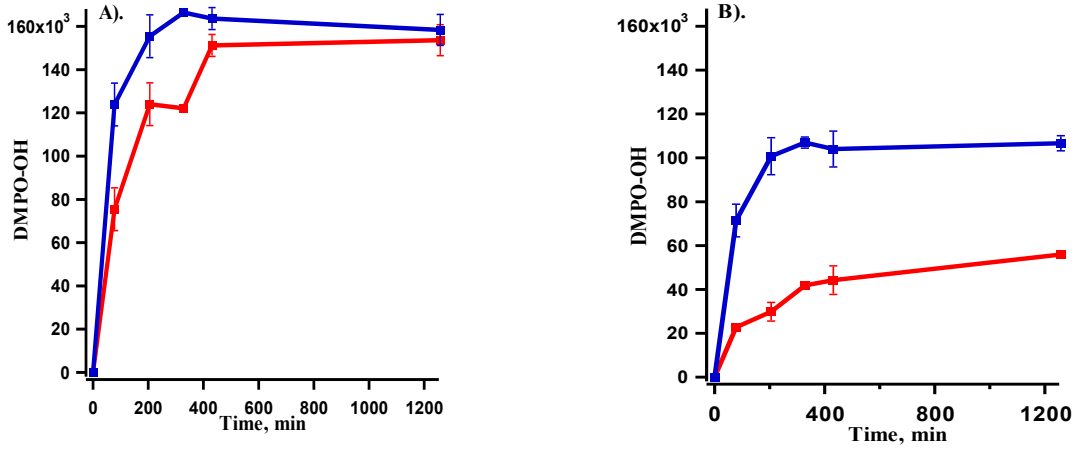

Figure 6.10 Density dependence of hydroxyl radical generation, A). Non-Centrifuged and B). Centrifuged EPFR-containing particles and Cu(II)O/silica particles. The blue line is the EPFR-containing particles and the red line is the control (Cu(II)O/silica) particles.

The concentration of hydroxyl radical was estimated from the previous studies with an assumption of 1-to-1 hydroxyl radical-to-DMPO stoichiometry and calibration using Tempol solution as standard [29]. Figure 6.11 depicts the concentration of hydroxyl radicals of centrifuged and non-centrifuged particles. In both cases, there was an increase in •OH generation

up to 1% Cu loading. Lighter particles (centrifuged) contain by far the highest activity, which correlates with surface-to-volume ratio dependency. There is an inverse relationship between the spins/gram and the DMPO-OH generation.

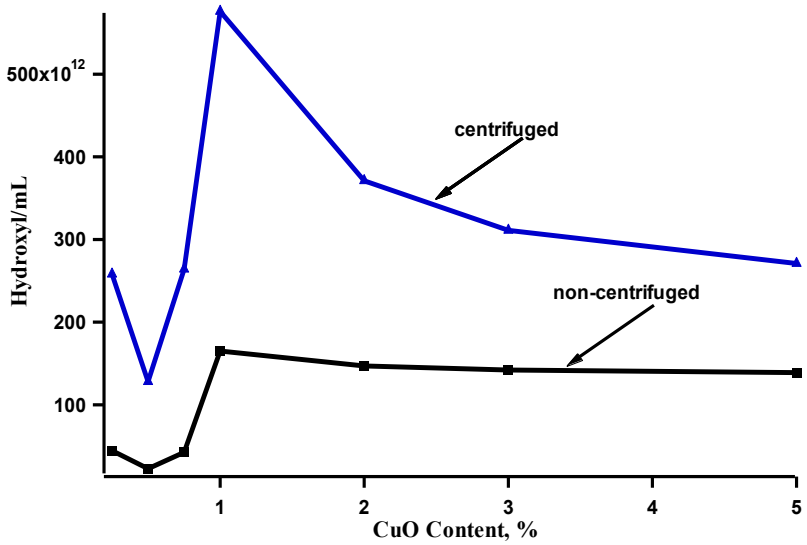

Figure 6.11 A comparison of centrifuged and non-centrifuged •OH radicals as a function of CuO content.

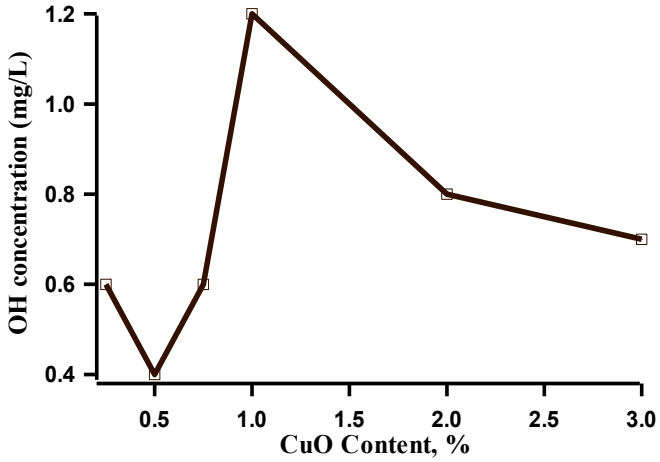

Figure 6.12 Hydroxyl radical concentration calculated at incubation time of 140 min.

The maximum [OH] of 1.2 mg/L was produced by 1% CuO-EPFR concentration (cf. Figure 6.12) of centrifuged particles. In an experiment, the hydroxyl solution of 0.68 mg/L decreased the Red Tide organisms from $11.74*10^6$/mL to $0.028*10^6$/mL, which was equivalent to 99.89% efficiency. Since the hydroxyl radical has a strong oxidation and dissociation effects, 90% chlorophyll was decomposed within 10 minutes by 0.68 mg/L [35].

6.4 Summary and Relevance to EPFRs Formation

In this chapter, the formation of EPFRs has been evidenced by the reactions of EPFRs precursors on fly ash surrogates. Combustion systems generate free radicals stabilized on the surface resulting in atmospheric lifetimes of several hours to several days. When inhaled, these Environmentally Persistent Free Radicals (EPFRs) generate reactive oxygen species (ROS) and oxidative stress in the host leading to pulmonary and cardiovascular dysfunction. Our series of studies indicated EPFRs are formed when hydroxyl- and chlorine-substituted aromatics chemisorbed on 5% Cu(II)O surfaces. This study reports the dependency of the EPFRs yields on a different metal loading in particles on silica. The EPFRs were generated by exposure of the vapors of phenol, monochlorophenol, and 1,2-dichlorobenzene to CuO/silica at 230 ^{0}C resulting in formation of phenoxyl- and semiquinoine-type radicals, with a characteristic EPR spectra of g-value ranging between 2.0044 to 2.005, respectively. The number of EPFRs formed per copper atom indicate the presence of maximum formation yield at 1% CuO loading for MCP. Generation of hydroxyl radicals by EPFRs with different copper oxide content was performed using the spin trapping agent, 5,5-dimethyl-1-pyrroline-N-oxide (DMPO).

In addition, the results presented here strongly suggest that both centrifuged and non-centrifuged particles of Cu(I)-EPFR are able to generate hydroxyl radicals. This has been demonstrated through spin trapping technique and detection of •OH radical by EPR [29, 30]. A

previous study with 5% Cu(II)O/silica demonstrated that EPFR are able to generate reactive oxygen species. As a consequence, EPFR are responsible for cell viability reduction and induction of asthma-like symptoms in rats [36]. Hydroxyl radical formation by various coal-fly ashes and PM is highly correlated to cause oxidative DNA-damage in lung epithelial [37-39].

6.5 References

1. Huffman, G.P., et al., *Characterization of fine particulate matter produced by combustion of residual fuel oil.* Journal of the Air & Waste Management Association, 2000. **50**(7): p. 1106-1114.

2. Allouis, C., F. Beretta, and A. D'Alessio, *Structure of inorganic and carbonaceous particles emitted from heavy oil combustion.* Chemosphere, 2003. **51**(10): p. 1091-1096.

3. Bell, M.L., et al., *Hospital admissions and chemical composition of fine particle air pollution.* American journal of respiratory and critical care medicine, 2009. **179**(12): p. 1115.

4. Peng, R.D., et al., *Emergency admissions for cardiovascular and respiratory diseases and the chemical composition of fine particle air pollution.* Environmental health perspectives, 2009. **117**(6): p. 957.

5. Dominici, F., et al., *Does the effect of PM10 on mortality depend on PM nickel and vanadium content? A reanalysis of the NMMAPS data.* Environmental Health Perspectives, 2007. **115**(12): p. 1701.

6. Lomnicki, S., et al., *Copper Oxide-Based Model of Persistent Free Radical Formation on Combustion Derived Particulate Matter.* Environ Sci Technol, 2008. **42**: p. 4982 - 4988.

7. Vejerano, E., S. Lomnicki, and B. Dellinger, *Formation and Stabilization of Combustion-Generated Environmentally Persistent Free Radicals on an Fe(III)2O3/Silica Surface.* Environmental Science & Technology, 2010. **45**(2): p. 589-594.

8. Vejerano, E., S. Lomnicki, and B. Dellinger, *Lifetime of combustion-generated environmentally persistent free radicals on Zn(ii)O and other transition metal oxides.* Journal of Environmental Monitoring, 2012. **14**(10): p. 2803-2806.

9. Vejerano, E., S.M. Lomnicki, and B. Dellinger, *Formation and Stabilization of Combustion-Generated, Environmentally Persistent Radicals on Ni(II)O Supported on a Silica Surface.* Environmental Science & Technology, 2012. **46**(17): p. 9406-9411.

10. Zhou, X., et al., *Size-Dependent Catalytic Activity and Dynamics of Gold Nanoparticles at the Single-Molecule Level.* Journal of the American Chemical Society, 2009. **132**(1): p. 138-146.

11. Wilson, O.M., et al., *Effect of Pd nanoparticle size on the catalytic hydrogenation of allyl alcohol.* Journal of the American Chemical Society, 2006. **128**(14): p. 4510-4511.

12. Bezemer, G.L., et al., *Cobalt Particle Size Effects in the Fischer−Tropsch Reaction Studied with Carbon Nanofiber Supported Catalysts.* Journal of the American Chemical Society, 2006. **128**(12): p. 3956-3964.

13. Grass, M., R. Rioux, and G. Somorjai, *Dependence of Gas-Phase Crotonaldehyde Hydrogenation Selectivity and Activity on the Size of Pt Nanoparticles (1.7–7.1 nm) Supported on SBA-15.* Catalysis Letters, 2009. **128**(1-2): p. 1-8.

14. Doyle, A.M., S.K. Shaikhutdinov, and H.-J. Freund, *Surface-Bonded Precursor Determines Particle Size Effects for Alkene Hydrogenation on Palladium.* Angewandte Chemie International Edition, 2005. **44**(4): p. 629-631.

15. Burda, C., et al., *Chemistry and Properties of Nanocrystals of Different Shapes.* Chemical Reviews, 2005. **105**(4): p. 1025-1102.

16. Lomnicki, S., et al., *A Copper Oxide-Based Model of Persistent Free Radical Formation on Combustion Derived Particulate Matter* Environmental Science & Technology, 2008. **42**(13): p. 4982-4988.

17. Lomnicki, S., et al., *Copper Oxide-Based Model of Persistent Free Radical Formation on Combustion-Derived Particulate Matter.* Environmental Science & Technology, 2008. **42**(13): p. 4982-4988.

18. Patterson, M.C., et al., *EPFR formation from phenol adsorption on Al2O3 and TiO2: EPR and EELS studies.* Chemical Physics, (0).

19. Boyd, S.A. and M.M. Mortland, *Dioxin radical formation and polymerization on Cu(II)-smectite.* Nature, 1985. **316**(6028): p. 532-535.

20. Lezna, R.O., et al., *Adsorption of phenol on gold as studied by capacitance and reflectance measurements.* Langmuir, 1991. **7**(6): p. 1241-1246.

21. Johnston, K., et al., *Adsorption structures of phenol on the Si (001)-(2× 1) surface calculated using density functional theory.* Physical Review B, 2010. **81**(23): p. 235428.

22. Lomnicki, S. and B. Dellinger, *A Detailed Mechanism of the Surface-Mediated Formation of PCDD/F from the Oxidation of 2-Chlorophenol on a CuO/Silica Surface.* The Journal of Physical Chemistry A, 2003. **107**(22): p. 4387-4395.

23. Alderman, S.L., et al., *An Infrared and X-ray Spectroscopic Study of the Reactions of 2-Chlorophenol, 1,2-Dichlorobenzene, and Chlorobenzene with Model CuO/Silica Fly Ash Surfaces.* Environmental Science & Technology, 2005. **39**(19): p. 7396-7401.

24. Khachatryan, L., R. Asatryan, and B. Dellinger, *Development of expanded and core kinetic models for the gas phase formation of dioxins from chlorinated phenols.* Chemosphere, 2003. **52**(4): p. 695-708.

25. Tsang, W., *Mechanisms for the Formation and Destruction of Chlorinated Organic Products of Incomplete Combustion.* Combustion Science and Technology, 1990. **74**(1-6): p. 99-116.

26. Pryor, W.A., *Oxy-Radicals and Related Species: Their Formation, Lifetimes, and Reactions.* Annual Review of Physiology, 1986. **48**(1): p. 657-667.

27. Finkelstein, E., G.M. Rosen, and E.J. Rauckman, *Production of hydroxyl radical by decomposition of superoxide spin-trapped adducts.* Molecular Pharmacology, 1982. **21**(2): p. 262-265.

28. Dellinger, B., et al., *Formation and stabilization of persistent free radicals.* Proceedings of the Combustion Institute, 2007. **31**(1): p. 521-528.

29. Khachatryan, L., et al., *Environmentally Persistent Free Radicals (EPFRs). 1. Generation of Reactive Oxygen Species in Aqueous Solutions.* Environmental Science & Technology, 2011. **45**(19): p. 8559-8566.

30. Khachatryan, L. and B. Dellinger, *Environmentally Persistent Free Radicals (EPFRs)-2. Are Free Hydroxyl Radicals Generated in Aqueous Solutions?* Environmental Science & Technology, 2011. **45**(21): p. 9232-9239.

31. Dellinger, B., et al., *Free Radicals in Tobacco Smoke.* Mini-Reviews in Organic Chemistry, 2011. **8**(4): p. 427-433.

32. Janzen, E.G. and B.J. Blackburn, *Detection and identification of short-lived free radicals by an electron spin resonance trapping technique.* Journal of the American Chemical Society, 1968. **90**(21): p. 5909-5910.

33. Hanna, P.M., W. Chamulitrat, and R.P. Mason, *When are metal ion-dependent hydroxyl and alkoxyl radical adducts of 5,5-dimethyl-1-pyrroline N-oxide artifacts?* Archives of Biochemistry and Biophysics, 1992. **296**(2): p. 640-644.

34. Burkitt, M.J., et al., *Generation of 5,5-Dimethyl-1-pyrrolineN-Oxide Hydroxyl and Scavenger Radical Adducts from Copper/H2O2Mixtures: Effects of Metal Ion Chelation and the Search for High-Valent Metal–Oxygen Intermediates.* Archives of Biochemistry and Biophysics, 1995. **323**(1): p. 63-70.

35. Zhang, Z., et al., *Killing of red tide organisms in sea enclosure using hydroxyl radical-based micro-gap discharge.* Plasma Science, IEEE Transactions on, 2006. **34**(6): p. 2618-2623.

36. Mahne, S., et al., *Environmentally persistent free radicals decrease cardiac function and increase pulmonary artery pressure.* American Journal of Physiology - Heart and Circulatory Physiology, 2012. **303**(9): p. H1135-H1142.

37. Shi, T., et al., *Hydroxyl radical generation by electron paramagnetic resonance as a new method to monitor ambient particulate matter composition.* Journal of Environmental Monitoring, 2003. **5**(4): p. 550-556.

38. Jan M. S. van Maanen, P.J.A.B., Ad Knaapen, Marcel van Herwijnen, Pauline A. E. L. Schilderman, Kevin R. Smith, Ann E. Aust, Maura Tomatis, Bice Fubini, *IN VITRO EFFECTS OF COAL FLY ASHES: Hydroxyl Radical Generation, Iron Release, and DNA Damage and Toxicity in Rat Lung Epithelial Cells.* Inhalation Toxicology, 1999. **11**(12): p. 1123-1141.

39. Kiruri, L.W., B. Dellinger, and S. Lomnicki, *Tar Balls from Deep Water Horizon Oil Spill: Environmentally Persistent Free Radicals (EPFR) Formation During Crude Weathering.* Environmental Science & Technology, 2013. **47**(9): p. 4220-4226.

CHAPTER 7 - EPFRS AND THEIR HALF-LIVES IN TAR BALLS FROM DEEP WATER HORIZON OIL SPILL[1]

7.1 Detection of EPFRs in Tar Balls

The fourth objective of this research was to identify/detect organic free radicals and transition metals in tar balls and investigate the EPFRs changes that occur with time in the environment. Since the presence of EPFRs have critical impact on the affected ecosystems, ROS studies were also conducted in PBS media. All experiments presented were performed using samples collected in the Gulf of Mexico following the DH incident.

7.1.1 Sample Characterization and Physical Appearance

The samples, based on their physical appearances, could be divided into 2 categories: hard, black, glossy material and soft, brown material. The latter is consistent with a typical appearance described in literature of tar balls containing weathered crude remnants, sand particles and bio-debris. Samples TB_{60}, TB_{90}, and TB_{360} belonged to this category. One sample, TB_0, had a black and glassy appearance [1]. Interestingly, this sample was collected at the very early stages of the DH incident, when the oilrig platform was still burning. A distinct difference of the appearance of the sample TB_0 compared to TB_{60}, TB_{90} and TB_{450} indicates a major chemical transformation upon release to the environment.

7.1.2 Initial Radical Concentrations

Sample TB_0. The physical appearance of the TB_0 sample (black, hard, and glassy) suggested the sample was a solidified pure asphaltene material. The solubility test of the

[1] Part of this manuscript is reproduced with permission from Kiruri, L. W.; Dellinger, B.; Lomnicki, S. Tar Balls from Deep Water Horizon Oil Spill: Environmentally Persistent Free Radicals (EPFR) Formation During Crude Weathering. *Environ. Sci. & Technol.* **2013,** *47* (9), 4220-4226. Copyright 2011. American Chemical Society.

samples was consistent with initial assumption, as the sample was completely dissolved in *tert*-buthylbenzene [2] (no residue left) and non-soluble in polar solvents or n-alkanes (isopropyl alcohol, n-hexane) [3, 4]. The EPR spectra of TB_0 revealed the presence of a single, symmetric and strong paramagnetic signal (cf. Figure 7.1) centered at 3454 Gauss, characterized by a g-value of 2.0035 and the ΔH_{p-p} of 5.1 Gauss. The parameters of the spectrum recorded were consistent with the radical species observed in the crude oil and originating from asphaltene species [5, 6]. The spin number of detected radicals (6.7×10^{18} spins/g of sample) was in the range of the number of radicals present in pure asphaltenes [7-10]. Unlike other reports, no spectral features were observed typical for the presence of metal centers, often present in asphaltenes from crudes [11-16]. Lack of spectral features characteristic to metal centers was an indication of non-presence of those metals in oxidation states with a paramagnetic electron. Reduction or oxidation of metal ions due to the interaction with organic material can result in disappearance of the metal-associated EPR signal.

The nature of the radical species in asphaltenes is not clearly understood. Unpaired electrons are thought to be delocalized across the aromatic π system stabilized by resonance on the intrinsic polyaromatic sheets of asphaltene molecule [6,17, 18].

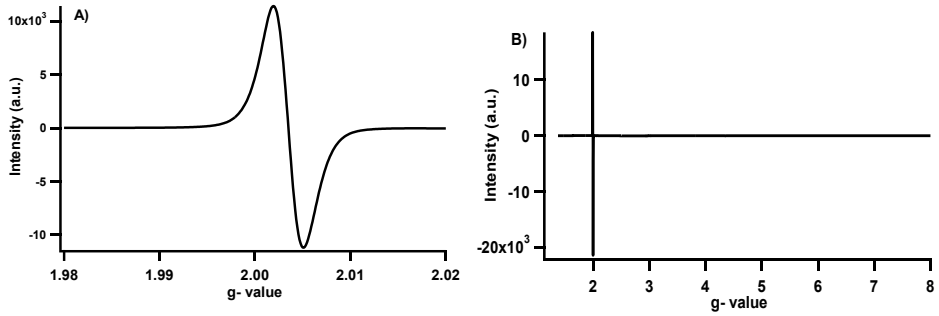

Figure 7.1 EPR spectra of TB_0 at room temperature. A) Spectrum at 200 Gauss field and B) at 1000 Gauss field, respectively.

This resonance stabilization of the observed radicals in asphaltenes contributes to their high persistency, as they remain unchanged almost indefinitely [19]. No changes were observed in the spin numbers of the collected sample, even after 2 years of exposure to ambient air. The mechanism of the radical formation in asphaltenes molecules is unknown [19]. Some studies have indicated the correlation between the paramagnetic signal and the number of transition metals (vanadyl groups in particular); however, studies are inconclusive [20, 21].

Tarballs TB_{60}, TB_{90}, TB_{450}. Tar balls collected 60,90 and 450 days after the DH incident exhibited a much more complex EPR spectrum compared to TB_0 (cf. Figure 7.2), indicating the presence of multiple organic radical species and paramagnetic metal ions.

For each of those samples a distinct organic radical signal was recorded at g ~ 2.0041 and with a $\Delta H_{p\text{-}p}$ ranging from 5.2 - 5.7 Gauss (cf. Figure 7.2A). While the width of this signal was increased only slightly, it's position was distinctly different from the one observed for sample TB_0. The broadening of the spectrum was an indication of more than one radical contribution to the overall spectra. Superposition of the signals of different species was further supported by the

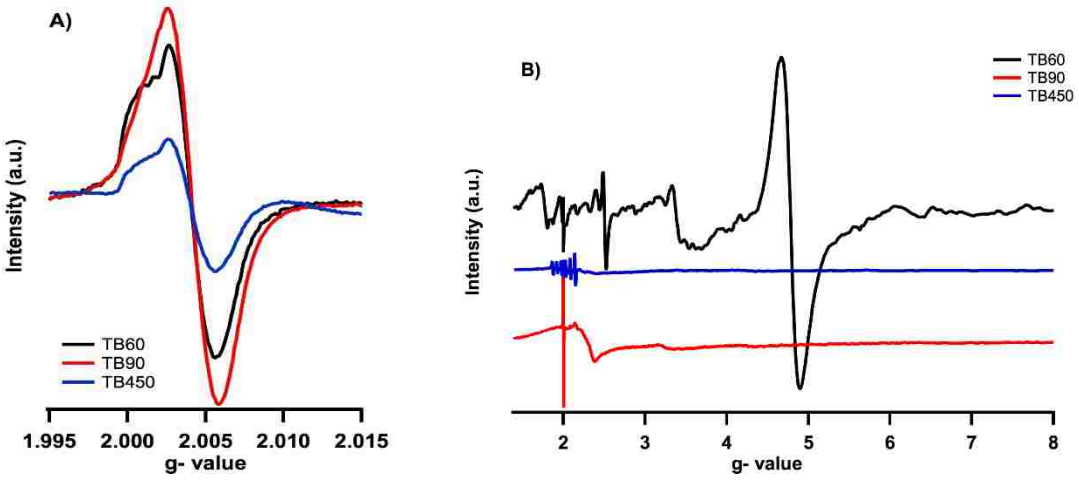

Figure 7.2 Spectra of TB_{60}, TB_{90} and TB_{450}: A). 50 Gauss field spectrum of organic radical and B). 1000 Gauss field spectrum.

lack of symmetry of the spectra. The shift in g value from 2.0035 to 2.0041 suggested the presence of more oxygen-centered radical species [21-24]. In the broad magnetic field of 1000 G several other paramagnetic species were also detected, not observed in TB_0 sample (cf. Figure 7.2B). Lines detected at g = 2.5 and g = 4.7 can be assigned as originating from paramagnetic Fe^{3+} ions - mutually interacting Fe^{3+} ions and Fe^{3+} ions in tetrahedral coordination, respectively [25, 26]. Theoretical calculations have demonstrated the g-value at 3.3 to represent Fe^{3+} in glassy environment [27]. Weak EPR lines in TB_{90} at g = 2.00, and g = 4.3 are characteristic for Fe^{3+} in a distorted tetragonal site, where Fe^{3+} ions substitutes for Si^{4+} in SiO_2 structures [28]. In the case of TB_{450}, a six-line hyperfine structure characteristic to the interaction of Mn(II) ions with its nuclear spin (I=5/2) was also observed [24, 28].

7.2 Sample aging and radical decay

Unlike TB_0, the concentration of the organic paramagnetic signals in samples TB_{60}, TB_{90} and TB_{450} decreased upon exposure to air outside the marine environment (cf. Figure 7.3), with a calculated 1/e half-life of 400-600 days. Slow radical decay further underlined the differences

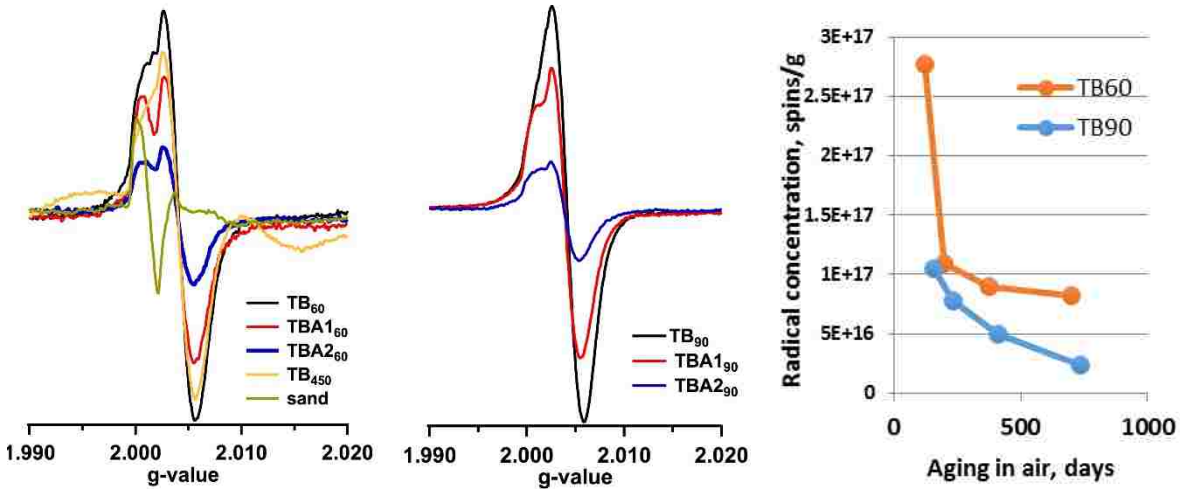

Figure 7.3 Comparison of the EPR spectra of TB_{60} and TB_{90} while aging in air.

between the asphaltene radical and the tar ball radicals. High delocalization of the paramagnetic electron in polyaromatic π system of asphaltenes results in indefinite stabilization by multi-ring resonance. As a result, asphaltene radicals are non-degrading and are resistant to environmental oxidation. A gradual radical decay of radicals in TB_{60}, TB_{90} and TB_{450} partially revealed the multi-component structure of the overall spectrum. One of the components of this spectrum at g = 2.0017 appears to be Fe^{3+} ions, which were also detected in a pure sand sample from the Gulf of Mexico beach (cf. Figure 7.3) with the remaining spectral components originating from the organic species.

7.4 Radical Extraction Analysis

The extraction of the samples with polar (isopropyl alcohol - IPP) and non-polar (*tert*-buthylbenzene- TBB) solvents resulted in a complete dissolution of the TB_0 in TBB (no residue remaining), and only slight dissolution in IPP (cf. Figure 7.4). The EPR spectra of the TBB extract revealed the presence of a weak signal at g = 2.0035 similar to that observed in original tar ball solid. No radicals were detected in the IPP extract. The extraction of TB_{60} and TB_{90} in TBB resulted in a distinct change in the EPR spectrum of the residue (cf. Figure 7.4) with the signal in the residue centered at g= 2.0017. The signal parameters and the physical appearance of the residue indicated the remaining part to be sand particles incorporated in tar ball. Unlike the case of TB_0, no paramagnetic signal was detected in the extract, indicating the lack of self-stabilization of the radicals in these 3 tar ball samples. Extraction of the TB_{60}, TB_{90} and TB_{450} samples with IPP resulted in a decrease in the radical concentration with no change in overall g-value in the solid residue and no radical signal in the extract.

Both TB aging and extraction have provided details on the components of the paramagnetic signal of TB_{60}, TB_{90} and TB_{450}. As observed for sample TB_0 and indicated in

literature, the g- values of asphaltenes ranges from 2.0028-2.0035 and are associated with carbon centered, ring delocalized radicals [5-7, 29]. Higher g-values were observed for TB_{60}, TB_{90} and TB_{450} samples (g= 2.0041) and are indicative of the presence of oxygen-centered radicals.

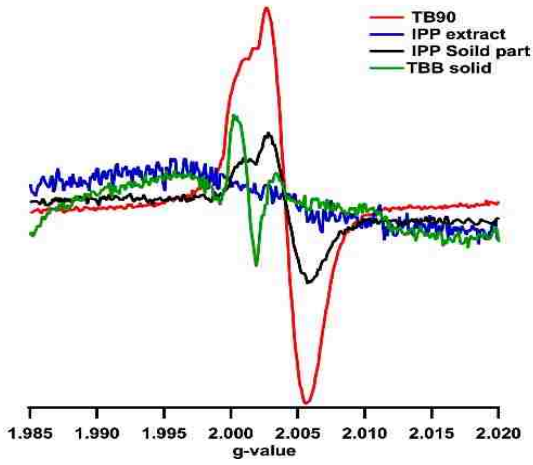

Figure 7.4 EPR spectra of TB_{90} before and after extraction with isopropyl alcohol and tert-butylbenzene.

In fact, the ability to extract a significant portion of the radicals with IPP is consistent with the enhanced polarity of the species containing oxygen atoms. Such extractability was not detected in the case of pure asphaltene samples. The disappearance of the radical signal in the extract for TB_{60}, TB_{90} and TB450 samples indicated the radicals in the tar balls were not stabilized and reactive when removed from the tar ball system.

The formation and stabilization of oxygen centered-radicals on the solid particles in the environmental samples may result from the interaction between the metal cations and aromatic molecules. Such phenomena has been observed and described for both combustion-generated particulates and in the soil samples [21-24]. We have previously demonstrated the formation of EPFRs on metal surfaces of Cu(II)O/Silica [21] and Fe(III)O/Silica [22] particles leading to the reduction of metal oxide via electron transfer and formation of phenoxyl or semiquinone-type

radicals. A similar mechanism may occur in the tar ball samples, where a presence of Fe^{3+} ion centers was detected. Using EPR spectral deconvolution procedures developed for metal-radical adducts [21-23] we were able to assign the g-values to the components of the observed spectra of TB_{60} and TB_{90}, (cf. Table 7.1). The presence of the Fe^{3+} ion centers (g=2.0015-2.0017) have been shown for both pure sand and, upon a complete extraction of the tar ball samples, indicating association of iron ions with sand in the tar balls. A component at g= 2.0033-34 is typical for the carbon-centered organic radicals and is most likely associated with the presence of asphaltene structures native to crude [30, 31]. The last component at g=2.0047-2.0049 is typical to the semiquinone radicals bound to the reduced metal ion center. These radicals in a semi-bonded state have singlet line signals and are stabilized by the metal center against oxidation and decomposition [22, 23].

Weathering of the spilled crude in the marine environment results in incorporation of sediments in the crude material and adsorption of organic matter to sand particles. The presence of iron in the sand particles resulted in the direct interaction of the adsorbed species, partial oxidation and formation of the surface stabilized radicals. This mechanism appears to be similar to the observed formation of EPFRs in the soils contaminated with pentachlorophenol (PCP) in the ambient environment [24]. It has been shown, that exposure of soils to pentachlorophenol result in the formation of radical species characterized by a singlet EPR spectrum with g value of 2.0031 and peak width of 6 Gauss [24]. These radicals are formed by an electron transfer

Table 7.1 EPR spectral deconvolution of tar ball samples

Peak # position	TB60	TB90	Structural assignment of radical
g1	2.0015	2.0017	Fe^{3+} center
g2	2.0033	2.0034	delocalized carbon centered
g3	2.0049	2.0047	Semiquinone type

reaction between the metal ion center in soil and adsorbed PCP molecule, resulting in primarily keto form of pentachlorophenoxy radical, due to the electronic effect of 5 chlorine atoms on benzene ring (hence, the lower g value).

In fact the presence of 6000-7000 ppm of PCP in soil resulted in 2.0×10^{18} radicals/ g of soil [24]. In the case of tar balls the concentration of the radicals is at the level of 2.0×10^{18} radicals /g of tar ball. Though the concentration is an order of magnitude lower compared to contaminated soils, it is surprisingly high, considering the fact that these radicals are formed from ambient condition of oxidation of residual organic matter, not by exposure to the reactive PCP contaminant. Interestingly, also the nature of the formed radicals is different, since tar ball EPFRs were identified as predominantly of semiquinone type.

7.5 Metal Analysis

The metals selected for analysis were Al, Cr, Fe, Mg, Mn, Mo, Si, Ti, V, and Zn. These metals were selected due to their potential risk to the environment and human health as well as mobilities in environment. The complete list of metal data (mg/kg) for all the tar balls is presented in Appendix 1.

7.6 Generation of OH Radicals by EPFRs in Tar Balls

The formation of EPFRs in tar balls indicates chemical changes in the crude during the weathering process in marine environment. Their presence in tar balls can have far-reaching environmental impacts - it has been shown before, that EPFRs in the particulate matter are active in formation of superoxide radicals and hydroxyl [32, 33]. Two tar ball samples have been tested for their OH radical generation potential based on the formation of DMPO-OH spin adduct: TB_0 and TB_{450} (cf. Figure 7.5). We have selected TB_0 sample to serve as a reference for the weathered tar ball as it contain exclusively asphaltene radicals. Difference in the OH radical

yield between TB_0 and TB_{450} is representing the change in the OH radical generation potency due to the formation of new radicals (EPFRs) resulting from weathering process. After only 1 h of suspending the tar balls in PBS solution (*vide supra*) TB_{450} have shown ~50% higher yield of DMPO-OH spin adduct and almost 2 fold higher amount of DMPO-OH formed after 12 h of reaction. Since the total radical concentration in TB_0 is 200 times that of TB_{450} ($\sim 6.0 \times 10^{18}$ and $\sim 3.0 \times 10^{16}$ spins/g, respectively) the overall yield of the OH radicals' formation from EPFRs is ~400 times that of asphaltene radicals. Such high OH radical formation potential by EPFRs in tar balls indicates their high environmental hazard. On the other hand, asphaltene radicals in TB_0 are also capable to generate OH radicals, however, due to their intrinsic nature they are not readily available for the reaction to occur.

7.7 Summary and Relevance to EPFRs Formation

In comparison with the other EPFR-particle systems, radicals found in tar balls, have

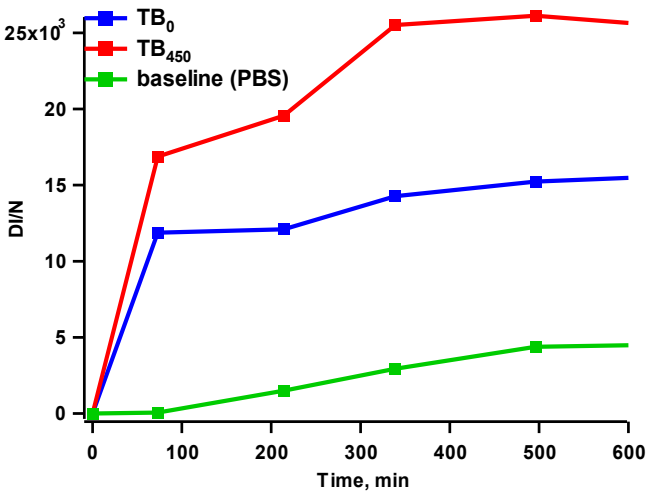

Figure 7.5 Formation of DMPO-OH adduct in the tar ball suspension in PBS.

long 1/e half-lives and can remain in the marine environment for a very long time. Surface bound radicals of both phenoxyl- and semiquinone-type radical have been shown to be able to generate

hydroxyl radicals through a cyclic chemical process, without substantial decay of the parent EPFR system [33, 34]. The newly discovered EPFR radicals are "bound" to the tar-ball matrix and as such their mobility inside the matrix is limited. Thus it is difficult to imagine them directly being involved in the transformation of the tar balls organic matter. However, they are product of the weathering or oxidation of organic matter and in that sense they are active in tar ball transformation. Also, they can be active indirectly, for example, generation of hydroxyl radicals, which in turn can react, with the organic matter of tar balls contributing to a further oxidation process.

Both *in vitro* and *in vivo* experiments have indicated initiation of cardiopulmonary disease from the particles containing EPFRs [35-39]. Though the large tar balls do not pose a direct threat for inhalation or ingestion, small sand particles exposed to crude oil can also contain oil-born radical species. These small sand particles can be windblown, become airborne, inhaled or digested. Presented in here is identification and discovery of the Environmentally Persistent free Radicals in tar balls during weathering process should be only the starting point of the research of this new species. It is of outmost importance to determine the environmental factors, such as, pH, salinity, water oxygen saturation etc, contributing to the formation of EPFRs as well as affecting their lifetime. Only then a full picture and understanding of the environmental effects of EPFRs in tar balls can be achieved.

7.8 References

1. Cimino, R., et al. *Thermodynamic modelling for prediction of asphaltene deposition in live oils*. in *SPE International Symposium on Oilfield Chemistry*. 1995.
2. Mannistu, K.D., H.W. Yarranton, and J.H. Masliyah, *Solubility Modeling of Asphaltenes in Organic Solvents*. Energy & Fuels, 1997. **11**(3): p. 615-622.

3. Johansen, E.J., et al., *Water-in-crude oil emulsions from the norwegian continental shelf Part I. Formation, characterization and stability correlations.* Colloids and Surfaces, 1988. **34**(4): p. 353-370.

4. Khulbe, K., et al., *Effects of solvents on free radicals of bitumen and asphaltenes.* Fuel processing technology, 1992. **32**(3): p. 133-141.

5. Guedes, C.L.B., et al., *EPR and Fluorescence Spectroscopy in the Photodegradation Study of Arabian and Colombian Crude Oils.* International Journal of Photoenergy, 2006. **2006**.

6. Montanari, L., et al., *Asphaltene radicals and their interaction with molecular oxygen: an EPR probe of their molecular characteristics and tendency to aggregate.* Applied Magnetic Resonance, 1998. **14**(1): p. 81-100.

7. Khristoforov, V.S., *Study of crude oil and some of its high molecular compounds using electron paramagnetic resonance (Review).* Chemistry and Technology of Fuels and Oils, 1971. **7**(8): p. 629-631.

8. Retcofsky H, L., et al., *Electron Spin Resonance Studies of Coals and Coal-Derived Asphaltenes*, in *Organic Chemistry of Coal*. 1978, American Chemical Society. p. 142-155.

9. Yen, T., *Structure of petroleum asphaltene and its significance.* Energy Sources, Part ARecovery, Utilization, and Environmental Effects, 1974. **1**(4): p. 447-463.

10. Schultz, K.F. and M.L. Selucky, *Esr measurements on asphaltene and resin fractions from various separation methods.* Fuel, 1981. **60**(10): p. 951-956.

11. Di Mauro, E., C.L.B. Guedes, and M.T. Piccinato, *EPR of Marine Diesel.* Applied Magnetic Resonance, 2007. **32**(3): p. 303-309.

12. Tagirzyanov, M.L., M.R. Yakubov, and G.V. Romanov, J. Can. Petrol. Technol., 2007. **46**(9): p. 9.

13. Dickson, F.E. and L. Petrakis, *Application of electron spin resonance and electronic spectroscopy to the characterization of vanadium species in petroleum fractions.* Analytical Chemistry, 1974. **46**(8): p. 1129-1130.

14. Altgelt, K.H. and M.M. Boduszynski, *Composition and analysis of heavy petroleum fractions*. Vol. 54. 1994: CRC Press.

15. Spencer, W., et al., *Chromatographic studies of vanadium compounds from Boscan crude oil.* Separation Science and Technology, 1982. **17**(6): p. 797-819.

16. Dechaine, G.P. and M.R. Gray, *Chemistry and Association of Vanadium Compounds in Heavy Oil and Bitumen, and Implications for Their Selective Removal†.* Energy & Fuels, 2010. **24**(5): p. 2795-2808.

17. Ferris, S., E. Black, and J. Clelland, *Aromatic structure in asphalt fractions.* Industrial & Engineering Chemistry Product Research and Development, 1967. **6**(2): p. 127-132.

18. Mujica, V., et al., *Caging of molecules by asphaltenes. A model for free radical preservation in crude oils.* Energy & fuels, 2000. **14**(3): p. 632-639.

19. Niizuma, S., et al., *Electron spin resonance study of free radicals in Athabasca asphaltene.* Fuel, 1977. **56**(3): p. 249-256.

20. Tagirzyanov, M.I., et al., *Method of Unification of the Relative Measurement Units for the Concentrations of V(IV) and Free Radicals in Crude Oils and Asphaltenes.* Russian Journal of Applied Chemistry, 2005. **78**(7): p. 1194-1196.

21. Lomnicki, S., et al., *Copper Oxide-Based Model of Persistent Free Radical Formation on Combustion-Derived Particulate Matter.* Environmental Science & Technology, 2008. **42**(13): p. 4982-4988.

22. Vejerano, E., S. Lomnicki, and B. Dellinger, *Formation and Stabilization of Combustion-Generated Environmentally Persistent Free Radicals on an Fe(III)2O3/Silica Surface.* Environmental Science & Technology, 2010. **45**(2): p. 589-594.

23. Vejerano, E., S.M. Lomnicki, and B. Dellinger, *Formation and Stabilization of Combustion-Generated, Environmentally Persistent Radicals on Ni(II)O Supported on a Silica Surface.* Environmental Science & Technology, 2012. **46**(17): p. 9406-9411.

24. dela Cruz, A.L.N., et al., *Detection of Environmentally Persistent Free Radicals at a Superfund Wood Treating Site.* Environmental Science & Technology, 2011. **45**(15): p. 6356-6365.

25. Kucherov, A.V., et al., *In situ high-temperature ESR characterization of FeZSM-5 and FeSAPO-34 catalysts in flowing mixtures of NO, C3H6, and O2.* Catalysis Letters, 1998. **56**(4): p. 173-181.

26. Kucherov, A.V. and A.A. Slinkin, *Introduction Fe(III) ions in cationic positions of HZSM-5 by a solid-state reaction, Fe(III) cations in HZSM-5, and Fe(III) lattice ions in ferrisilicate.* Zeolites, 1988. **8**(2): p. 110-116.

27. Golding, R.M., T. Singhasuwich, and W.C. Tennant, *An analysis of the conditions for an isotropic g-tensor in high-spin d5 systems.* Molecular Physics, 1977. **34**(5): p. 1343-1350.

28. Sur, S. and T. Cooney, *Electron paramagnetic resonance study of iron(III) and manganese(II) in the glassy and crystalline environments of synthetic fayalite and tephroite.* Physics and Chemistry of Minerals, 1989. **16**(7): p. 693-696.

29. Piccinato, M.T., C.L.B. Guedes, and E. Mauro, *EPR characterization of organic free radicals in marine diesel.* Applied Magnetic Resonance, 2009. **35**(3): p. 379-388.

30. Yen, T.F., J.G. Erdman, and A.J. Saraceno, *Investigation of the Nature of Free Radicals in Petroleum Asphaltenes and Related Substances by Electron Spin Resonance.* Analytical Chemistry, 1962. **34**(6): p. 694-700.

31. Scotti, R. and L. Montanari, *Molecular structure and intermolecular interaction of asphaltenes by FT-IR, NMR, EPR.* Structures and Dynamics of Asphaltenes, 1998: p. 79-113.

32. Kelley, M.a., et al., *Model Particulate Matter Containing Persistent Free Radicals Exhibit Reactive Oxygen Species Production.* Free Radical Biology and Medicine, 2011. **51,** p. S134.

33. Khachatryan, L., et al., *Environmentally Persistent Free Radicals (EPFRs). 1. Generation of Reactive Oxygen Species in Aqueous Solutions.* Environmental Science & Technology, 2011. **45**(19): p. 8559-8566.

34. Khachatryan, L. and B. Dellinger, *Environmentally Persistent Free Radicals (EPFRs)-2. Are Free Hydroxyl Radicals Generated in Aqueous Solutions?* Environmental Science & Technology, 2011. **45**(21): p. 9232-9239.

35. Mahne, S., et al., *Environmentally persistent free radicals decrease cardiac function and increase pulmonary artery pressure.* American Journal of Physiology - Heart and Circulatory Physiology, 2012. **303**(9): p. H1135-H1142.

36. Lord, K., et al., *Environmentally persistent free radicals decrease cardiac function before and after ischemia/reperfusion injury in vivo.* Journal of Receptors and Signal Transduction, 2011. **31**(2): p. 157-167.

37. Balakrishna, S., et al., *Environmentally persistent free radicals amplify ultrafine particle mediated cellular oxidative stress and cytotoxicity.* Particle and Fibre Toxicology, 2009. **6**(1): p. 11.

38. Timonen, K. and J. Pekkanen, *Air pollution and respiratory health among children with asthmatic or cough symptoms.* Am J Respir Crit Care Med, 1997. **156**: p. 546 - 552.

39. Fahmy, B., et al., *In vitro and in vivo assessment of pulmonary risk associated with exposure to combustion generated fine particles.* Environ Toxicol Pharmacol, 2010. **29**(2): p. 173-82.

CHAPTER 8 - SUMMARY

Nanoparticles are emitted from combustion and thermal systems and then transported to vastly in the environment [1]. These nanoparticles are composed of organic and inorganic species including metals such as copper, iron, zinc, nickel, titania, and alumina [2]. The association of the metal-organic compound result in a surface-stabilized complexes of carbon- and oxygen-centered radical's structure [3] hence, the name environmentally persistent free radicals (EPFRs). When inhaled, EPFRs undergo cycling and cause oxidative stress which lead to cardiopulmonary dysfunction and even cancer [4, 5]. We identified three steps in the formation of EPFRs. In the first step, the molecular adsorbate physisorbs on the surface of the terminal hydroxyl group of the metal oxide. The step involves chemisorption on the surface through elimination of H_2O/HCl or both (cf. Scheme 8.1). Elimination of a single component (H_2O or HCl) results in the formation of monodentate, whereas double elimination of both components results in bidentate [6-10]. After chemisorption, the electron from the oxygen atom is then transferred to the metal cation from the adsorbate to form a surface-associated radical and further reducing the metal cation.

8.1 Computational Modelling of Initial Steps in PCDD/Fs Formation

8.1.1. EPFRs Formation on Copper Oxide Clusters

We investigated the stability and reactivity of CuO-EPFRs complexes using three density functionals. We used previously optimized neutral $(CuO)_n$, with n = 1- 8, clusters for this study [11]. The reaction was initiated through addition of water to form terminal hydroxyl groups on the metal oxide surfaces and then addition of PCDD/Fs precursor (phenol, *o*-chlorophenol, and *p*-chlorophenol) to form surface-associated radicals. The addition of water resulted in the rupture of a Cu-O and the formation of two OH groups, one of which was the target for a phenolic

compound addition. The ruptured Cu-O bond was typically a bond involving a strained Cu-O-Cu bond. The reaction energies, bond lengths, and Bader charges were then established. Reactions of small hydroxylated clusters with EPFRs precursors were more exoergic than larger hydroxylated clusters. As evidenced by examination of molecular orbitals, a phenolic-bound radical was formed. The exoergic energies is an indication that organic compound can bind to CuO nanoclusters. Bader charge distributions was used to assess the degree of electron transfer from phenolic species to metal cluster. A low degree of electron transfer was observed for small clusters (CuO - Cu_5O_5). There was essentially no electron transfer for the large clusters studied

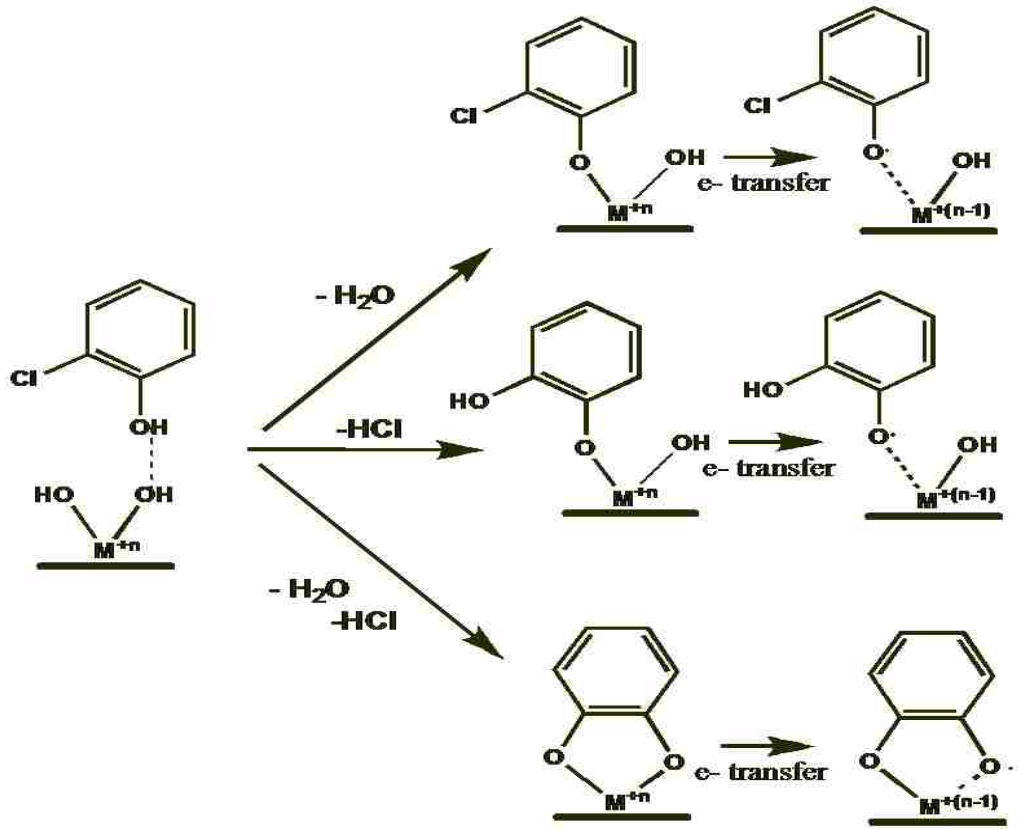

Scheme 8.1 Formation of 2-chlorophenoxyl-, 2-hydroxyphenoxyl-, and semiquinone-type EPFRs from reactions of 2-chlorophenol with a transition metal oxide.

(Cu_6O_6 - Cu_8O_8), and this suggest that the catalytic sites are likely to be small “islands" of metal

oxide clusters. Interestingly, the small clusters are more exoergic and thus more reactive than larger clusters.

In addition, we were able to predict reaction sites for Cu_4O_4 – Cu_8O_8 clusters using Bader charge analysis. The interaction of Cu-Cl bond contributes to *o*-chlorophenol stabilization. Our calculated results shows that reaction energies for chemisorption of 1,2-DCBz are slightly lower than those of 2-CP. A previous study demonstrated that the rate of chemisorption of 1,2-DCBz is ~ 10x slower than that of 2-CP [12]. The concentrations of chlorinated benzenes observed in incinerator effluent are 100x greater [13] than those of chlorinated phenols. This suggests that the number of PCDD/Fs that result from chlorinated benzenes are greater than those formed from chlorinated phenols. These reactions of adsorbed phenol and chlorinated phenols are therefore responsible for PCDD/Fs formation.

8.1.2 EPFRs Formation on Aluminum Oxide Clusters

We also investigated the reaction energies, potential energy surfaces, and activation energies to elucidate the stability and reactivity of aluminum oxide-EPFRs complexes using density functional theory. We employed GRRM [14] coupled with g09 package [15] to search for the alumina global cluster. The formation of EPFRs was initiated by addition of water to alumina clusters to form hydroxyl surfaces that reacted with PCDD/Fs precursors (phenol, *o*-chlorophenol, and *p*-chlorophenol). The addition of water molecule to Al_2O_3 did not disrupt the Al_2O_2 rhombus structure. However, the average bond length of the rhombus structure increased from 1.77 Å to 1.81 Å. For Al_4O_6 cluster, the ring was disrupted after addition of water molecule and subsequent H-atom transfer. The exoergic reaction energies indicate that organic compounds are likely to bind to alumina surfaces. Interestingly, the Al_4O_6 cluster is more exothermic and thus more reactive than Al_2O_3 cluster. Thus, we suggest that formation and stabilization of

EPFRs on alumina may depend on the cluster size. 2-chlorophenol adsorbs weakly to the surface due to displacement of both O atoms of the alumina cluster and the Cl atom of the phenolic compound. In all cases, the unpaired electron is localized on phenoxyl part which agrees with the experimental findings. These results clearly show that the formation of EPFRs from phenol and chlorinated phenols on alumina surfaces may be significant in conversion of surface-bound radicals to PCDD/Fs.

8.2 Effects of Cu(II)O/SiO_2 Content on EFPRs Yield and Persistency

Our study suggests the dependency of EPFRs yields and their persistency on metal loading in particles of: 0.25, 0.5, 0.75, 1, 2, and 3% CuO/Silica. The EPFRs were generated through exposure of particles to adsorbate vapors at 230 ^{0}C: phenol, 2-chlorophenol (2-CP), and 1,2-dichlorobenzene (DCBz). Adsorption resulted in the formation of surface-bound phenoxyl- and semiquinoine-type radicals with characteristic EPR spectra displaying a g-value ranging from ~2.0037 - 2.006. Phenoxyl- and semiquinone-type radicals are environmentally persistent and thus biologically active. They are stable in the gas phase, but they can further be stabilized through association with catalytically active metals. EPFRs were measured using electron paramagnetic resonance (EPR) and their concentration calculated based on 2,2-diphenyl-1-picrylhydrazyl (DPPH) standard. In addition, their lifetimes in ambient condition were determined. Our previous studies of EPFRs based on the same concentration of metals (5% by weight as oxide) in particulates indicated that almost every transition metal that was under study yielded EPFRs on particle surfaces [7-9, 16]. The yields and persistence of EPFRs showed dependency on the metal concentration. For example, longer lifetimes of EPFRs were recorded between 0.5 - 0.75% CuO content. Large distribution of metal concentration in particulate matter

therefore affects yield, lifetime, and chemical reactivity of the EPFRs. The size of metal/metal oxide cluster is therefore pivotal property in the catalytic activity [17-22].

Formation of EPFRs on < 5% Cu(II)/silica undergoes the same mechanism as oxides of 5% Cu(II), Fe(III), Ni(II), Zn(II), and aluminum oxide. The highest EPFRs yield was observed for CuO concentrations between 1 - 3% in relation to 2-CP and Phenol adsorption. However, radical density, which is expressed as the number of radicals per copper atom, was highest at 0.75 – 1% CuO loading. For 1,2-dichlorobenzene adsorption, radical concentration increased linearly with decreasing copper content. At the same time, a qualitative change in the formed radicals was observed – from semiquinone to chlorophenoxyl radicals.

The lifetime of these EPFRs show a strong dependence on the concentration of CuO content. Our previous study of different adsorbates on 5% CuO on silica gel based particulates resulted in half-lives of 27-74 min. The half-lives of various adsorbates on 0.25 – 5% CuO on silica (Cabosil) studied herein ranged from 7 - 25 h. The two longest lifetimes, 23 h and 22 h, were observed for phenoxyl-type radicals on 0.5% CuO and chlorophenoxyl-type radicals on 0.75% CuO, respectively. Longer half-lives were established for EPFRs on Ni(II)O, $Fe(III)_2O_3$, and Zn(II) of several days to months. For instance, the lifetime of EPFRs formed on Zn(II) domains were the longest observed among the transition metal oxides studied and ranged from 3 to 73 days [8].

8.3 Hydroxyl Radical Generation

The generation of ROS by EPFRs was conducted using spin trapping techniques confirming our hypothesized cycle that combines the radical transformation with the metal cationic center as a medium for Fenton reaction and a source of ROS [4, 5]. The EPFRs particles generated more DMPO-OH adduct compared with non-EPFRs particles. The intensity of the

DMPO-OH adduct from both the EPFRs and non-EPFRs particles increased with incubation time to a maximum at ~400 min. On average, the DMPO-OH spin adducts formed in EPFRs particles was twice that of non-EPFRs particles. The detection of 4-line spectrum from non-EPFRs is attributed to nucleophilic addition of water to DMPO [23]. On the basis of particle size, the centrifuged particles resulted in higher DMPO-OH generation compared with non-centrifuged particles. DMPO-OH generation depends on the initial concentration of EPFRs. At the maximum, 1% CuO content, 1.2 mg/L of [OH] was generated.

8.4 Tar Balls from BP Oil Spill

Tar balls collected from the Gulf of Mexico shores of Louisiana and Florida after the BP oil spill have shown the presence of paramagnetic spectra characteristic of organic free radicals as well as transition metal ions; predominantly iron(III) and manganese(II) [24]. The two types of organic radicals were identified: an asphaltene radical species typically found in crude oil (g = 2.0035) and a new type of radical resulting from the environmental transformations of crude oil (g = 2.0041-47). Pure asphaltene radicals which are stable and unreactive in air are resonance stabilized over a polyaromatic structure [25]. The new radicals were identified as products of partial oxidation of crude components and result from the interaction of the oxidized aromatics with metal ion centers. These radicals are similar to semiquinone-type observed in combustion-generated particulate and contaminated soils. In comparison with the other EPFR-particle systems, radicals found in tar balls, have longer 1/e lifetimes and can remain in the marine environment for a very long time.

8.5 Recommendations for Further Work

Semiquinone radicals are known to be very potent species that can undergo redox cycling [26] and therefore, are implicated in oxidative stress, which results to cardiopulmonary

dysfunction [27]. Based on this fact, the author suggests further studies be done on the generation of hydroxyl radicals on different concentrations of CuO content dosed with 1,2-dichlorobenzene vapors. In addition, other transition metals such as iron, nickel, titanium, and zinc can be investigated. This will determine whether these redox-active metals are significant in ROS generation.

To further investigate the effect of size in the formation of EPFRs, dendrimer templates should be used since they exert a high degree of control over size, composition, and structure of catalytically active nanoparticles in the < 3nm size range [18]. Dendrimer nanoparticles are well suited for studying the effect of particle size on catalytic function [28]. This can be achieved by using constant moles of Cu and vary the Cu/dendrimer ratio to yield dendrimer- encapsulated nanoparticles (DEN) having different CuO content. The size distribution of metal nanoparticles synthesized within dendrimers is very narrow due to the well-defined composition and structure of the dendrimer template [29].

In theoretical studies, the author suggests addition of more than one water molecule to the metal oxides studied herein. However, this may lead to disruption of the overall geometry. The EQ1 (Al_2O_3 cluster) is only 2.4 kcal/mol higher in energy than EQ0 and therefore, it is present in significant amounts even at room temperature. EQ1′ is present too at room temperature and reaches significant concentrations at high temperatures. The author further suggests calculations of EQ1 and EQ1′ with phenol and chlorinated phenols. The transition state theory can be employed to establish the overall rate of conversion of phenol reactants to phenyl species.

8.6 References

1. Kittelson, D.B. *Nanoparticle Emissions from Internal Combustion Engines*. in *The Royal Society Discussion Meeting, Ultra Fine Particles in the Atmosphere*. 2000.

2. Buzea, C., I.I. Pacheco, and K. Robbie, *Nanomaterials and nanoparticles: sources and toxicity.* Biointerphases, 2007. **2**(4): p. MR17-MR71.

3. McFerrin, C.A., *Elementary Reactions Involved in Pollutant-Forming Mechanisms*, 2007, Faculty of the Louisiana State University and Agricultural and Mechanical College in partial fulfillment of the requirements for the degree of Doctor of Philosophy in The Department of Chemistry by Cheri Ann McFerrin BS, Louisiana State University.

4. Khachatryan, L., et al., *Environmentally Persistent Free Radicals (EPFRs). 1. Generation of Reactive Oxygen Species in Aqueous Solutions.* Environmental Science & Technology, 2011. **45**(19): p. 8559-8566.

5. Khachatryan, L. and B. Dellinger, *Environmentally Persistent Free Radicals (EPFRs)-2. Are Free Hydroxyl Radicals Generated in Aqueous Solutions?* Environmental Science & Technology, 2011. **45**(21): p. 9232-9239.

6. Patterson, M.C., et al., *EPFR formation from phenol adsorption on Al2O3 and TiO2: EPR and EELS studies.* Chemical Physics, 2013. **422**(0): p. 277-282.

7. Vejerano, E., S.M. Lomnicki, and B. Dellinger, *Formation and Stabilization of Combustion-Generated, Environmentally Persistent Radicals on Ni(II)O Supported on a Silica Surface.* Environmental Science & Technology, 2012. **46**(17): p. 9406-9411.

8. Vejerano, E., S. Lomnicki, and B. Dellinger, *Lifetime of combustion-generated environmentally persistent free radicals on Zn(ii)O and other transition metal oxides.* Journal of Environmental Monitoring, 2012. **14**(10): p. 2803-2806.

9. Vejerano, E., S. Lomnicki, and B. Dellinger, *Formation and Stabilization of Combustion-Generated Environmentally Persistent Free Radicals on an Fe(III)2O3/Silica Surface.* Environmental Science & Technology, 2010. **45**(2): p. 589-594.

10. Lomnicki, S., et al., *Copper oxide-based model of persistent free radical formation on combustion-derived particulate matter.* Environ Sci Technol, 2008. **42**: p. 4982 - 4988.

11. Bae, G.-T., B. Dellinger, and R.W. Hall, *Density Functional Calculation of the Structure and Electronic Properties of CunOn (n = 1−8) Clusters.* The Journal of Physical Chemistry A, 2011. **115**(11): p. 2087-2095.

12. Alderman, S.L., et al., *An Infrared and X-ray Spectroscopic Study of the Reactions of 2-Chlorophenol, 1,2-Dichlorobenzene, and Chlorobenzene with Model CuO/Silica Fly Ash Surfaces.* Environmental Science & Technology, 2005. **39**(19): p. 7396-7401.

13. Blumenstock, M., et al., *Estimation of the dioxin emission (PCDD/FI-TEQ) from the concentration of low chlorinated aromatic compounds in the flue and stack gas of a hazardous waste incinerator.* Journal of Analytical and Applied Pyrolysis, 1999. **49**(1–2): p. 179-190.

14. Ohno, K. and S. Maeda, *A scaled hypersphere search method for the topography of reaction pathways on the potential energy surface.* Chemical Physics Letters, 2004. **384**(4–6): p. 277-282.

15. Frisch, M.J., et al., *Gaussian 09, Revision B.01*, 2009: Wallingford CT.

16. Lomnicki, S., et al., *Copper Oxide-Based Model of Persistent Free Radical Formation on Combustion Derived Particulate Matter.* Environ Sci Technol, 2008. **42**: p. 4982 - 4988.

17. Zhou, X., et al., *Size-Dependent Catalytic Activity and Dynamics of Gold Nanoparticles at the Single-Molecule Level.* Journal of the American Chemical Society, 2009. **132**(1): p. 138-146.

18. Wilson, O.M., et al., *Effect of Pd nanoparticle size on the catalytic hydrogenation of allyl alcohol.* Journal of the American Chemical Society, 2006. **128**(14): p. 4510-4511.

19. Bezemer, G.L., et al., *Cobalt Particle Size Effects in the Fischer−Tropsch Reaction Studied with Carbon Nanofiber Supported Catalysts.* Journal of the American Chemical Society, 2006. **128**(12): p. 3956-3964.

20. Grass, M., R. Rioux, and G. Somorjai, *Dependence of Gas-Phase Crotonaldehyde Hydrogenation Selectivity and Activity on the Size of Pt Nanoparticles (1.7–7.1 nm) Supported on SBA-15.* Catalysis Letters, 2009. **128**(1-2): p. 1-8.

21. Doyle, A.M., S.K. Shaikhutdinov, and H.-J. Freund, *Surface-Bonded Precursor Determines Particle Size Effects for Alkene Hydrogenation on Palladium.* Angewandte Chemie International Edition, 2005. **44**(4): p. 629-631.

22. Burda, C., et al., *Chemistry and Properties of Nanocrystals of Different Shapes.* Chemical Reviews, 2005. **105**(4): p. 1025-1102.

23. Hanna, P.M., W. Chamulitrat, and R.P. Mason, *When are metal ion-dependent hydroxyl and alkoxyl radical adducts of 5, 5-dimethyl-1-pyrroline N-oxide artifacts?* Archives of biochemistry and biophysics, 1992. **296**(2): p. 640-644.

24. Kiruri, L.W., B. Dellinger, and S. Lomnicki, *Tar Balls from Deep Water Horizon Oil Spill: Environmentally Persistent Free Radicals (EPFR) Formation During Crude Weathering.* Environmental science & technology, 2013. **47**(9): p. 4220-4226.

25. Montanari, L., et al., *Asphaltene radicals and their interaction with molecular oxygen: an EPR probe of their molecular characteristics and tendency to aggregate.* Applied Magnetic Resonance, 1998. **14**(1): p. 81-100.

26. Squadrito, G.L., et al., *Quinoid redox cycling as a mechanism for sustained free radical generation by inhaled airborne particulate matter.* Free Radical Biology and Medicine, 2001. **31**(9): p. 1132-1138.

27. Nel, A.E., D. Diaz-Sanchez, and N. Li, *The role of particulate pollutants in pulmonary inflammation and asthma: evidence for the involvement of organic chemicals and oxidative stress.* Current opinion in pulmonary medicine, 2001. **7**(1): p. 20-26.

28. Lomnicki, S.M., et al., *Size-selective synthesis of immobilized copper oxide nanoclusters on silica.* Materials Science and Engineering: B, 2010. **175**(2): p. 136-142.

29. Somorjai, G.A. and J.Y. Park, *Molecular Factors of Catalytic Selectivity.* Angewandte Chemie International Edition, 2008. **47**(48): p. 9212-9228.

APPENDIX 1. SUPPORTING INFORMATION FOR EPFRS FORMATION

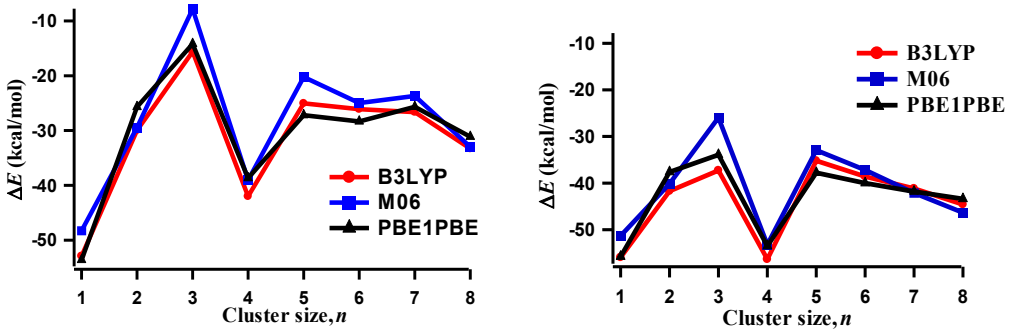

Figure A1.1 Reaction energies (kcal/mol) of copper oxide clusters with water: A). GENECP and B). LANL2DZ basis set.

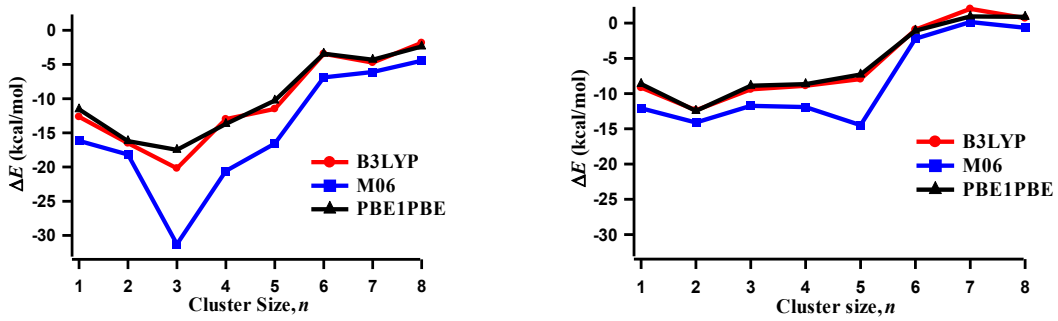

Figure A1.2 Reaction energies (kcal/mol) of hydroxylated copper oxide clusters with phenol: A). GENECP and B). LANL2DZ basis set.

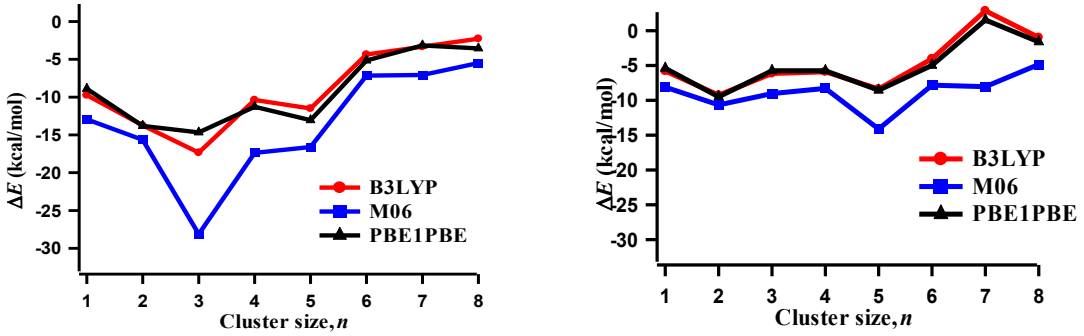

Figure A1.3 Reaction energies (kcal/mol) of hydroxylated copper oxide clusters with *o*-chlorophenol: A). GENECP and B). LANL2DZ basis set.

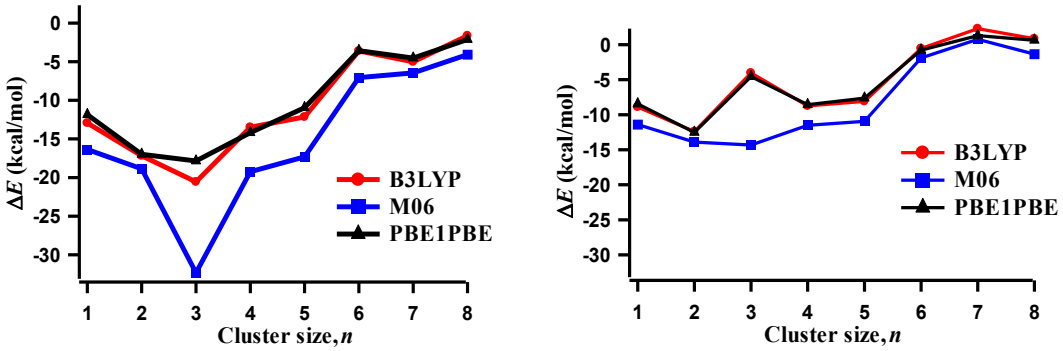

Figure A1.4 Reaction energies (kcal/mol) of hydroxylated copper oxide clusters with *p*-chlorophenol: A). GENECP and B). LANL2DZ basis set.

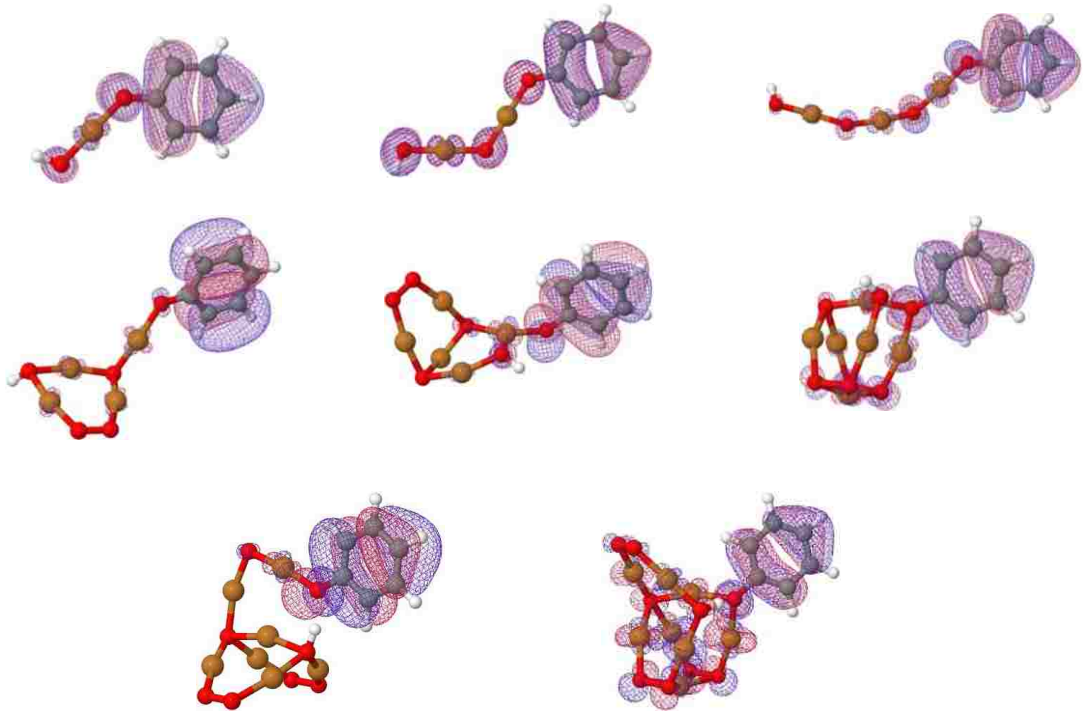

Figure A1.5 Molecular orbitals of phenoxyl-type EPFRs showing the location of the unpaired electron.

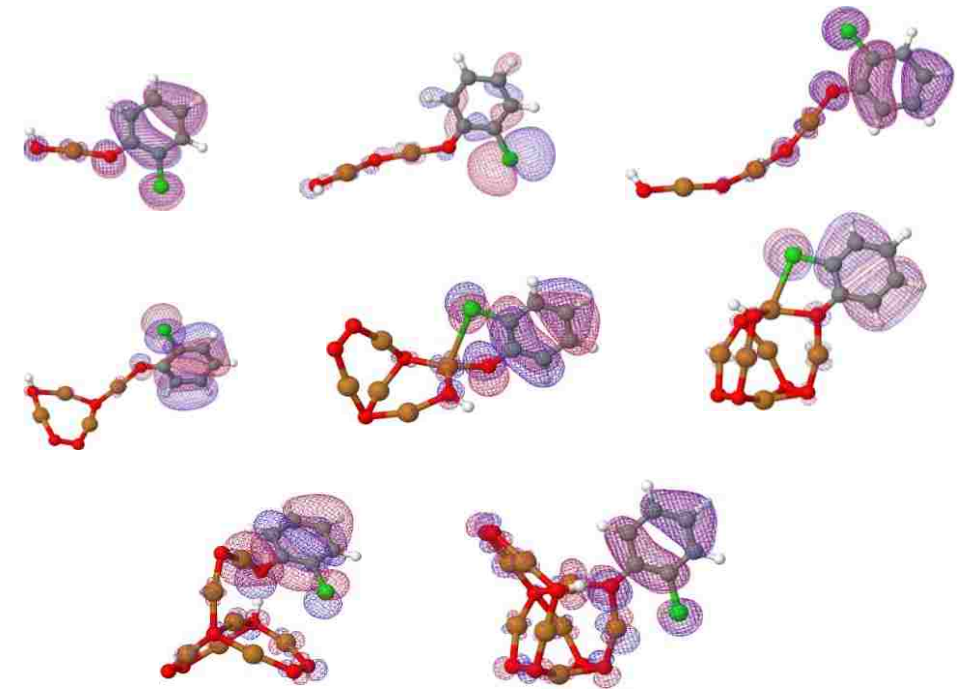

Figure A1.6 Molecular orbitals of 2-chlorophenoxyl-type EPFRs showing the location of the unpaired electron.

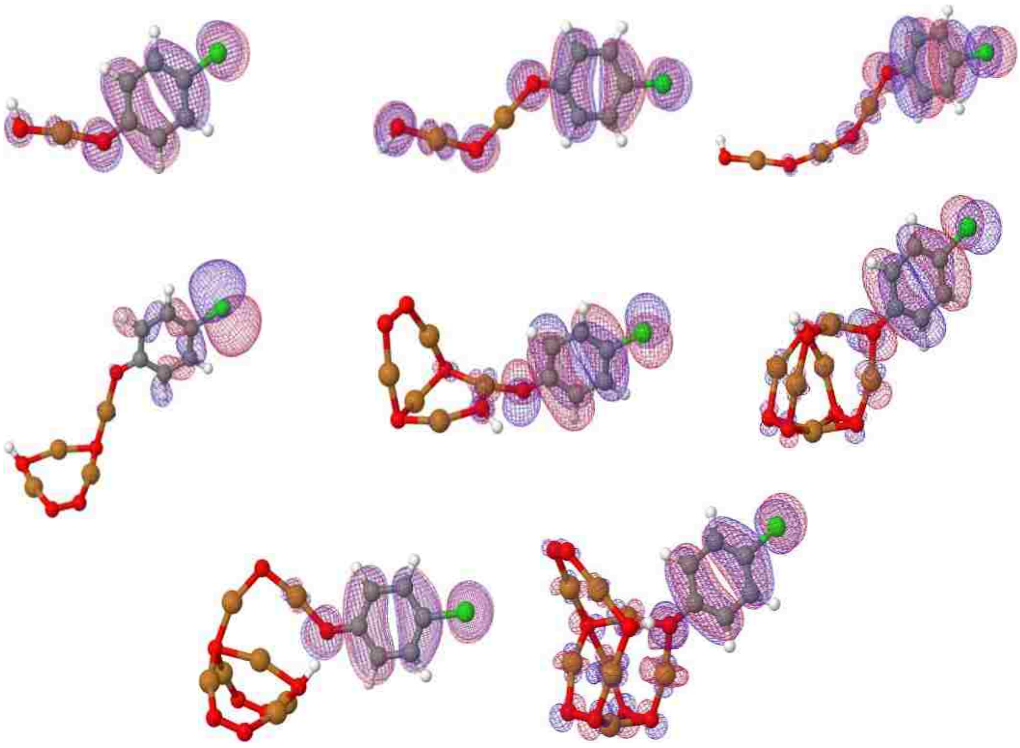

Figure A1.7 Molecular orbitals of 4-chlorophenoxyl-type EPFRs showing the location of the unpaired electron.

Table A1.1 Spin states, ionization energies (IE), electron affinities (EA), and atomization energies (AE) for Al_2O_3 and Al_4O_6 clusters Energies are in eV and are calculated using B3LYP/6-311+G* model chemistry.

Clusters	Spin State	IE	EA		AE
Al_2O_3	triplet	9.18	3.41		9.45
Al_4O_6	singlet	9.56	2.21		11.65

Table A1.2 Entropies and Gibbs free energies of the various complexes, relative to reactants at 298.15 K. Units in Cal/mol and kcal/mol

Precursor	$Al_2O_4H_2$ 'OC'		TS		'OC'Al_2O_3 H_2O		'OC'Al_2O_3+ H_2O	
	ΔS	ΔG	ΔS	ΔG	ΔS	ΔG	ΔS	ΔG
phenol	-41.1	-14.3	-45.7	7.8	-41.7	-5.2	-7.7	-9.6
o-chlorophenol	-41.7	-12.7	-45.8	9.1	-40.8	-6.6	-7.5	-7.1
p-chlorophenol	-41.9	-13.4	-45.7	7.9	-42.0	-5.7	-8.1	-10.4

Table A1-3 Entropies and Gibbs free energies of the various complexes, relative to reactants at 298.15 K. Units in Cal/mol and kcal/mol

Precursor	$Al_4O_7H_2$ 'OC'		TS		'OC'Al_4O_6 H_2O		'OC'Al_4O_6+ H_2O	
	ΔS	ΔG	ΔS	ΔG	ΔS	ΔG	ΔS	ΔG
phenol	-29.2	-37.2	-34.3	-28.5	-28.6	-41.1	-4.4	-27.2
o-chlorophenol	-29.5	-35.0	-32.7	-27.2	-29.9	-42.4	-5.0	-25.2
p-chlorophenol	-29.7	-36.4	-35.0	-28.4	-28.6	-41.9	-4.0	-27.7

Table A1.3 Metal Analysis

Sample	Si	Al	Fe	Mg	Zn	Ti	Cr	V
TB_0	46676	6549.2	32.956	275.66	6.7228	7.49	0.077	
TB_{60}	39984	5714.8	29.582	246.12	0.364	7.448	0.0504	
TB_{90}	39340	6484.8	32.06	261.8	0.322	6.9874	0.0658	0.1022
TB_{360}	37184	4774	23.338	226.66	0.0196	15.372	0.091	

APPENDIX 2. AMERICAN CHEMICAL SOCIETY'S POLICY ON THESES AND DISSERTATIONS (FORM)

American Chemical Society's Policy on Theses and Dissertations

If your university requires you to obtain permission, you must use the RightsLink permission system. See RightsLink instructions at http://pubs.acs.org/page/copyright/permissions.html.

This is regarding request for permission to include **your** paper(s) or portions of text from **your** paper(s) in your thesis. Permission is now automatically granted; please pay special attention to the **implications** paragraph below. The Copyright Subcommittee of the Joint Board/Council Committees on Publications approved the following:

> Copyright permission for published and submitted material from theses and dissertations
> ACS extends blanket permission to students to include in their theses and dissertations their own articles, or portions thereof, that have been published in ACS journals or submitted to ACS journals for publication, provided that the ACS copyright credit line is noted on the appropriate page(s).
>
> Publishing **implications** of electronic publication of theses and dissertation material
> Students and their mentors should be aware that posting of theses and dissertation material on the Web prior to submission of material from that thesis or dissertation to an ACS journal may affect publication in that journal. Whether Web posting is considered prior publication may be evaluated on a case-by-case basis by the journal's editor. If an ACS journal editor considers Web posting to be "prior publication", the paper will not be accepted for publication in that journal. If you intend to submit your unpublished paper to ACS for publication, check with the appropriate editor prior to posting your manuscript electronically.

Reuse/Republication of the Entire Work in Theses or Collections: Authors may reuse all or part of the Submitted, Accepted or Published Work in a thesis or dissertation that the author writes and is required to submit to satisfy the criteria of degree-granting institutions. Such reuse is permitted subject to the ACS' "Ethical Guidelines to Publication of Chemical Research" (http://pubs.acs.org/page/policy/ethics/index.html); the author should secure written confirmation (via letter or email) from the respective ACS journal editor(s) to avoid potential conflicts with journal prior publication*/embargo policies. Appropriate citation of the Published Work must be made. If the thesis or dissertation to be published is in electronic format, a direct link to the Published Work must also be included using the ACS Articles on Request author-directed link – see http://pubs.acs.org/page/policy/articlesonrequest/index.html

* Prior publication policies of ACS journals are posted on the ACS website at http://pubs.acs.org/page/policy/prior/index.html

If your paper has **not** yet been published by ACS, please print the following credit line on the first page of your article: "Reproduced (or 'Reproduced in part') with permission from [JOURNAL NAME], in press (or 'submitted for publication'). Unpublished work copyright [CURRENT YEAR] American Chemical Society." Include appropriate information.

If your paper has already been published by ACS and you want to include the text or portions of the text in your thesis/dissertation, please print the ACS copyright credit line on the first page of your article: "Reproduced (or 'Reproduced in part') with permission from [FULL REFERENCE CITATION.] Copyright [YEAR] American Chemical Society." Include appropriate information.

Submission to a Dissertation Distributor: If you plan to submit your thesis to UMI or to another dissertation distributor, you should not include the unpublished ACS paper in your thesis if the thesis will be disseminated electronically, until ACS has published your paper. After publication of the paper by ACS, you may release the entire thesis (**not the individual ACS article by itself**) for electronic dissemination through the distributor; ACS's copyright credit line should be printed on the first page of the ACS paper.

10/10/03, 01/15/04, 06/07/06, 04/07/10, 08/24/10, 02/28/11

APPENDIX 3. COPYRIGHTS PERMISSION FORMS

Copyright Clearance Center RightsLink®

Home | Account Info | Help

ACS Publications High quality High impact

Title:	Tar Balls from Deep Water Horizon Oil Spill: Environmentally Persistent Free Radicals (EPFR) Formation During Crude Weathering
Author:	Lucy W. Kiruri, Barry Dellinger, and Slawo Lomnicki
Publication:	Environmental Science & Technology
Publisher:	American Chemical Society
Date:	May 1, 2013

Logged in as: Lucy Kiruri
Account #: 3000701217
LOGOUT

PERMISSION/LICENSE IS GRANTED FOR YOUR ORDER AT NO CHARGE

This type of permission/license, instead of the standard Terms & Conditions, is sent to you because no fee is being charged for your order. Please note the following:

- Permission is granted for your request in both print and electronic formats, and translations.
- If figures and/or tables were requested, they may be adapted or used in part.
- Please print this page for your records and send a copy of it to your publisher/graduate school.
- Appropriate credit for the requested material should be given as follows: "Reprinted (adapted) with permission from (COMPLETE REFERENCE CITATION). Copyright (YEAR) American Chemical Society." Insert appropriate information in place of the capitalized words.
- One-time permission is granted only for the use specified in your request. No additional uses are granted (such as derivative works or other editions). For any other uses, please submit a new request.

BACK | CLOSE WINDOW

RightsLink®

Home | Account Info | Help

Title: Density Functional Calculation of the Structure and Electronic Properties of CunOn (n = 1−8) Clusters

Author: Gyun-Tack Bae, Barry Dellinger, and Randall W. Hall

Publication: The Journal of Physical Chemistry A

Publisher: American Chemical Society

Date: Mar 1, 2011

Logged in as:
Lucy Kiruri
Account #:
3000701217

LOGOUT

PERMISSION/LICENSE IS GRANTED FOR YOUR ORDER AT NO CHARGE

This type of permission/license, instead of the standard Terms & Conditions, is sent to you because no fee is being charged for your order. Please note the following:

- Permission is granted for your request in both print and electronic formats, and translations.
- If figures and/or tables were requested, they may be adapted or used in part.
- Please print this page for your records and send a copy of it to your publisher/graduate school.
- Appropriate credit for the requested material should be given as follows: "Reprinted (adapted) with permission from (COMPLETE REFERENCE CITATION). Copyright (YEAR) American Chemical Society." Insert appropriate information in place of the capitalized words.
- One-time permission is granted only for the use specified in your request. No additional uses are granted (such as derivative works or other editions). For any other uses, please submit a new request.

If credit is given to another source for the material you requested, permission must be obtained from that source.

BACK CLOSE WINDOW

Copyright Clearance Center RightsLink®

Home | Account Info | Help

ACS Publications High quality. High impact.

Title: Potential for Misidentification of Environmentally Persistent Free Radicals as Molecular Pollutants in Particulate Matter

Author: Hieu Truong, Slawo Lomnicki, and Barry Dellinger

Publication: Environmental Science & Technology

Publisher: American Chemical Society

Date: Mar 1, 2010

Logged in as:
Lucy Kiruri
Account #:
3000701217

LOGOUT

PERMISSION/LICENSE IS GRANTED FOR YOUR ORDER AT NO CHARGE

This type of permission/license, instead of the standard Terms & Conditions, is sent to you because no fee is being charged for your order. Please note the following:

- Permission is granted for your request in both print and electronic formats, and translations.
- If figures and/or tables were requested, they may be adapted or used in part.
- Please print this page for your records and send a copy of it to your publisher/graduate school.
- Appropriate credit for the requested material should be given as follows: "Reprinted (adapted) with permission from (COMPLETE REFERENCE CITATION). Copyright (YEAR) American Chemical Society." Insert appropriate information in place of the capitalized words.
- One-time permission is granted only for the use specified in your request. No additional uses are granted (such as derivative works or other editions). For any other uses, please submit a new request.

If credit is given to another source for the material you requested, permission must be obtained from that source.

BACK CLOSE WINDOW

RightsLink®

Home | Account Info | Help

Title: Formation and Stabilization of Combustion-Generated Environmentally Persistent Free Radicals on an Fe(III)2O3/Silica Surface

Author: Eric Vejerano, Slawomir Lomnicki, and Barry Dellinger

Publication: Environmental Science & Technology

Publisher: American Chemical Society

Date: Jan 1, 2011

Logged in as:
Lucy Kiruri
Account #:
3000701217

LOGOUT

PERMISSION/LICENSE IS GRANTED FOR YOUR ORDER AT NO CHARGE

This type of permission/license, instead of the standard Terms & Conditions, is sent to you because no fee is being charged for your order. Please note the following:

- Permission is granted for your request in both print and electronic formats, and translations.
- If figures and/or tables were requested, they may be adapted or used in part.
- Please print this page for your records and send a copy of it to your publisher/graduate school.
- Appropriate credit for the requested material should be given as follows: "Reprinted (adapted) with permission from (COMPLETE REFERENCE CITATION). Copyright (YEAR) American Chemical Society." Insert appropriate information in place of the capitalized words.
- One-time permission is granted only for the use specified in your request. No additional uses are granted (such as derivative works or other editions). For any other uses, please submit a new request.

If credit is given to another source for the material you requested, permission must be obtained from that source.

BACK CLOSE WINDOW

Copyright Clearance Center RightsLink®

Home | Account Info | Help

ACS Publications High quality. High impact.

Title: Role of Free Radicals in the Toxicity of Airborne Fine Particulate Matter

Author: Barry Dellinger et al.

Publication: Chemical Research in Toxicology

Publisher: American Chemical Society

Date: Oct 1, 2001

Logged in as:
Lucy Kinuri
LOGOUT

PERMISSION/LICENSE IS GRANTED FOR YOUR ORDER AT NO CHARGE

This type of permission/license, instead of the standard Terms & Conditions, is sent to you because no fee is being charged for your order. Please note the following:

- Permission is granted for your request in both print and electronic formats, and translations.
- If figures and/or tables were requested, they may be adapted or used in part.
- Please print this page for your records and send a copy of it to your publisher/graduate school.
- Appropriate credit for the requested material should be given as follows: "Reprinted (adapted) with permission from (COMPLETE REFERENCE CITATION). Copyright (YEAR) American Chemical Society." Insert appropriate information in place of the capitalized words.
- One-time permission is granted only for the use specified in your request. No additional uses are granted (such as derivative works or other editions). For any other uses, please submit a new request.

If credit is given to another source for the material you requested, permission must be obtained from that source.

BACK CLOSE WINDOW

Lucy Kiruri <lkirur1@tigers.lsu.edu> Oct 30 (3 days ago)

to Gyun-Tack, gtbae, Randall

Dear Tack,

I am writing to request for permission to use some of the work in "Computational Modeling of the Initial Steps in Copper Oxide-Catalyzed Formation of Poly-Chlorinated Dibenzo Dioxins and Furans" in my dissertation.

Thank you.

배균택 Oct 31 (2 days ago)

to me

Hi, Lucy. Sorry late email. Yes, You can put it in your disseration. Good luck!!! Thanks tack

Gyun-Tack Bae, Ph.D.
Assistant Professor
Department of Chemical Education
Chungbuk National University
82-216 410 Seongbong-ro Heungdeok-gu,
Cheongju Chungbuk 361-763, South Korea
Office: 216
Phone: +82-43-261-2733
Fax: +82-43-263-2723 (department)
Email: gtbae@chungbuk.ac.kr

THE VITA

Lucy W. Kiruri was born in Nakuru, Kenya to Mr. Samuel T. Kamau and Mrs. Mary W. Tatha. She attended Kiguoya Primary School from 1987 to 1994. She enrolled at Jomo Kenyatta High School for her certificate of Secondary School education. She completed her Bachelor of Science in Chemistry from Kenyatta University in 2004 and her Masters of Science in Chemistry from the same institution in 2009. In Fall 2009, she joined Louisiana State University where she's pursuing her doctoral degree in physical and computational chemistry under the directions of Prof. Barry Dellinger and Prof. Randall Hall. She will receive her Doctor of Philosophy degree in December 2013.